Alma Mater Studiorum - Università di Bologna

DOTTORATO DI RICERCA IN

SCIENZE BIOTECNOLOGICHE, BIOCOMPUTAZIONALI, FARMACEUTICHE E FARMACOLOGICHE

Ciclo 36

Settore Concorsuale: 05/G1 - FARMACOLOGIA, FARMACOLOGIA CLINICA E FARMACOGNOSIA

Settore Scientifico Disciplinare: BIO/14 - FARMACOLOGIA

GASTROINTESTINAL STROMAL TUMORS: ARBUTUS UNEDO L. AS A SOURCE OF NOVEL CHEMOTHERAPEUTICS & MECHANISMS BEHIND METASTASIS

Presentata da: Aldo Di Vito

Coordinatore Dottorato

Maria Laura Bolognesi

Supervisore

Patrizia Hrelia

Co-supervisore

Sabrina Angelini

Esame finale anno 2024

Alma Mater Studiorum – Università di Bologna

PhD program in

BIOTECHNOLOGICAL, BIOCOMPUTATIONAL, PHARMACEUTICAL AND PHARMACOLOGICAL SCIENCES

Cycle 36th

Gastrointestinal stromal tumors: *Arbutus unedo L.* as a source of novel chemotherapeutics & mechanisms behind metastasis

Author

Aldo Di Vito, M.D

Supervisor

Professor Patrizia Hrelia, Ph.D

Co-supervisor

Professor Sabrina Angelini, Ph.D

Coordinator of the PhD Program

Professor Maria Laura Bolognesi, Ph.D

Go instead where there is no path and leave a trail

Ralph Waldo Emerson

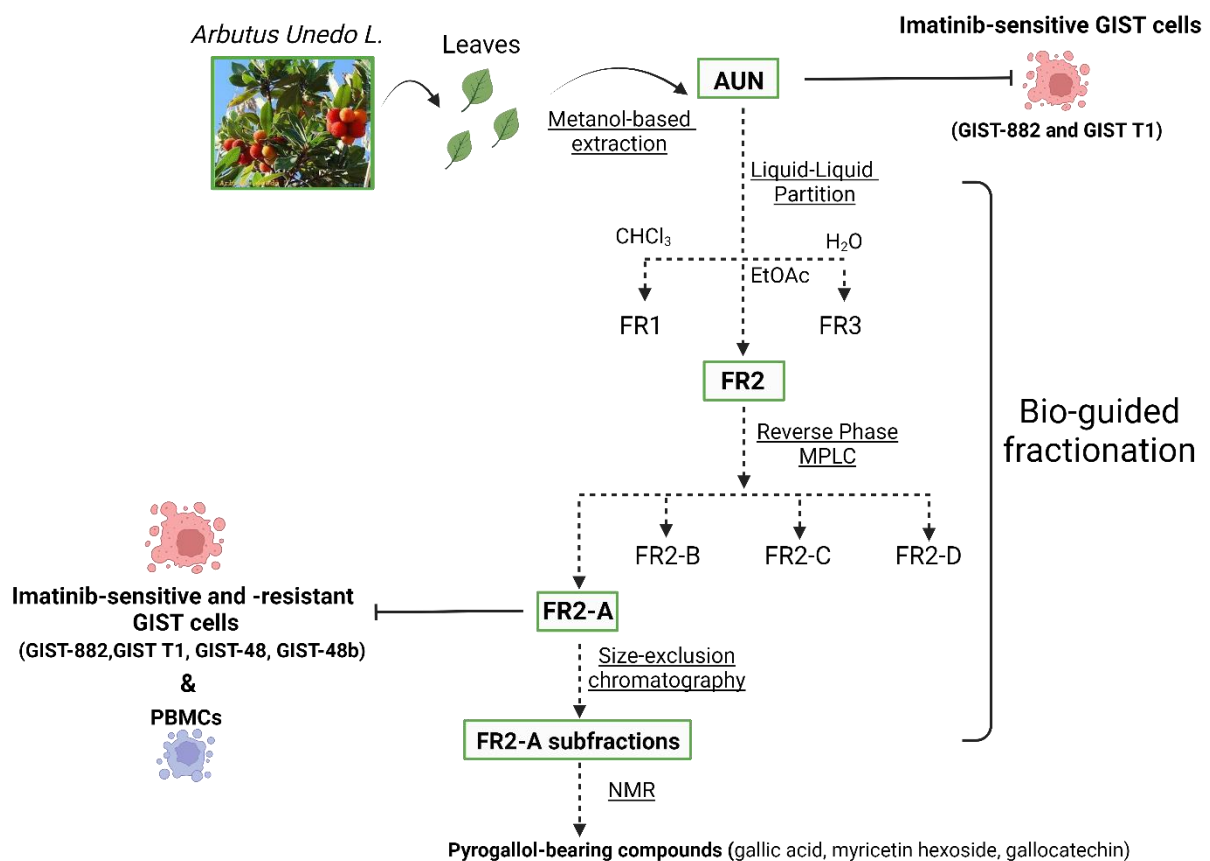# ABSTRACT

Gastrointestinal stromal tumors (GIST) are mesenchymal neoplasms frequently caused by a gain of function mutation in KIT or PDGFRα, two tyrosine kinase receptors (TKR). For this reason, they are successfully treated with imatinib, a tyrosine kinase inhibitor (TKI). However, the therapy is typically long-term ineffective due to imatinib resistance, which represents the main issue in the clinic of GISTs. Although numerous efforts have been made in the last two decades to develop novel therapies for imatinib-resistant GISTs, the approvals of multi-target TKIs have only improved the clinical outcomes modestly. Emblematic is the recent failure of ripretinib in the phase III INTRIGUE trial, decisively marking the end of the paradigm only based on the central role of KIT secondary mutations in imatinib resistance, and the consequent seeking of multi-target TKIs as the solution. Consistent with this clinical result, preclinical studies have revealed numerous mechanisms of resistance that are not targetable with multi-target TKIs, indicating that imatinib resistance is more multifaceted than initially hypothesized and explaining the modest efficacy of these latter. In this scenario, the absence of drugs capable of long-term counteracting the rise of imatinib-resistant subclones unavoidably leads to progressive disease and metastasis. In particular, the onset of metastases remarkably impacts the median overall survival and determines the most GIST-related deaths. Therefore, new therapy proposals are needed. Here, we present two project lines investigating novel strategies to counteract imatinib-resistant GISTs.

Bio-guided fractionation of AUN to identify novel chemotherapeutics in GISTs

Considering the multifaceted landscape of imatinib resistance, seeking a broad-spectrum therapy, such as traditional chemotherapy, could represent a solution to target most imatinib-resistant subclones simultaneously. However, available traditional chemotherapeutics have shown low partial response in GISTs, and none have been approved for the therapy. Numerous chemotherapeutics were discovered in the plant kingdom, and others could still be hidden. *Arbutus unedo L.* could be a source of novel hit or lead compounds because its extracts were associated with a broad-spectrum anti-cancer activity in various cellular models. Since the leaf extract of *Arbutus unedo L.* (AUN) also impaired the viability of GIST cells, we applied bio-guided fractionation to isolate and unveil the bioactive compounds responsible for the pharmacological activity. The bio-guided fractionation of AUN led to the isolation of FR2-A, a fraction that efficiently targeted both imatinib-sensitive and -resistant cell lines via a KIT-independent mechanism. The multi-spectrum activity of FR2-A was not

GIST-specific due to cytotoxicity observed in Peripheral Blood Mononuclear Cells (PBMCs), a healthy cellular model. Interestingly, doxorubicin, a traditional chemotherapeutic not approved in GIST due to a low partial response, showed similar cytotoxicity in PBMCs and a well-known myelosuppressive side effect in patients. Therefore, the doxorubicin-like cytotoxic profile suggested that bioactive compounds in FR2-A could belong to the class of traditional chemotherapeutics. The further bio-guided fractionation of FR2-A and nuclear magnetic resonance (NMR) analysis of the derived subfractions revealed that pyrogallol-bearing compounds were exclusively present in those that maintained the pharmacological activity in GIST cellular models, highlighting the interest in these phytochemicals. Further studies are required to validate these compounds for GIST treatment.
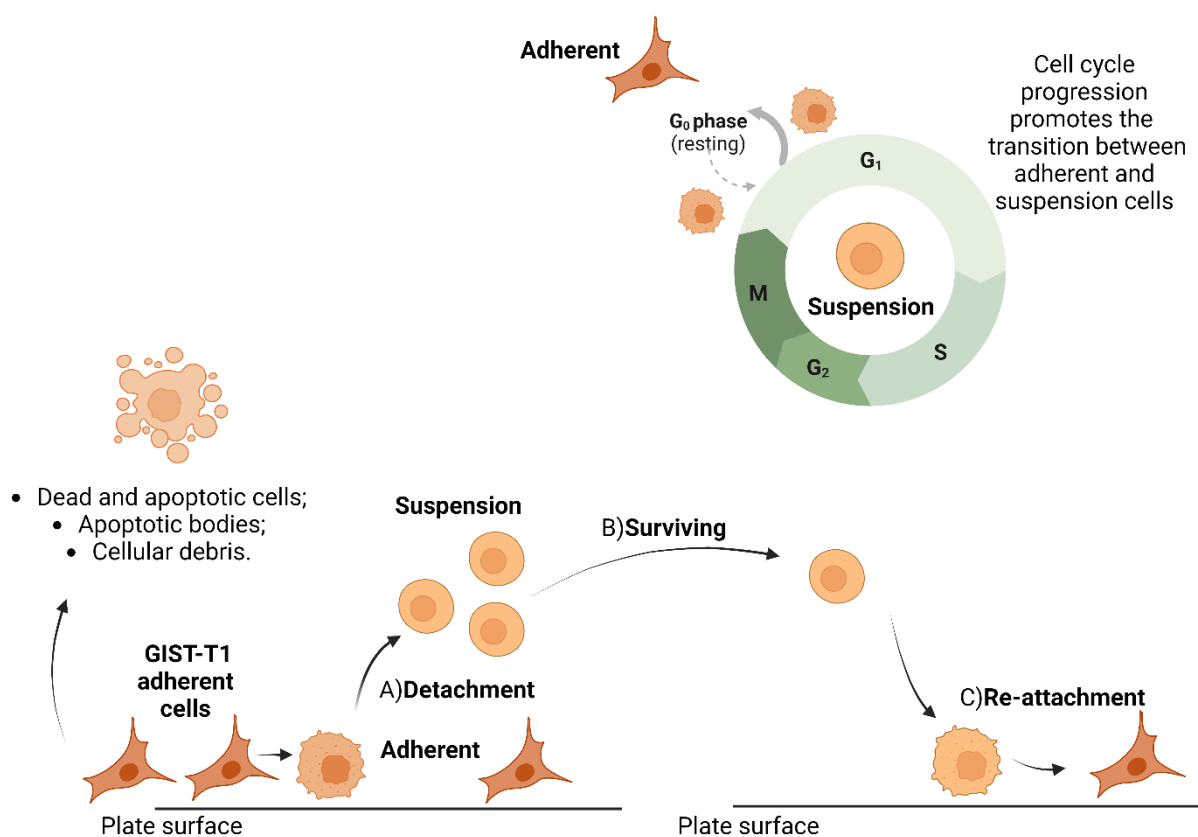

Graphical abstract - Created with BioRender.com.

An *in vitro* model for the study of metastasis in GIST

An alternative therapeutic strategy that could ameliorate the life expectancy of patients with an unresectable and imatinib-resistant GIST could be targeting the metastatic cascade. Indeed, preventing the tumor progression to metastasis could remarkably increase the median overall

survival. However, the mechanisms behind GIST metastasis are mostly unknown, and no validated targets have been reported. This is also attributable to the lack of reliable preclinical models for the study of metastasis in GISTs. Therefore, we established a novel *in vitro* metastasis model and characterized it to shed light on novel strategies to prevent metastasis. In detail, certain adherent GIST-T1 cells spontaneously detach from the plate surface, survive in suspension, and colonize a new tissue culture plate if seeded, thus mimicking the metastatic cascade *in vitro*. This process was associated with cell plasticity, which modified their phenotype to detach from the plate surface, transiently acquiring the status of suspension cells. Noteworthy, we unveiled that this plasticity strictly depended on the cell cycle. Indeed, these cells showed an elongated shape when adherent and quiescent. The entry into the cell cycle promoted the acquisition of a circular phenotype and the movement in the cell suspension. Cells divide in suspension and re-attach to the plate surface when the cell cycle is completed. Further studies are required to decipher the molecular mechanisms behind the transition between adherent and suspension cells and vice-versa. Moreover, validating this *in vitro* model *in vivo* is crucial to strengthen the significance of the established findings.

Graphical abstract - Created with BioRender.com.

Table of Contents

KEYWORDS

Gastrointestinal stromal tumors; GIST; plant extract; *Arbutus unedo L.*; Bio-guided fractionation; natural compound; Pyrogallol-bearing compounds; metastatic cascade; metastasis; *in vitro* metastasis model.

ABBREVIATIONS

7-AAD, 7-amino actinomycin D; **A. unedo;** Arbutus unedo L.**; AUN,** the extract obtained from the leaves of Arbutus unedo L. **CR**, complete response; **CTC,** circulating tumor cell; **dt,** doubling time; **EGIST,** extra-GIST; **FDA,** Food and drug administration; **GI,** gastrointestinal; **GIPACT,** gastrointestinal pacemaker cell tumor; **GIST,** gastrointestinal stromal tumor; **ICC,** interstitial cells of Cajal; **LMS,** leiomyosarcoma; **lncRNA,** long non-coding RNA; **miR,** miRNA; **NP,** natural compound; **ORR,** overall response rate; **OS,** overall survival; **PDGFRα,** platelet-derived growth factor receptor; **PDGFα,** the platelet-derived growth factor; **PFS,** progressive free survival; **PS,** phosphatidylserine; **SCF,** Stem Cell Factor; **SD,** stable disease; **SEER,** Surveillance, Epidemiology, and End Results Program database; **TC,** tissue culture-treated plates **TKI,** tyrosine kinase inhibitor; **TKR,** tyrosine kinase receptors; **WT,** wild-type;

DEFINITIONS [(d)]

Gain of function mutation = A mutation that promotes new or deregulated gene product functions.

Adjuvant therapy = A therapy commonly delivered after tumor resection to destroy remaining cancer cells.

Anoikis = Anoikis is a form of programmed cell death that occurs when cells detach from the surrounding extracellular matrix (Adeshakin et al., 2021).

cLogP value = cLogP is the calculated log of the partition coefficient, which represents the solubility of a molecule in octanol/water. It measures how much of a solute dissolves e in an immiscible biphasic system of lipids (fats, oils, organic solvents) and water.

Complete response = the disappearance of all target lesions.

Doubling time (dt) = the time required for doubling the number of cells.

Epithelial-mesenchymal transition (EMT) = biological process that allows a polarized epithelial cell, which usually interacts with the basement membrane via its basal surface, to undergo multiple biochemical changes that enable it to assume a mesenchymal cell phenotype, which includes enhanced migratory capacity.

Familial GISTs = GISTs associated with an inherited germline mutation. The onset of the disease is between the ages of 25 and 50.

High-risk GIST = A GIST is considered high-risk if the tumor is >10 cm with any mitotic index, >5 cm with a mitotic count >5/50 number per high-power field (HPF), or if it underwent rupture during resection (Poveda et al., 2017).

Neo-adjuvant therapy = therapy delivered before surgery to promote tumor shrinkage or make surgery less invasive and more effective.

Objective response rate (ORR) = the proportion of patients who have a partial or complete response to therapy.

Overall survival (OS) = the time which begins at diagnosis (or at the start of treatment) and up to the time of death

Partial response = A partial response is defined as at least a 30% decrease in the sum of all cancer lesions.

Patient-derived xenograft (PDX) = models of cancer where part of the patient's tumor is implanted into an immunodeficient or humanized mouse. PDX models better simulate the biology of human tumors and are particularly useful for evaluating drug efficacy.

Primary GISTs = a GIST that grows at the anatomical site where tumorigenesis began.

Progressed-free survival = the length of time during and after the therapy in which a patient lives without the disease progression.

SEER stages = classification of tumors in localized, regional, and distant (metastatic): "**localized**" is used for malignancies that are confined to the organ of origin; "**regional**" for tumors that are spread to adjacent tissues instead; "**distant**" (metastatic) for tumors that colonize a tissue located in an area not physically in contact with the organ of origin.

Size-exclusion chromatography (SER) = This technique separates molecules based on size through gel filtration. The gel consists of spherical beads containing pores of a specific size distribution. Separation occurs when molecules of different sizes are included or excluded from the pores within the matrix.

Soft tissue sarcoma = cancer that begins in the muscle, fat, fibrous tissue, blood vessels, or other supporting tissues.

Sporadic GIST = a non-inherited GIST that is commonly diagnosed after age 50. Sporadic GIST harbors somatic mutations, which only affect the tumor tissue.

Stable disease = Stable disease is defined as fitting the criteria neither for progressive disease nor a partial response.

Syngeneic mouse models = Syngeneic mouse models are tumors derived from murine cancer cells engrafted on genetically identical mouse strains.

Thin-layer chromatography (TLC) = TLC is a chromatographic technique useful for separating organic compounds. It consists of a stationary phase immobilized on a glass or plastic plate and an organic solvent. The liquid sample is then deposited as a spot on the stationary phase. The bottom edge of the plate is placed in a solvent reservoir, and the solvent moves up the plate by capillary action. When the solvent front reaches the other edge of the stationary phase, the plate is removed from the solvent reservoir. The different compounds in the mixture move up the plate at different rates due to differences in their portioning behavior between the mobile liquid phase and the stationary phase. The visualization of the compound movement, for example, with a UV light, constitutes the TLC profile of that mixture.

TNM classification = classification based on tumor size and invasion of surrounding tissues (T1-T4), the distance of the involved lymph nodes (N1-N3), and the presence or absence of metastases (M0-M1) (Amin et al., 2017).

TP53 gene = a tumor suppressor gene that encodes for p53. p53 plays a crucial role in the regulation or progression of the cell cycle. p53 is mutated in over 50% of human cancers (Ozaki & Nakagawara, 2011).

Xenogeneic tumor model = model in which a tumor from an individual of one species is transplanted into or grafted onto an organism of another species.

1. INTRODUCTION

1.1. Gastrointestinal stromal tumors

1.1.1. General clinical background

Gastrointestinal stromal tumors (GISTs) are soft tissue sarcomas[d] typically found in the gastrointestinal (GI) tract, especially in the stomach (about 55% of cases) or in the small intestine (30%) (Corless et al., 2011). The colorectum, the esophagus, and the appendix are rarely affected (<8%) (Figure 1). Certain GISTs originate outside the GI tract in the omentum or the mesentery and are referred to as extra-GISTs (EGISTs) for this reason (<10%) (Sawaki, 2017).
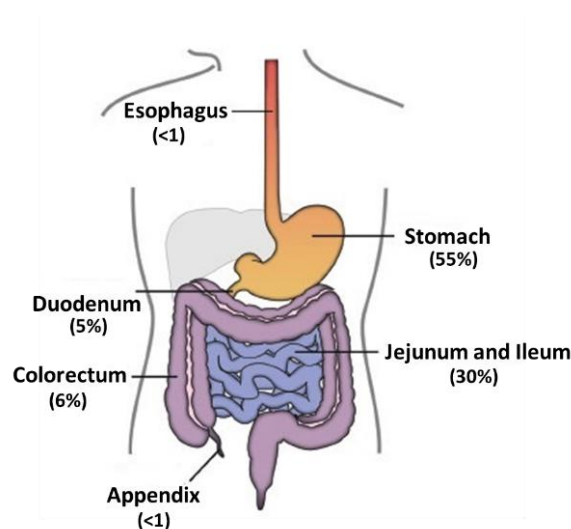
Figure 1. The relative frequencies of GISTs in GI tissues (Foo et al., 2012).

The median age at diagnosis is about 60 years old. Numerous findings indicate that they are mainly caused by oncogenic mutations that individuals acquire during their lifetimes. Hence, age represents the first risk factor for developing sporadic GISTs[d]. Nevertheless, familial GIST[d] cases are observed before age 50 due to the inheritance of germline mutations, which promote an early disease onset (Postow & Robson, 2012). Even if they are the most common mesenchymal neoplasms of the GI apparatus, GISTs are classified as rare tumors given the annual incidence of 10-15 per million (Søreide et al., 2016). Despite this, an increasing frequency of localized[d] GISTs has been recently reported in countries like the Netherlands and the USA, but the absence of an equal increase in metastatic GISTs suggests that these observations could be primarily linked to the improvement of the diagnostic tools (N. Patel & Benipal, 2019; Sepe et al., 2009; van der Graaf et al., 2018). Regarding

epidemiology, differences have been observed between geographic areas and ethnic groups (Søreide et al., 2016). For example, significant differences were even highlighted between different regions of China, suggesting that genetics and the environment could be additional risk factors. No differences have been observed between genders.

1.1.2. History of GIST classification and biomarkers

The classification of GISTs is relatively recent. GISTs were long misclassified and considered to originate from progenitors of smooth muscle cells, such as gastrointestinal leiomyomas, leiomyoblastomas, and leiomyosarcomas, or to be tumors of neural crest, such as schwannomas or nerve sheath tumors. The first mention of GISTs as a specific class of sarcoma is dated 1983, when Michael T. Mazur and H. Brent Clark reported a brilliant reappraisal of twenty-eight tumors initially classified as gastric leiomyomas or leiomyosarcomas, starting to raise doubts about the histogenesis of certain of them (Mazur & Clark, 1983). In detail, despite an analogous viewing with light microscopy, nine tumors didn't recapitulate the canonical features of smooth or Schwann cells in terms of ultrastructure and immunohistochemical. Corroboration of these doubts was published soon after, revealing a remarkable distance between GISTs and smooth muscle-related tumors (Schaldenbrand & Appelman, 1984). Indeed, GISTs don't express any muscle differentiation marker, showing frequent positive staining to CD34 (Miettinen et al., 1995; van de Rijn et al., 1994). A few years later, the cellular origin and molecular etiology of GISTs became incontrovertible (Hirota, 1998). Among a panel of fifty-eight GI cancers, nine were classified as authentic leiomyomas or schwannomas, while the remaining forty-nine were diagnosed as GISTs. Among GISTs, 94% expressed KIT (CD-117), a tyrosine kinase receptor (TKR) encoded by the c-kit gene. The percentage of KIT positivity was even higher than CD34, which was instead expressed in 87% of cases. Noteworthy, non-GIST tumors were consistently KIT negative, indicating that the expression of KIT could be a selective and main hallmark of GISTs. The authors then compared the immunohistochemistry of KIT-positive tumors to that of Interstitial cells of Cajal (ICCs), a crucial member of the GI neuromuscular apparatus that contributes to the regulation of motility by acting as pacemakers, neuromuscular mediators, and mechanoreceptors (Sanders et al., 2006). Hirota and colleagues reported an analogous co-expression of KIT and CD34 in GISTs and ICCs, supporting the concept that ICCs could arguably represent the progenitor of GISTs. Despite fewer citations, another study published a few months later similarly concludes that GISTs may originate from the oncogenic version of the stem cells, which are commonly involved in the differentiation toward ICCs, even

coining an alternative name for GISTs, such as Gastrointestinal pacemaker cell tumors (GIPACTs) (Kindblom et al., 1998).

Regarding the etiology, the sequencing of the c-kit gene in GIST specimens highlighted mutations in the exons that encode for the juxtamembrane domain of KIT (Hirota, 1998). These mutations determine the constitutive phosphorylation of KIT in cellular models, independently from the binding of Stem Cell Factor (SCF), the KIT ligand. The stable expression of a mutated version of KIT in cellular models was sufficient to promote tumor growth in mice, thus displaying an oncogenic role. The unveiled role of KIT as a disease driver marked the beginning of a new era in the GIST clinics.

More recently, a novel biomarker, DOG1, has been included in the antigen palette for the diagnosis of GIST, allowing a further improvement of the capability to differentiate GISTs from other mesenchymal GI cancers (Miettinen et al., 2009; West et al., 2004). Immunostaining of 139 GISTs showed that 136 (97.8%) expressed DOG1, even in KIT negativity. Only 0.01% of the non-GIST tumors were immunoreactive for DOG1, indicating a high selectivity of the DOG1-based staining in GISTs. An example of KIT and DOG1 co-staining in GIST and leiomyosarcoma (LMS) is shown in Figure 3A. Noteworthy, ICCs can be successfully stained with anti-DOG1 antibodies, confirming the close homology with GISTs. The current workflow for classifying and diagnosing GIST includes KIT, DOG-1, and, if necessary, CD34 as biomarkers (Figure 3B). Desmin and S-100 antigens are instead evaluated as markers of myogenic or neurogenic tumors, respectively (Nishida et al., 2016).
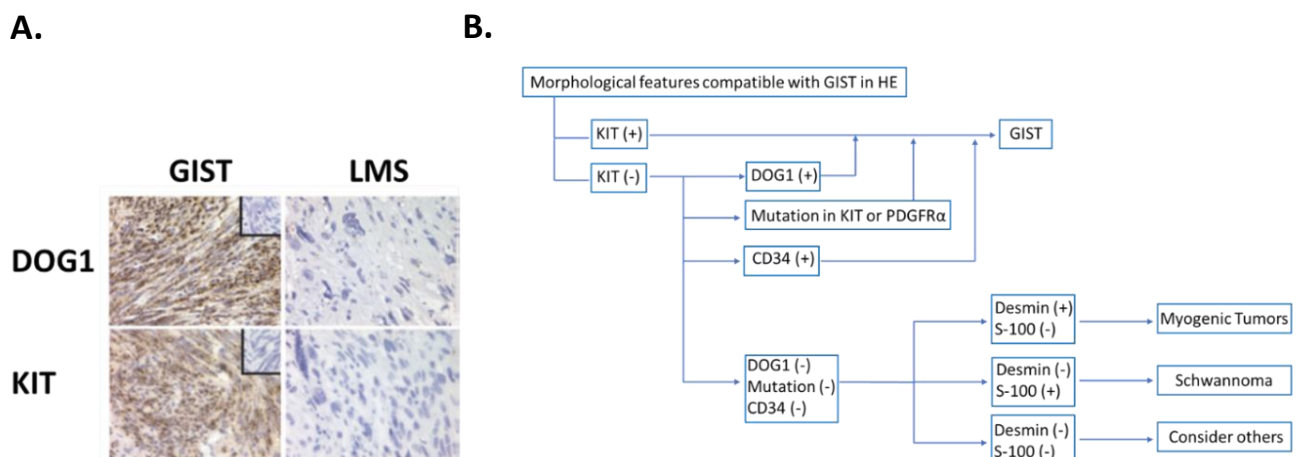
Figure 2. A. *In situ* hybridization of GIST or LMS samples with antisense probes to *DOG1* and *KIT*. The corresponding negative control probes are included in the top right corner of the GIST sample (West et al., 2004). **B.** Workflow for the diagnosis of GISTs by immunohistochemistry and genotyping. HE means hematoxylin–eosin staining (Nishida et al., 2016).

1.1.3. Oncogenic mutations in primary GISTs

According to the findings from Hirota and co-authors, most of the primary GISTs[(d)] (70-80% of cases) harbor a gain of function mutation[(d)] in c-kit (Niinuma et al., 2018). In addition, although rare, GISTs can also be driven by a gain of function mutation in PDGFRA (5-8%), a gene that encodes for the platelet-derived growth factor receptor (PDGFRα), a further TKR. KIT or PDGFRα mutants are commonly defined as "mutually exclusive", which means that no primary GISTs have been diagnosed with a gain of function mutations on both TKRs simultaneously, and the single presence is sufficient for tumorigenesis (Lasota & Miettinen, 2006). KIT and PDGFRα belong to the type III receptor tyrosine kinase family and are physiologically inactive in their monomeric forms (Hanks et al., 1988). The binding of SCF or the platelet-derived growth factor (PDGFα), the corresponding dimeric ligands, triggers the receptor homodimerization, the auto-transphosphorylation of specific tyrosine residues in an intracellular receptor region, and the signal transduction (Fretto et al., 1993; Lev et al., 1992). As shown in Figure 3, Gain of function mutations explicate their oncogenic properties through the constitutive receptor function via a ligand-independent mechanism which promotes the aberrant stimulation of PI3K/AKT/mTOR, RAS/MAPK and STAT3 downstream pathways, commonly found activated in GIST extracts (Duensing et al., 2004; Rubin et al., 2001). C-kit and PDGFRA are not randomly mutated, but in-frame deletions, insertions, substitutions, or combinations of these latter selectively hit gene regions crucial in receptor activation and regulation. Hence, KIT is typically mutated in the extracellular domain (exon 8 and 9), in the juxtamembrane domain (exon 11), in the ATP-binding domain (exon 13), and the activation loop of the tyrosine kinase domain (exon 17).
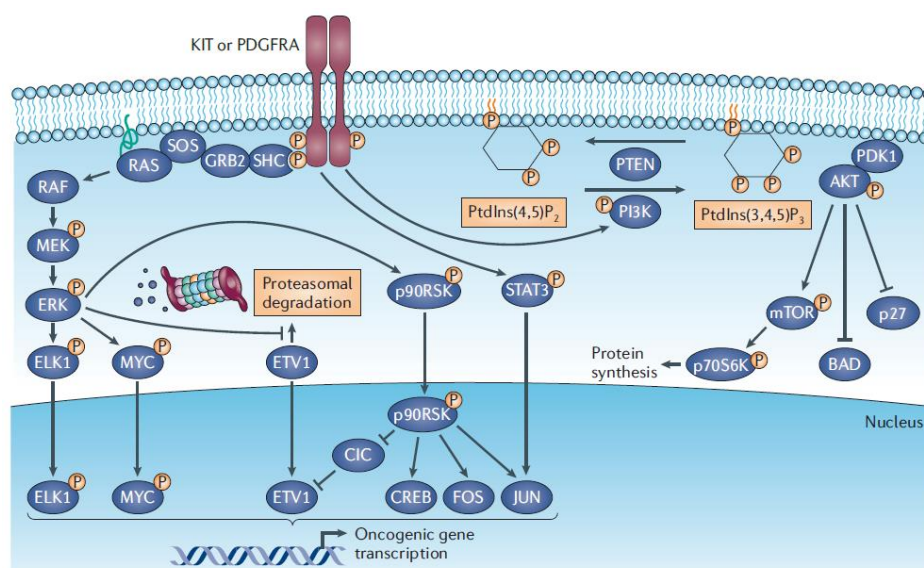
Figure 3. Oncogenic signaling in KIT or PDGFRα mutated GISTs (Corless et al., 2011).

Approximately 70% of all GIST cases harbor a mutation in exon 11, which compromises the regulatory function of the juxtamembrane domain, known for its role in the prevention of the swinging between the inactive and active conformation of the activation loop (Mol et al., 2004). Exon 11 mutations frequently affect 557 to 559 in series codons, which represent a hot spot mutation site. The importance of the juxtamembrane domain is also confirmed by rare mutations observed in intron 10. The Deletion of 3-8bp in the junction sequence with the exon 11 affects the splicing, leading to in-frame deletions in the produced mRNA and, consequently, in the juxtamembrane domain (Wozniak et al., 2012). Instead, exon 9, exon 13, and exon 17 mutations are less common (about 10% of all cases) (Lasota et al., 2008). PDGFRα is structurally homologous to KIT and shows a similar tumorigenic function in the case of gain of function mutations. Therefore, PDGFRA can be analogously mutated in the juxtamembrane domain (exon 12), in the ATP-binding domain (exon 14), or in the activation loop (exon 18) (Hirota et al., 2003). The substitution at position 842 in the activation loop of an aspartic acid (D) with a valine (D842V) is the most frequent, being detected in about 5% of GIST patients and representing about 60-65% of all PDGFRα mutations (Rizzo et al., 2021). Although the panel of observed mutations in KIT or PDGFR mutations are similarly tumorigenic, they could be associated with different prognoses and clinical outcomes. For example, larger tumor size, high mitotic rate, high-risk factor, and poor disease-free survival has been reported in the case of mutations in the 557 and 558 KIT codons compared to the other mutation in the exon 11 (Wozniak et al., 2014). Mutations also seem to correlate with the tumor location. Exon 9 mutations in KIT are observed in the small intestine and colon, while D842V mutation in PDGFRα mainly in the stomach, omentum, and mesentery (Antonescu et al., 2004). KIT and PDGFRα mutations are analogously observed in middle-aged individuals with familial GIST syndrome (Chompret et al., 2004; Hirota et al., 2002). Tumors without alterations in c-kit or PDGFRA genes (10-15%) are classified as KIT/PDGFRα wild type (WT) GISTs (Wada et al., 2016). WT GISTs are primarily associated with mutations promoting Succinate dehydrogenase deficiency (SDH). The loss of SDH leads to the accumulation of succinate, which supports the stabilization of HIF1-α and, consequently, a remarkable change in gene expression (Gill, 2012). SDH-deficient WT GISTs are commonly characterized by overexpression of the Insulin-like growth factor 1 receptor (IGF1R), which, analogously to KIT and PDGFRα, aberrantly boosts MAPK and PI3K/AKT downstream signals (Brahmkhatri et al., 2015; Chou et al., 2012). Alterations in RAS family genes and BRAF have also been detected in WT GISTs (Miranda et al., 2012). A summary of mutations observed in sporadic GISTs is shown in Table 1.

KIT mutations (70-80%)	PDGFRα mutations (5-8%)	KIT/PDGFRα WT (10-15%)
• Exon 11 (70%)	• Exon 18 D842V (5%)	• SDH (8%)
• Exon 9 (5-10%)	• Exon 18 non D842V (3%)	• RAS (<1%)
• Exon 13 (<1%)	• Exon 12 (<1%)	• BRAF (<1%)
• Exon 17 (<1%)	• Exon 14 (<1%)	• others (<1%)

Table 1. Genetic profile of sporadic GISTs. Summary of the mutation frequency.

1.2.   GIST therapy

1.2.1. Surgery and resistance to traditional chemotherapy

Surgery has been the mainstay of GIST clinical management and represented the unique treatment available before the approval of imatinib (Dematteo et al., 2002). Patients who underwent a successful tumor resection had a median overall survival[d] (OS) of 66 months, while individuals with an unresectable or metastatic GIST of about 22 (DeMatteo et al., 2000). Primary GISTs hang from the tissue of origin, usually allowing a resection with negative margins. However, tumor rupture and intraperitoneal dissemination are the main risks of the procedure due to the soft and fragile structure of the tumor mass, frequently leading to tumor recurrence (about 40%). Therefore, the lack of adjuvant therapy, as well as neo-adjuvant, significantly impaired patient prognosis. The interpretation of clinical trials in GISTs is not straightforward due to the common misclassification before the 2000s and because few trials differentiated GISTs from other mesenchymal sarcomas in the GI. Nevertheless, if metastatic cancers originally related to LMSs in the gastrointestinal tissue were instead of GISTs, the partial response (PR) to traditional chemotherapies can be estimated. As shown in Figure 4, the estimated PR to therapeutic regimens is generally low (<10%). The lack of responsiveness to traditional chemotherapy was confirmed in one of the few trials that accurately differentiates GISTs and LMSs. A combination therapy based on dacarbazine, mitomycin C, doxorubicin, cisplatin, and growth factors as support, promoted a PR of 4% and 67% in patients with GIST or LMS, respectively, corroborating the resistance of GISTs to traditional chemotherapy (Edmonson et al., 2002). The higher levels of P-glycoprotein and multidrug resistance protein in GISTs with respect to LMSs could contribute to the observed results (Plaat et al., 2000). Hence, none of the traditional chemotherapeutics have been approved for GIST therapy. Analogously to chemotherapy, studies have displayed that GISTs are commonly resistant to radiotherapy, preventing its clinical use nowadays (Gatto et al., 2017). Nevertheless, certain clinical cases suggest that it could

provide an objective response, long-term control of the disease, and not remarkable toxicity. Further studies are required to extend this insight in a larger patient cohort, defining clinical setting, dosage, and combination with imatinib.

TABLE 1. Response Rates to Chemotherapy in Patients With Metastatic GIST

Regimen	Partial Response		Reference
	n	n (%)	
DOX + DTIC	43	3 (7%)	56
DOX + DTIC +/− IF	60	10 (15%)	57
DOX + DTIC+ IF	11	3 (27%)	58
IF + VP-16	10	0 (0%)	59
Paclitaxel	15	1 (7%)	60
Gemcitabine	17	0 (0%)	61
Liposomal DOX	15	0 (0%)	62
DOX	12	0 (0%)	62
DOX or docetaxel	9	0 (0%)	63
High-dose IF	26	NR (0–8%)	64
EPI + IF	13	0 (0%)	61,65
Various (e.g., DOX, gemcitabine, CT2584)	40	4 (10%)	21
DTIC + MMC + DOX + CDDP + GM−CSF	21	1 (5%)	20
TOTAL	266	22 (8.3%)	

Abbreviations: DOX, doxorubin; DTIC, dacarbazine; IF, ifosfamide; CDDP, cisplatin; VP16, etoposide; EPI, epirubicin; NR, not reported.

Figure 4. Partial response to traditional chemotherapy in patients with a metastatic GIST (Dematteo et al., 2002).

1.2.2. Targeted therapy with imatinib

Imatinib, known by the brand name Gleevec®, is a tyrosine kinase inhibitor (TKI) developed to target BCR-ABL1 in chronic myelogenous leukemia (Rossari et al., 2018). The kinase domains of KIT and PDGFRα show homology with ABL1 and were successfully inhibited by imatinib in GIST preclinical models (Heinrich et al., 2000; Tuveson et al., 2001). The first encouraging clinical response was observed in a patient with a metastatic GIST, a middle-aged Finnish woman who received imatinib daily. Magnetic resonance imaging (MRI) and positron-emission tomography (PET) revealed a remarkable metabolic response of the tumor with rare or mild side effects, paving the way for further validations (Joensuu et al., 2001). 946 patients with an unresectable or metastatic KIT-positive GIST were included in the III phase trial EORTC 62005, and progression-free survival (PFS) was assessed as the primary endpoint (Verweij et al., 2004). The study divided patients into two groups that received 400 or 800mg of imatinib daily. At the median follow-up (25 months), 44% of the first group and 50% of the second didn't show progression. Despite the significant difference between the two groups, a subsequent study did not confirm better efficiency of the high dose,

leading to the statement that 400mg could be the standard (Blanke et al., 2008). The response rates were similar between the two groups, promoting complete response (CR) in 5% of patients, PR in 47%, and stable disease (SD) in 32%. The OS was around 57 months, a remarkable increase with respect to the historical control represented by doxorubicin (Figure 5).
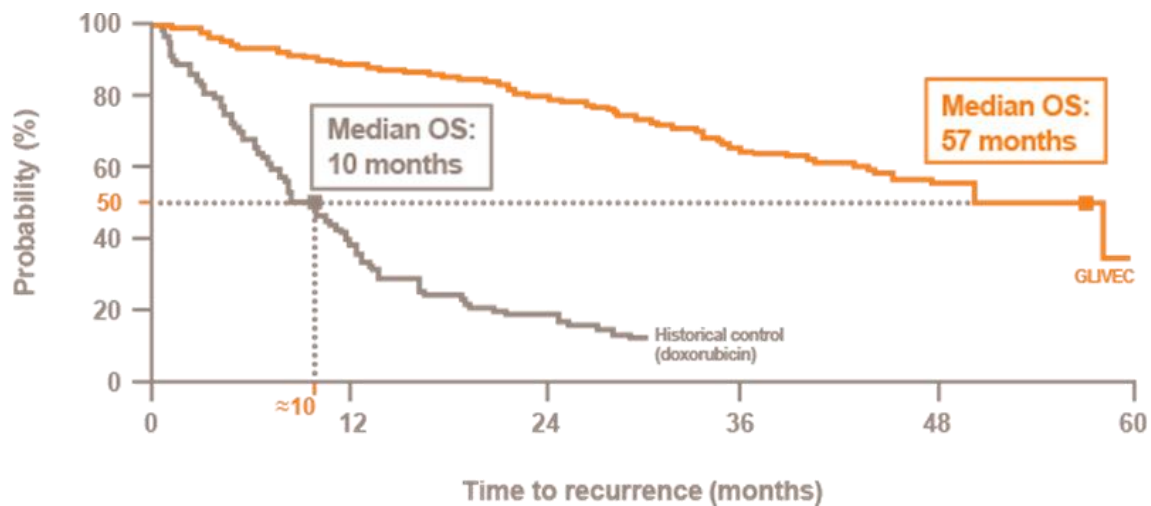
Figure 5. The OS in patients with advanced or metastatic GISTs who received imatinib (Glivec) or doxorubicin. Data from EORTC 62005 compared with historical controls from the European Organization for Research and Treatment of Cancer (EORTC) database (Verweij et al., 2004).

Interestingly, the mutation status of KIT influences the responsiveness to imatinib. Patients with exon 9 mutations can achieve a similar prognosis with those that harbor exon 11 mutations only if they receive a higher dosage (800mg vs. 400mg), indicating that KIT mutants could show different sensitivity to imatinib (Gastrointestinal Stromal Tumor Meta-Analysis Group (MetaGIST), 2010). In addition, adjuvant therapy significantly reduced the risk of recurrence in patients after the resection of a primary GIST (Blanke et al., 2008). Only 8% of patients continuously treated with imatinib for one year had tumor recurrence or died; this percentage increased to 20% in the placebo group. Subsequently, it was demonstrated that a 3-year treatment could even better control the recurrence of an intermediate or high-risk GIST, thus being recommended in patients who underwent resection (Raut et al., 2018; Reichardt et al., 2012). Few recurrent cases were reported in patients who respected the 3-year compliance and decided not to discontinue the treatment. On the contrary, the disease frequently recurs in patients in case of imatinib discontinuation. Recently, the 5-year treatment compared to the 3-year has been even associated with better prognosis in patients where a primary tumor was resected with a rupture (Kang et al., 2022). Moreover, imatinib is also efficient as a neo-adjuvant therapy (Hohenberger et al., 2012). Pre-surgery treatment (about 6-12 months) can be helpful to reduce the tumor mass, allowing the resection of not-operable GISTs or promoting

operations less mutilating. This strategy is often practiced in GISTs located in the gastroesophageal junction, the duodenum, or the rectum. Overall, imatinib has represented the magic bullet for GIST clinical management, improving the life expectancy of patients with unresectable or metastatic GISTs, promoting a decrease in the size of unresectable tumors and consequential their resection, and reducing the risk of recurrence (Balachandran & DeMatteo, 2014; Strebhardt & Ullrich, 2008).

1.2.3. Primary resistance to imatinib and avapritinib approval

The first challenge in the management of patients with unresectable or metastatic GISTs is the lack of responsiveness to imatinib. Indeed, disease progression has been commonly observed in a subset of patients (about 20%) since the beginning of therapy. This resistance is classified as primary and is observed in the case of WT GISTs or due to the presence of specific resistant KIT or PDGFRα mutants. WT GISTs belong to a heterogeneous tumor subclass without a common deregulated target. For this reason, no efficient molecular targeted therapy has been established so far (Kays et al., 2018). Regarding the resistant mutants, avapritinib, a novel TKI, was developed to selectively target these mutations, including the most frequent D842V in PDGFRα (Evans et al., 2017). In the NAVIGATOR phase I trial, patients with primary resistance, characterized by D842V or further exon 18 mutations in PDGFRA, were treated with avapritinib (Heinrich et al., 2020). The overall response rate (ORR) was 87%, with CR in 9% of patients and PR in 78%, while the toxicity was manageable. The promising results promoted the approval of avapritinib (AYVAKIT®) as an alternative first-line treatment in case of unresectable or metastatic GISTs which are resistant to imatinib due to the presence of PDGFRA exon 18 mutations, including the D842V (Dhillon, 2020a). The mPFS provided by avapritinib is about 29 months, which is in line with what was observed in patients with imatinib-sensitive GISTs (about 20 months).

1.2.4. Adaptive and survival processes

As previously indicated, imatinib only promotes CR in 5% of cases, while most patients display a partial reduction of the tumor mass followed by stable disease. However, this stationary condition is not permanent but is strictly dependent on the continuous administration of imatinib. Indeed, its withdrawal leads to the rapid conversion of stable disease into progressive disease, suggesting that stabilized tumor mass, despite being successfully targeted, survives and enters a temporary resting state (Blay et al., 2007). Preclinical studies have demonstrated that sensitive GIST cells can counteract the mechanism of action of imatinib, evading apoptosis through adaptive and survival processes, such as quiescence and autophagy. Garcia-Valverde and colleagues reported Atrogin-1

overexpression because of imatinib treatment, independently from the mutation status of KIT (García-Valverde et al., 2021). The expression of Atrogin-1 is finely regulated by KIT downstream pathways, which prevent the translocation in the nucleus of the transcription factor FOXO3a. On the contrary, the inhibition of KIT determines FOXO3a dephosphorylation, its migration in the nucleus, and consequent transcription of Atrogin-1 mRNAs. Authors unveiled that the overexpression of Atrogin-1 is associated with stimulation of cell quiescence and less apoptosis susceptibility, as testified by reduction of caspase-3 and PARP-1 cleavage. This study corroborates earlier findings in which quiescence was already observed in response to imatinib in sensitive GIST-882 cells via the cyclin-dependent kinase (CDK) regulator p27^{Kip1} and the DREAM multiprotein complex (Boichuk et al., 2013; Y. Liu et al., 2008). Quiescence is not the only adaptive mechanism but is part of a complex and intertwined system in which autophagy can also be involved (Ravegnini et al., 2017). Gupta and co-workers observed autophagy markers after imatinib treatment in quiescent imatinib-sensitive GIST-T1, suggesting that autophagy could promote the recycling of inhibited KIT receptors to replace them with the new translated (Gupta et al., 2010). According to these insights, the downregulation of microRNA 30a (miR30a) was observed in GIST-882 and GIST-T1 due to imatinib treatment (Chen et al., 2020). Its downregulation contributes to autophagy stimulation, leading to the upregulation of Beclin-1, a crucial autophagy player and a target of miR-30a. A similar autophagy stimulation has also been reported via HOTAIR recently, a long noncoding RNA (lncRNA) that is overexpressed in response to imatinib in GIST-882 and GIST-T1 (Zhang et al., 2021). Notably, the simultaneous targeting of quiescence or autophagy in association with imatinib increases the percentage of apoptotic cells, corroborating that both quiescence and autophagy activation can significantly contribute to mitigating the effect of imatinib in GISTs. Moreover, the transient nature of both phenomena explains why patients require continuous therapy to prevent disease progression; indeed, GIST cells in these adaptive states can quickly modify their metabolism and newly enter the cell cycle.

1.2.5. Secondary resistance to imatinib

Secondary resistance, also named "acquired resistance", occurs in patients after an initial and successful response to the therapy (Hamid & Petreaca, 2020). Figure 6 quickly summarizes what likely takes place in the case of an imatinib-sensitive GIST. As described in the previous paragraph, continuous treatment with imatinib leads to progression-free survival, a clinical state in which good management of patient life is guaranteed. Nevertheless, even if the tumor mass is not growing, the clonal composition of the tumor changes. While sensitive subclones are directed toward apoptosis

or survive to imatinib via adaptive and survival processes, a small subclone population, arguably present from the beginning of the therapy, continues to proliferate, gradually becoming a significant part of the tumor mass. At that moment, typically observed within 24 months, the growth of resistant subclones becomes predominant and promotes disease progression.
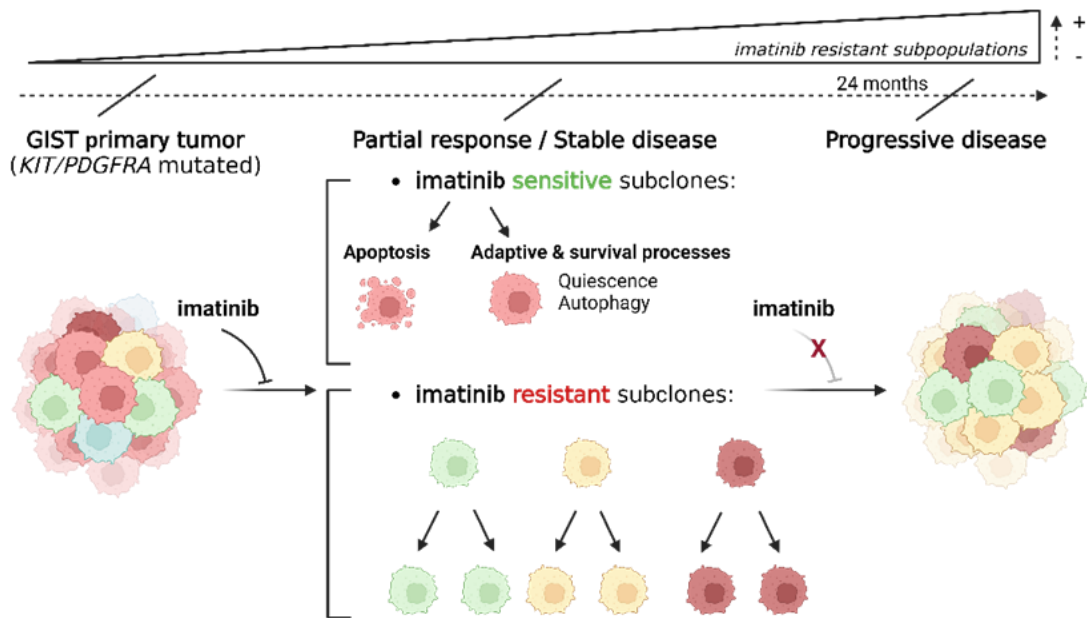
Figure 6. The frequent clinical scenario in the case of imatinib-sensitive GISTs. Imatinib mostly leads to a partial reduction of tumor mass via apoptosis induction. Then, control of tumor growth is observed (stable disease). This is mainly caused by the capacity of GIST cells to counteract imatinib through adaptive and survival processes, such as quiescence and autophagy. During the treatment, certain imatinib-resistant subclones, probably present in the tumor mass since the beginning of the therapy, can continue to proliferate. This small tumoral subpopulation gradually becomes remarkable and able to sustain progressive disease within 24 months. Created with BioRender.com.

Considering the crucial role in tumorigenesis, c-kit was deeply analyzed in patients who showed secondary resistance to imatinib. In addition to the first in exon 11 or 9 commonly reported in primary GISTs, a further mutation was detected in specimens of 7 out of 15 patients who underwent resection (Antonescu et al., 2005). For this reason, these mutations, never detected in nonresistant patients, were classified as secondary. They were primarily identified in exon 17, leading to an aminoacidic substitution in the activation loop, such as D820Y, Y823D, and N822K. Instead, V654A and T670I substitutions, induced by mutations in exon 13 or exon 14, were identified in the ATP-binding domain less frequently. In confirmation of this, a further study also reported the presence of c-kit secondary mutations in about 70% of the specimens of imatinib-resistant GISTs (Nishida et al., 2008). In some patients, more than one secondary mutation in the same exon or two or three was observed (Wardelmann et al., 2006). Consistent with the clonal evolution theory, a primary mutation was consistently detectable in the same allele of the secondary mutation in each tumor

sample. Noteworthy, multiple secondary mutations were identified in different lesions collected from the same patient, indicating that resistant subclones could independently originate and co-exist in GISTs (Wardelmann et al., 2006).

1.2.6. The approval of multi-target TKIs: sunitinib and regorafenib

Testing of imatinib in cell lines that harbor primary or a combination of primary and secondary mutations confirmed their correlation with the resistance (Serrano et al., 2019). As testified by the IC_{50} in the µM range, imatinib loses the capacity to recognize KIT once it acquires a secondary mutation (table 2). Indeed, on the contrary, imatinib efficiently targets cells with only primary mutations (GIST-T1, GIST-882, and GIST-430) at a low nM range. Therefore, numerous research projects were focused on developing a novel TKI to target imatinib-resistant KIT mutants successfully.

GIST cell line	KIT mutation	Imatinib (1st line)	Sunitinib (2nd line)	Regorafenib (3rd line)
GIST-T1	Ex. 11	4.5	5	35
GIST-430	Ex. 11	35	10	150
GIST-882	Ex. 13	300	70	800
GIST-430/654	Ex. 11 + Ex. 13 (V654A)	2500	45	2000
GIST-T1/670	Ex.11 + Ex. 14 (T670I)	> 10000	30	60
GIST-T1/816	Ex.11 + Ex. 17 (D816E)	1500	> 10000	550
GIST-T1/820	Ex. 11 + Ex. 17 (D820A)	1500	> 10000	600
GIST-T1/829	Ex. 11 + Ex. 19 (D829P)	3000	10000	2500
GIST-48b	KIT independent	>10000	> 10000	> 10000
GIST-226	KIT independent	>10000	> 10000	> 10000

Table 2. IC_{50} (nM) of imatinib, sunitinib, and regorafenib and in GIST cell lines harboring a different combination of primary and secondary mutations. The table is adapted starting from Table 1 in the publication of Serrano et al., 2019.

Sunitinib (Sutent®) was the first multi-target TKI that displayed the capability to recognize KIT in case of V654A or T670I substitutions in the ATP-binding domain (GIST-430/654 and GIST-T1/760), receiving the approval of FDA in 2006 as second-line treatment in case of resistance or intolerance to imatinib. Sunitinib newly promoted SD in 40-50% of patients with good tolerability (Demetri et al., 2006; George et al., 2009). However, the ORR was only about 6%, while the mPFS was 6-8 months. Differently to imatinib and sunitinib, Regorafenib, a further multi-target TKI, despite a mild pharmacological potency (IC_{50} about 500-600 nM), successfully recognizes D816E and D820A

substitutions in the activation loop (Table 2). Nevertheless, regorafenib is a weaker inhibitor of certain primary exon 13 mutations (IC$_{50}$ about 800 nM) and does not show efficacy against the V654A substitution in the ATP binding domain. Overall, sunitinib and regorafenib show a complementary activity, targeting mutations in the ATP binding domain or the activation loop, respectively (Figure 7). These preclinical findings suggested that regorafenib could be useful to counteract subclones not previously targeted by imatinib and sunitinib. In the third phase clinical trial GRID, Regorafenib was administered to patients who showed disease progression after imatinib and sunitinib treatment (Demetri et al., 2013). Regorafenib newly provided SD in 60-70% of patients with a median PFS of 4.8 months, significantly longer than 0.9 months observed in the placebo group. In line with sunitinib, the ORR was low (4.5%). The FDA approved Regorafenib (Stivarga®) as the third-line treatment for patients with failure of imatinib and sunitinib in 2012.

KIT mutated clones

	Primary mutations (exon 11 or exon 9)	Primary mutations + secondary mutations in exon 13 or 14 (ATP binding pocket)	Primary mutations + secondary mutations in exon 17 or 18 (activation loop)
GIST cells			
IMATINIB	Sensitive	Resistant	Resistant
SUNITINIB	Sensitive	Sensitive	Resistant
REGORAFENIB	Sensitive	Resistant	Sensitive
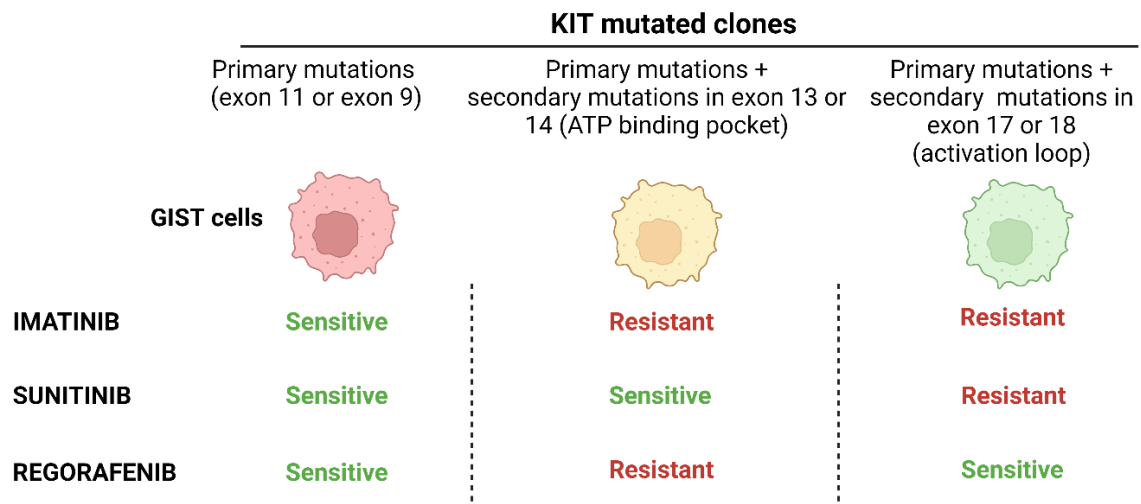
Figure 7. Recognition of GIST cells that harbor primary mutations (commonly in the exon 11 or 9) or secondary in addition to primary mutations. Imatinib successfully targets cells with primary mutations but does not recognize subclones with secondary mutations in the ATP binding pocket (exons 13 and 14) or the activation loop (exons 17 and 18). Differently, sunitinib selectively recognizes cells with mutations in exons 13 and 14, while regorafenib is efficient against that with mutations in exons 17 and 18. The color of the subclones (GIST cells) is intentionally maintained in agreement with that shown in Figure 6, which means the selection of resistant subclones with an additional secondary mutation in KIT. Created with BioRender.com.

1.2.7. Ripretinib, an unexpected failure

Despite an improvement in the outcome, sunitinib and regorafenib have modestly improved patients' perspectives, mainly providing a further but short control of the disease. Table 2 shows sunitinib and regorafenib do not recognize the entire panel of KIT mutants associated with imatinib resistance and disease progression (Serrano et al., 2019) (Figure 7). Therefore, it was proposed that their modest efficacy could depend on this targeting weakness and the consequent proliferation of

untargeted resistant subclones. Ripretinib was developed as PAN KIT-PDGFRα inhibitor and considered the long-awaited step forward thanks to the broader recognition of KIT and PDGFRα mutants with respect to the already approved TKIs (Lostes-Bardaji et al., 2021; Smith et al., 2019). In detail, while imatinib, sunitinib, and regorafenib display targeting weaknesses towards such mutants or mutant families, ripretinib similarly and potently impairs cells with KIT primary mutations, as well as those that additionally harbor a secondary mutation in the ATP binding domain or the activation loop (50 nM<IC_{50}<200 nM). These promising preclinical data supported the evaluation of ripretinib in patients with an unresectable or metastatic GIST that was resistant or intolerant to the previous treatment lines (Blay et al., 2020). Ripretinib met the first endpoint in the third phase trial INVICTUS, significantly improving the mPFS compared with placebo from 1.0 to 6.3 months and exhibiting a well-tolerated imatinib-like toxicity profile. About 10% of patients showed PR, while most displayed SD. Based on this data, the FDA approved ripretinib (Qinlock®) as the fourth line in 2020 for treating GISTs already treated and resistant to the other approved TKIs (Dhillon, 2020b). In addition, recognizing more imatinib-resistant subclones compared to sunitinib, ripretinib was also evaluated in the INTRIGUE trial as an alternative second-line treatment instead of sunitinib (Bauer et al., 2022). However, ripretinib has not recently met the primary endpoint, being not superior to sunitinib in terms of PFS. However, fewer grade 3/4 adverse effects and better tolerability were worth mentioning. Overall, despite encouraging preclinical properties and the possibility to target subclones that evade the mechanisms of action of imatinib, sunitinib, and regorafenib, ripretinib has not provided the expected outcome improvement. Indeed, as the fourth-line treatment, ripretinib does not provide a longer mPFS than sunitinib and regorafenib. Moreover, the administration of ripretinib as a hypothetical better second-line does not promote an amelioration of prognosis compared to sunitinib. Both clinical results indicate that secondary resistance to imatinib is more than what was initially and exclusively associated with secondary mutations in c-kit or PDGFRA, suggesting a complex and multifaceted landscape behind imatinib resistance.

1.2.8. The multifaceted landscape behind imatinib secondary resistance

Numerous preclinical studies have reported secondary resistance independent from secondary mutations in c-kit or PDGFRA (Di Vito et al., 2023). The PI3K/AKT/mTOR pathway is crucial at KIT or PDGFRα downstream (Bosbach et al., 2017). The substitution of tyrosine 719 with phenylalanine (Y719F) prevents the rise of GISTs in a mouse model with an oncogenic mutation in the juxtamembrane domain of KIT. This tyrosine residue, once phosphorylated, is involved in the

recruiting of PI3K and the activation of downstream pathways. Thus, being decisive in GIST development, the role of PI3K/AKT/mTOR signaling cascade in imatinib resistance has been primarily investigated. PTEN, a well-recognized tumor suppressor that regulates PI3K, is downregulated due to methylation of the promoter in GIST-T1R, a cell line resistant to imatinib and sunitinib (J. Yang et al., 2012). The absence of PTEN promotes the aberrant activation of AKT/mTOR even under imatinib and sunitinib treatment, supporting the concept that alternative dysregulations at KIT or PDGFRα downstream can similarly cause resistance without a direct counteraction of imatinib. Moreover, recent findings have highlighted that alternative kinases can substitute KIT or PDGFRα in resistant cellular models, making the imatinib treatment inefficient. Over-expression of FGFR2α, a TKR that belongs to the FGF receptors (FGFRs) family, was observed in an imatinib-resistant cell line, GIST-T1R, which was isolated from GIST-T1 after a continuous treatment with imatinib (Boichuk et al., 2017). The interesting characteristic of this cell line was the loss of KIT, which FGFR2α functionally replaced. Indeed, the impairment of its activity with BGJ398, an inhibitor of FGFRs, selectively affected the viability of GIST-T1R. At the same time, no effect was reported in the progenitor GIST-T1, corroborating the novel function of FGFR2α instead of KIT. The overexpression of FGFR2α is not an isolated case; additional TKRs have been reported with a compensatory role in case of loss of KIT. Low expression of AXL is commonly observed in KIT-positive and imatinib-sensitive lines. Interestingly, the expression was considerably upregulated in KIT-negative GIST cells such as GIST-54, GIST-62, and GIST-552 (Tu et al., 2018). AXL knockdown remarkably reduced cell viability in these cells, while no effect was observed in KIT-positive and AXL-negative cells, suggesting that AXL could drive disease progression instead of KIT in certain imatinib-resistant GISTs. MET, a further TKR, was upregulated in HG-209 cells, an imatinib-resistant model in which a low level of KIT was detected (Cohen et al., 2015). Interestingly, the opposite expression levels are commonly observed in imatinib-sensitive GIST-882 and GIST-T1. Incubation with HGF, a MET ligand, exclusively stimulates proliferation in HG209, supporting the idea that the oncogenic stimulus may originate from MET in the absence of KIT. Even if the research of alternative oncogenic drivers has mainly focused on TKRs, non-receptor TKs and non-receptor serine/threonine kinases have also been associated with imatinib resistance in GIST. For example, overexpression of Aurora kinase A (AURKA), already identified as a negative prognostic factor, mediates imatinib resistance in GIST-T1 cells (Cheng et al., 2021; Yeh et al., 2014). In addition, dysregulation of miRs has also been identified in resistant GISTs. Lower levels of miR-320 correlate with rapid imatinib resistance in GIST patients (Gao et al., 2014). In line with this finding, an additional miR, miR-218, was downregulated in imatinib-resistance GIST-

430 cells with respect to GIST-882 (Fan et al., 2015). Interestingly, the transfection of a miR-218 mimic promoted the restoration of imatinib resistance in GIST-430. Further mechanisms of imatinib secondary resistance have been highlighted and recently summarized (Hu et al., 2022). Therefore, tumor subclones can activate a plethora of mechanisms to counteract the imatinib mechanism of action. Noteworthy, numerous are independent of secondary mutations in KIT or PDGFRα, being not directly targetable with multi-target TKIs, including the best-in-class ripretinib (Figure 8).
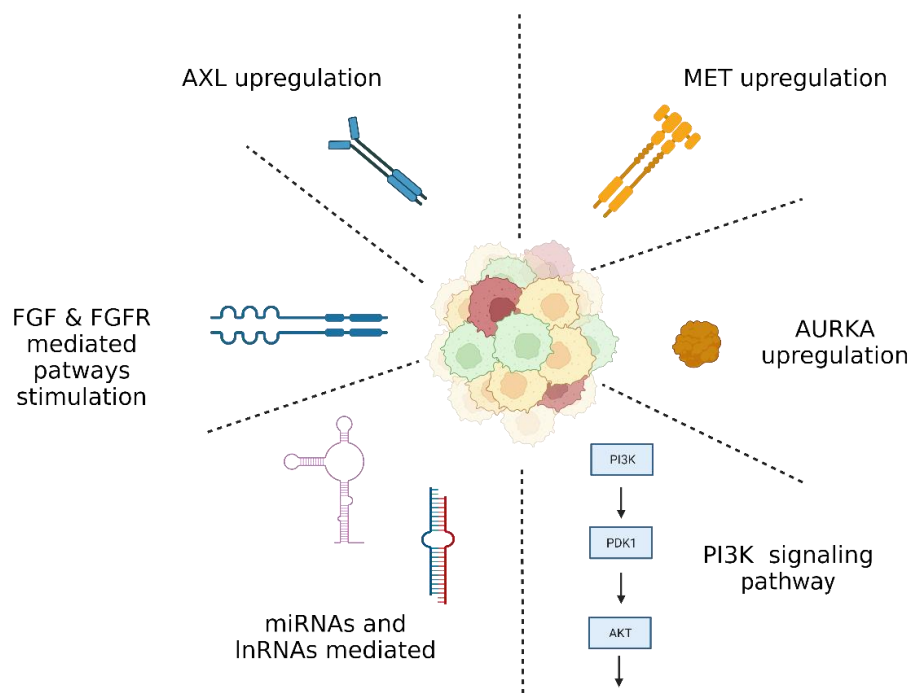
Figure 8. Mechanisms associated with imatinib resistance in preclinical studies. These mechanisms are not targetable with imatinib and other TKIs, including the best-in-class ripretinib. The involvement of these mechanisms could explain the modest effect observed in clinics with multi-target TKIs as additional treatment lines. The same color scheme as Figure 6 is applied. Created with BioRender.com.

1.3.   Metastasis and preclinical models in GISTs

1.3.1. General background

The process through which cancer cells leave the tumor mass and colonize a distant tissue is termed "metastasis". Despite the improvement of early diagnosis and therapy, it has been estimated that metastasis continues to cause about 70% of solid tumor-related deaths (Dillekås et al., 2019). According to the TNM classification[d], the presence of metastases represents the late stage of tumor development since its incidence frequently correlates with the tumor size. Indeed, patients with a T2 stage show a 20% higher risk of developing metastases than those with a T1 (Klein, 2009). Cancer cells could require the accumulation of numerous genetic, epigenetic, and morphological aberrancies before acquiring a metastatic behavior, which may more easily occur after a significant number of proliferation rounds. In confirmation of this, mutations of the tumor suppressor gene TP53[d] are rarely observed in the T1 stage of breast cancers but are common in T3, suggesting that high-size tumors potentially accumulate more mutations, including those that promote metastasis (Olivier et al., 2006). Nevertheless, certain studies support that metastasis could occur in earlier tumor stages, albeit infrequently. Metastasis requires the completion of numerous serial steps, which have led to the definition of the "metastatic cascade": a) detachment of cancer cells from the primary tumor and invasion into surrounding tissue; b) entrance into the blood or lymphatic vessels as circulating tumor cells; c) survival to anoikis[d], as well as to chemical or physical stresses outside the tumor environment and in the circulation; d) extravasation into a distant tissue; e) survival and colonization of the new tissue (Figure 9) (Fares et al., 2020).
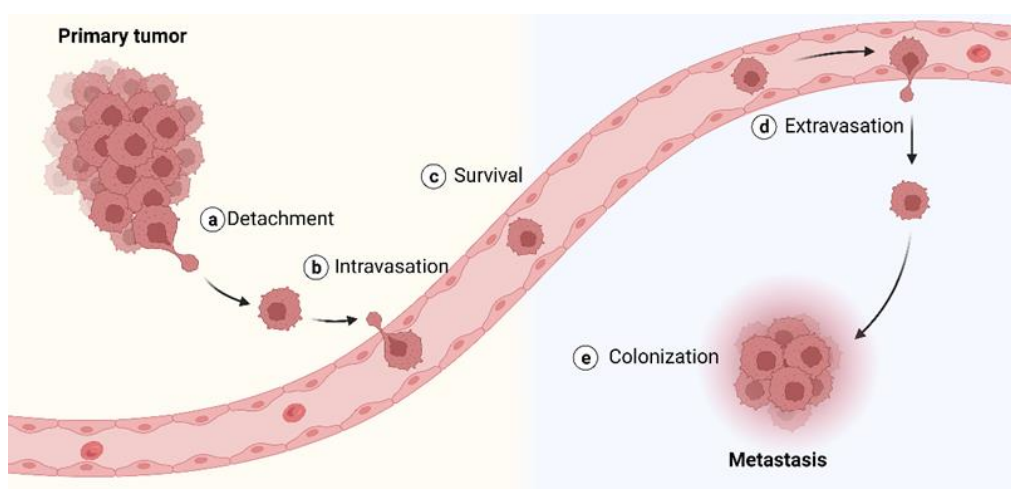
Figure 9. The key steps of metastasis include detachment from the primary tumor mass, intravasation, survival, extravasation, and colonization of a distant tissue. Created with BioRender.com

To complete this complex process, tumor cells require the transient modification of their physical and biological properties, a phenomenon commonly defined as cellular plasticity (Pérez-González et al., 2023).

The theory based on the congenial metaphor of the "seed and soil" proposed by Stephen Paget at the end of the 19th is still accepted and underlines the crucial role of the microenvironment for the successful colonization of a distant tissue (Langley & Fidler, 2011; Paget, 1989). Numerous circulating cancer cells (CTCs) can be detected in the blood of cancer patients, but most cells fail to metastasize (Luzzi et al., 1998). These could be related to the short half-life in the blood, approximately 2 hours, arguably induced by shear stress or the immune system, or the difficulty in finding a proper "soil" for the genesis of a pre-metastatic niche (Eslami-S et al., 2022; Strilic & Offermanns, 2017). For example, inflammation and the activation of nuclear factor-kB (NF-kB) in local fibroblasts contribute to establishing a suitable microenvironment for CTC colonization in the lung (Du et al., 2020). Even if some organs, such as the liver and lung, are commonly colonized due to facilitated extravasation of CTCs arguably promoted by anatomical reasons, certain tumors show metastatic organotropism, indicating that CTCs could require a specific "soil" (Lorusso & Rüegg, 2012; Minn et al., 2005). Several findings suggest that metastasis mechanisms could be tumor-specific and strictly dependent on the microenvironment, making the therapeutic approach particularly challenging (Majidpoor & Mortezaee, 2021). Therefore, the diagnosis of metastatic cancer, including in GIST patients, continues to be associated with a terminal label.

1.3.2. Metastasis in GISTs

As described in the previous paragraphs, imatinib resistance leads to progressive disease in patients with an advanced and unresectable GIST. In this clinical scenario, tumor progression and metastasis can only be delayed but not avoided with the current therapies. Metastases are commonly found in the liver (96%) and only rarely in the lung (2%) or in the bones (2%); these latter are commonly associated with that in the liver (D. Y. Yang et al., 2019). Only a single case of brain metastasis is reported in the Surveillance, Epidemiology, and End Results Program database (SEER). According to the SEER, metastases significantly reduce the median OS, which is commonly higher than 60 months in the case of non-metastatic GISTs. The presence of liver metastases reduces the median OS to about 50 months, while the impairment of lungs or bones is even associated with a median OS of 15 and 8 months, respectively.

Unfortunately, even if clinical data indicate that the progression of unresectable GISTs toward metastasis represents the major obstacle to a prolonged life expectancy, the mechanisms involved in the metastatic cascade are mostly unknown, and few players, especially adhesion proteins, have been reported in the last years. Curious is the case of Snail, a zinc-finger transcriptional repressor, which controls the Epithelial-Mesenchymal transition[d] (EMT) in epithelial cancers, promoting less expression of E-cadherin. This adhesion protein promotes cell-cell interactions. Despite the mesenchymal nature of GISTs, primary tumors that have already progressed up to the rise of metastases show higher mRNA levels of Snail and lower levels of E-cadherin with respect to specimens collected from patients with a non-metastatic GIST (S. Liu et al., 2014). This suggests that an intensification of the gene signature commonly observed during the EMT could also be crucial in GIST metastasis. Analogously, the downregulation of SPARCL1 (secreted protein acidic and rich in cysteine-like protein 1), a glycoprotein of the extracellular matrix that is involved in cellular adhesion and motility, has been correlated with the presence of metastases at the time of initial GIST diagnosis (Shen et al., 2018). The downregulation of SPARCL1 in GIST-882 does not affect cell viability but promotes cell migration and invasion. In confirmation of this, xenograft GIST-882 models with stable silencing of SPARCL1 give rise to a higher number of liver metastasis than those developed with progenitor GIST-882, suggesting a potential role in the first phases of the metastatic cascade. In a subsequent publication, authors unveiled that the downregulation of SPARCL1 is strictly related to that concomitant of the Lysine demethylase 6 A (KDM6A), which regulates the transcription of SPARCL1 through H3K27 demethylation (Shen et al., 2022). This finding confirms the necessity of a wide epigenetic rearrangement in cancer cells for acquiring a metastatic behavior that can likely induce remarkable changes in gene expression, including that observed in SPARCL1. Furthermore, the involvement of a further adhesion protein in the metastatic cascade role has been recently reported. *In vitro* findings indicate that the high expression of the cell adhesion molecule 1 (CADM1) inhibits proliferation, migration, and invasion but is crucial for the adhesion and migration through a monolayer of umbilical vein endothelial cells (HUVEC), an *in vitro* model of intravasation (Yuan et al., 2022). This study corroborates the plasticity required to pass through the different phases of the metastatic cascade. Indeed, the expression of CADM1 could be necessary during the extravasation but not compatible with other steps of metastasis.

1.3.3. *In vivo* model of metastasis

Developing suitable preclinical models is crucial to deciphering the complexity behind metastasis. Although various *in vivo* models have been developed to study metastasis, such as chicken embryos, zebrafish, and flies, mouse models are the most used because of their homologies to human beings (Hebert et al., 2023). Autochthonous tumor models developed thanks to genetic engineering or chemical-induced carcinogenesis can recapitulate the disease entirely, from tumorigenesis to metastasis. However, tumorigenesis, tumor growth, and metastasis are long-lasting, making those models time-consuming and expensive. This limitation can be partially overcome through the injection of murine (syngeneic model)[d] or human (xenogeneic model)[d] cancer cells directly into the interested tissue or circulation, accelerating the rise of the primary tumor or metastases, respectively. Nevertheless, cell lines are typically grown *in vitro* before the injection, and tumor subpopulations with better *in vitro* adaptability but a lower recapitulation of *in vivo* tumor features can be selected. Autochthonous or syngeneic mouse models are preferable since they maintain the physiological microenvironment, preserving the close relationship between metastatic cells, the natural stroma, and the immune system. Indeed, the transplantation of human or allogeneic mouse cells requires immunocompromised mice to prevent rejection by the adaptive immune system, thus excluding the well-recognized contribution to metastasis associated with this latter (Blomberg et al., 2018). In addition, incompatibility between human and murine receptor-ligand pairs could be present in xenogeneic models, impairing specific processes commonly active in syngeneic models. Despite these limitations, human and murine cell lines are still used since they can recapitulate the remarkable genetic and genomic alterations widely observed in cancer. Indeed, genetically engineered models are developed by precisely manipulating oncogenes, hence only harboring a few genetic alterations compared to naturally mutated cancer cells. The limit associated with the growth of cancer cells *in vitro* and their subsequent injection could be bypassed with the patient-derived xenografts (PDX) model [d], but the low metastasis rate observed in this model has prevented its successful use for the study of metastasis until now. Each mouse model shows some peculiar disadvantages, and the choice of which should be used depends on the scientific aim. The use of mouse models is also limited by the difficulties of performing extensive screening of drugs or studying the involvement of numerous putative genes. Therefore, developing accurate *in vitro* models could enable the evaluation of only the most promising candidates *in vivo*, minimizing ethical implications and respecting the 3Rs principles (Hubrecht & Carter, 2019).

1.3.4. *In vitro* models of metastasis

In vitro cell culture has represented the cornerstone of cancer research, enabling the study of tumor cell biology and drug development (Boussommier-Calleja, 2020). The main advantage of *in vitro* models is the possibility of affordably dissecting the role of genes in cancer-related processes through their transient or stable deregulation. In particular, the recent innovation of the CRISPR/CAS-9 tool allows a gene editing that has never been available before (Ran et al., 2013). However, metastasis complexity makes *in vitro* recapitulation challenging. The use of specific assays, such as migration and invasion, has provided crucial insights regarding the mechanisms that regulate the movement of cancer cells, representing a suitable model for mimicking the migration of cancer cells to reach the lymphatic system or blood circulation (Katt et al., 2016). Regarding the subsequent stages of the metastatic cascade, many steps forward have been taken in the last decade, and numerous cutting-edge models of metastasis have been developed. For example, microfluidic-based and three-dimension (3D) models for the study of cancer cell extravasation, the role of mechanic forces in metastasis, as well as for the simulation of the entire metastatic cascade (Bersini et al., 2014; Malandrino et al., 2018; Ni et al., 2019). Progress in 3D bioprinting could also bring promising results in the following years (Albritton & Miller, 2017). Recently, Vargas-Accarino et al. proposed a microfluidic independent and 2D cellular model to quickly and affordably study malignancy and metastatic properties *in vitro* (Vargas-Accarino et al., 2021). Tumor cells that grow adherent to plate surfaces spontaneously give rise to cellular elements in suspension typically recognized as dead cells, apoptotic bodies, or cellular debris. Notwithstanding, the authors demonstrated that there could also be living cells among dead or dying cells that reattach if seeded in a new culture plate, hence mimicking specific steps of the metastatic cascade *in vitro*. Despite obvious limitations, cell cultures and more advanced *in vitro* models display significant benefits, especially in terms of time, costs, and replacement/reduction of animals, fulfilling a complementary role with *in vivo* models and reciprocally overcoming the corresponding limits.

1.4.   Plant extracts as a promising source of therapeutics

1.4.1. The History of plant-derived drugs in cancer therapy and plant extracts

Natural compounds (NPs), including those derived from plants, have been historically used for therapeutic aims, as testified by Greek, Chinese, Indian, and Arabian traditional medicines (Khan, 2014). Based on these findings, numerous NPs have been isolated and evaluated as therapeutics. The chemical and physical properties of NPs confer potential advantages for the drug discovery process compared to chemically synthesized ones. Indeed, they are characterized by higher numbers of H-bond acceptors and donors, lower cLogP value[(d)], rigidity, and a wide area of chemical space (Atanasov et al., 2021). NPs are structurally "evolved" to play a biological function, thus owning an intrinsic capacity to interact with cellular structures. Moreover, their uses in traditional medicine may be proof of potential efficacy and safety. A recent review has estimated that 1/3 of all small-molecule drugs approved between 1981 and 2019 were NPs or their derivatives (Newman & Cragg, 2020). In particular, numerous NPs derived from plants, such as vincristine, etoposide, and taxanes, are currently employed successfully in cancer treatment (Naeem et al., 2022). Vincristine, isolated from the periwinkle *Catharanthus roseus*, inhibits the assembly of microtubules and has remarkably improved the efficacy of the treatment in Hodgkin's disease and some forms of leukemia (Noble, 1990). Etoposide, an epipodophyllotoxin derived from the mandrake plant *Podophyllum peltatum* or the wild chervil *Podophyllum emodi*, is an inhibitor of topoisomerase II approved with bleomycin and cisplatin for testicular cancer therapy (Williams et al., 1987). It induces DNA breaks via the stabilization of the enzyme-DNA complex. Paclitaxel, originally isolated from the bark of the yew tree *Taxus brevifolia*, and its analog docetaxel impede the disassembly of microtubules, showing a remarkable anti-tumor effect in different cancers, such as breast and ovarian (Wani et al., 1971). Despite these and other successes, drawbacks have limited NP-based drug discovery projects, primarily those pursued by pharmaceutical companies (Henrich & Beutler, 2013). Indeed, the constitution of a pure NP-based library is not straightforward since only about 250,000 NPs have been isolated and characterized, and many of them cannot be sufficiently purified for testing their pharmacological activities in preclinical studies, thus preventing a successful application of high throughput screenings (HTS). Furthermore, patenting NPs can be limited depending on the legislation of the different countries (Harrison, 2014). Instead, chemically modified NPs could be more easily patented, but applying Structure-Activity Relationship (SAR) may be a hurdle due to the complex chemical structures of NPs with challenging synthetic routes. Nevertheless, seeking new

plant-derived compounds is still considered a promising approach for drug discovery, and many unknown NPs could still be hidden in the vegetal kingdom. Indeed, numerous studies have reported that crude plant extracts can induce apoptosis in preclinical models, including *in vivo,* suggesting the potential presence of novel chemotherapeutics (Rajabi et al., 2021). For example, the extract from the leaves of *Hibiscus sabdariffa* induces apoptosis in LNCaP cells, a model of androgen-dependent prostate cancer. The administration of the extract through the diet in mice that harbor a xenograft LNCaP tumor promotes a significant decrease in tumor burden via the increase of FasL, Bax, and cleaved caspase-3 (Lin et al., 2012). Although these observations corroborate the ancient use of plants in traditional medicine, occidental medicine compulsorily demands pure molecules in clinics. Therefore, isolating plant bioactive NPs is required. However, this process could be challenging due to the complexity of the phytochemical mixture commonly contained in plant extracts.

1.4.2. Arbutus unedo L. as a promising source of anticancer phytochemicals

Arbutus unedo L. (*A. unedo*) is an evergreen shrub or small tree belonging to the Ericaceae family. It is commonly found in regions with hot summers and mild rainy winters, especially in Mediterranean countries (Morgado et al., 2018). *A. unedo* is particularly resistant to hard environmental conditions like drought and low temperatures. Being diffused in most of the Greek coast, this plant was highly used by ancient people, including in traditional medicine. Therefore, its potential uses for pharmacological purposes have been investigated. Extracts produced from different parts of *A. unedo* have revealed numerous pharmacological effects in preclinical studies, such as antiaggregant, antidiabetic, antihypertensive, anti-inflammatory, antioxidant, and antitumoral. Regarding this latter, it has been recently reported that the extract of *A. unedo* leaves obtained through a methanol-based extraction impairs the viability of U2OS cells, a model of osteosarcoma, supporting the concept that *A. unedo* could be a promising source for novel chemotherapeutics (Cappadone et al., 2019). In addition, the extract does not affect HUVEC cells, a healthy cellular model, suggesting that it could show a good toxicity profile. However, more studies are needed to clarify which phytochemicals are responsible for this activity and which are their biological targets. Indeed, leaves contain a large diversity of NPs, such as phenolic compounds, essential oils, and α-tocopherol (Bessah & Benyoussef, 2012; Erkekoglou et al., 2017; Kivçak & Mert, 2001). Focusing on the phenolic compounds, which are drawing the attention of the scientific community for a potential role as anti-cancer, leaves harbor tannins, flavonoids (for example, catechin gallate, and myricetin), phenolic glycosides (quercitrin, isoquercitrin, and hyperoside), and iridoid glucosides (Abotaleb et al., 2020; Morgado et al., 2018). Several polyphenols, such as arbutin, ethyl gallate, galloyl arbutin,

gallocatechin, and others, have also been identified and could similarly be promising for cancer treatment (Briguglio et al., 2020; Cháirez-Ramírez et al., 2021). Interestingly, plant extract composition, including that of *A. unedo*, is not standard but can change based on geographic location and seasons. This indicates that certain extracts could show anti-cancer activity only if extracted from plants grown in a particular soil and at precise moments of the year. For example, leaves collected from Croatia harbor more hyperoside and quercitrin in January than in June.

Figure 11. *Arbutus unedo L.* tree (A); Ripe (B) and unripe fruits (C); Arbutus unedo flowers (D). (Morgado et al., 2018)

1.4.3. Bio-guided fractionation: a strategy for identifying active NPs

Bio-guided fractionation is an approach that has been used to isolate and characterize active NPs from plant extracts (Liao et al., 2023; Mani et al., 2022). In detail, as shown in Figure 10, the process commonly starts with the fractionation of NPs in the crude plant extract using a liquid-liquid partition in different solvents based on their solubilities. A biological assay then assesses which fraction among those produced continues to preserve the pharmacological function. Various in-series fractionation steps are typically required to reduce the complexity of the starting extract sufficiently. Hence, chromatography-based techniques, such as reverse phase and size exclusion, are commonly

performed after the first phytochemical liquid-liquid partition. Analytical methods, such as NMR, could be used to monitor the successful advancement of the process and to confirm the gradual reduction of the fraction complexity. Once active NPs are enriched, analytical methods, such as NMR, infrared spectroscopy (IR), and mass spectrometry (MS), can elucidate the structure of the bioactive phytochemical.

Nevertheless, bio-guided fractionation is time-consuming and sometimes inefficient in discovering novel compounds (Demarque et al., 2020). Metabolomics, a novel approach developed in the 21st century, can represent valuable support in discovering NPs from plants (M. Patel et al., 2021). It consists of powerful bioinformatic tools that match NMR and MS data with annotated spectroscopic databases, allowing the identification of NPs in the plant extract. Comparing the metabolomes of numerous plant extracts, it is possible to hypothesize which NP is responsible for the biological activity without prior fractionation. This approach can be applied when the objects of the study are plant extracts derived from plants belonging to the same family, extracted with different solvents, or obtained from different soils and seasons. Indeed, few metabolites are expected to change remarkably in this context, and observing a different biological activity could immediately focus the attention on specific metabolites identified thanks to the matching of analytical data with that available in the databases, which are present in higher concentrations, thus avoiding performing the bio-guided approach for each extract. Recent publications have shown that the same active compound can be identified using traditional bio-guided fractionation or metabolomics approaches (Demarque et al., 2020; Graziani et al., 2018). Nevertheless, as indicated, applying metabolomics strictly requires that the biological activity is associated with a small panel of metabolites that changes between similar extracts. Moreover, numerous compounds remain unknown, and a metabolomics approach to characterize them without experimental isolation and analysis is required to be developed (Nakabayashi & Saito, 2013). Therefore, even if metabolomics could provide advantages in plant drug discovery, the bio-guided fractionation approach continues to be considered the primary approach to isolate and identify NPs with interesting pharmacological activity from plant extract.
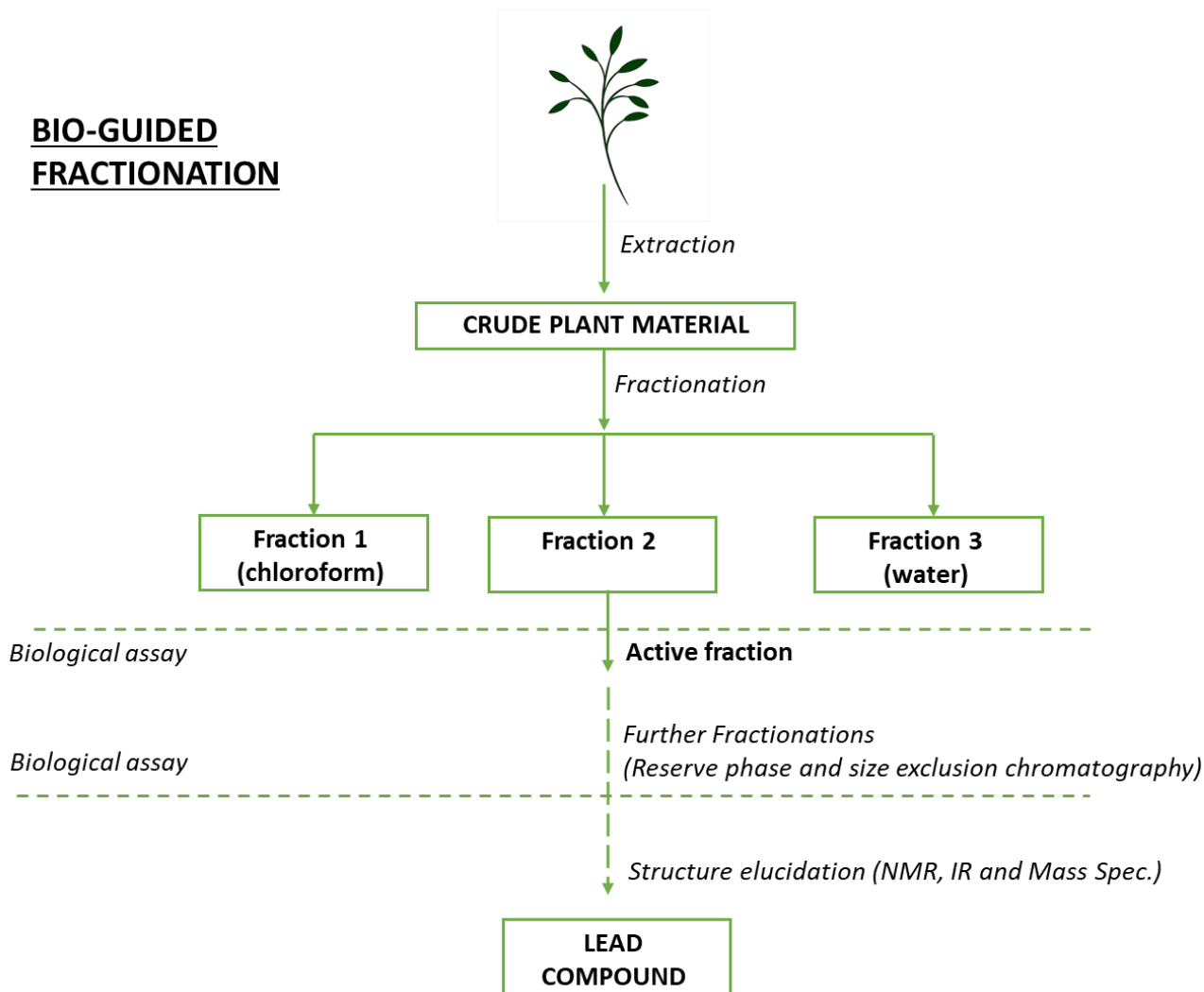
Figure 10. Bio-guided fractionation workflow. The crude extract is commonly fractionated based on chemical properties, separating phytochemicals based on the solubility in different solvents (liquid-liquid partition), whose extremes are represented by water and a water-immiscible solvent like chloroform. The fractions obtained with the separation method are then tested with a biological assay to identify the most active ones. This process is repeated to reduce the chemical complexity of the extract. In particular, the bio-guided fractionation proceeds using chromatography-based tools, such as reverse-phase and size-exclusion. Analytical methods, such as NMR, IR, and mass spectrometry, allow the identification of bioactive phytochemicals, if already known and present in databases, or contribute to their characterization.

2. HYPHOTESES AND PROJECT AIMS

Imatinib has significantly improved the clinical outcome of patients with unresectable and advanced GISTs since they are frequently caused by a gain of function mutation in KIT or PDGFRα. Nevertheless, imatinib is rarely curative, mainly promoting the temporary stabilization of the disease. The major obstacle for patients is progressive disease, typically observed within 24 months due to imatinib resistance, making the discovery of novel therapies the primary medical need in GIST research. Secondary mutations in KIT or PDGFRα, which counteract imatinib, have been found in resistant GISTs, supporting the development of novel multi-target TKIs for their targeting. However, the approval of developed multi-target TKIs, which more efficiently target secondary mutated KIT or PDGFRα, has improved prognosis modestly. Emblematic is the recent result of the phase III INTRIGUE trial, in which ripretinib, the best-in-class TKI, cannot long control disease progression, indicating that the secondary mutations in KIT or PDGFRα are only "the tip of the iceberg" in imatinib resistance, which is more multifaceted than that was initially thought. As a confirmation of this, preclinical studies have unveiled numerous mechanisms of resistance not successfully targetable by the multi-target TKIs, thus explaining the modest effect of these latter. In this clinical scenario, tumor progression and metastasis can be only delayed but not prevented with current therapies.

The lack of specificity of traditional chemotherapy is commonly considered a limit due to the numerous side effects commonly observed in clinics. Nevertheless, the mechanism of action of standard chemotherapeutics, which triggers apoptosis interfering with the synthesis and function of DNA, RNA, and proteins, could also represent an advantage. We advanced the hypothesis that its low specificity could target numerous imatinib-resistant subclones, regardless of the mechanisms they resist imatinib. Unfortunately, none of the traditional chemotherapeutics in clinics were approved for GIST therapy due to insufficient PR. Therefore, identifying novel chemotherapeutics for GIST treatment could be a promising strategy. The vegetal kingdom has historically been a source of traditional anti-cancer drugs and could still harbor unknown hit or lead compounds. We focused on the extract obtained from the leaves of *A. unedo* (hereafter referred to as AUN only), which has already been associated with anti-cancer activity in osteosarcoma U2OS cells, suggesting the presence of bioactive compounds. Moreover, it has been reported that AUN contains numerous phenolic or polyphenolic phytochemicals, which are attracting the scientific community's interest as potential anticancer agents. Based on these findings, **we hypothesized that AUN could also affect**

GIST cells, and its bio-guided fractionation could unveil novel chemotherapeutics for GIST treatment ("Bio-guided fractionation of AUN to identify chemotherapeutics for GIST treatment").

Moreover, without an efficient long-term therapy, anti-metastatic drugs could prevent the progression of unresectable and advanced GIST toward metastasis, representing an alternative strategy for extending the OS. However, the mechanisms behind GIST metastasis are mostly unknown, and more effort is required to identify promising molecular targets. However, to the best of our knowledge, no *in vivo* or advanced *in vitro* models for the study of metastasis in GIST have been developed. For this reason, **our second aim was the development of a reliable *in vitro* model for the study of metastasis** ("An *in vitro* model for the study of metastasis in GISTs"). Vargas Accarino and co-authors have recently reported that certain adherent cells can spontaneously give rise to viable cells that survive in suspension and reattach if seeded in a new tissue culture plate, mimicking specific steps of the metastatic cascade *in vitro*. According to these findings, **we hypothesized that GIST-T1 cells**, **established from a metastasis related to a primary GIST, could have maintained metastatic properties *in vitro* and could be used as a model for the preliminary study of metastasis in GISTs.**

3. RESULTS

3.1. Bio-guided fractionation of AUN to identify chemotherapeutics for GIST treatment

3.1.1. AUN impairs the viability of imatinib-sensitive GIST cells

AUN was first tested in GIST-882, an imatinib-sensitive cell line harboring a gain of function mutation in KIT. The treatment dosage was determined based on the concentrations commonly associated with a pharmacological effect of plant extracts in the literature. To properly evaluate if AUN could impair cell proliferation, cells were treated for 72 hours (h) since it approximates the doubling time[d] (d_t). AUN significantly affected the viability of GIST-882 cells in a dose-dependent manner (Figure 1). In detail, the cell viability decreased by about 75% because of the 200 µg/mL treatment, while a faint but significant reduction (around 25%) was observed in cells treated with 100 µg/mL. Instead, no effect was induced by 50 µg/mL. 200 µg/mL similarly reduced the viability by about 60-70% in GIST-T1, a further imatinib-sensitive cell line with a different gain of function mutation in KIT (Supplementary Figure 1A).
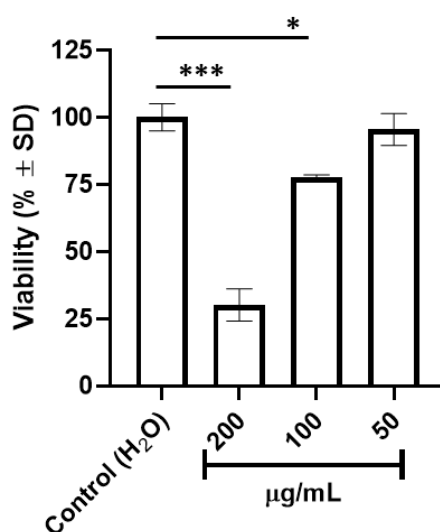
Figure 1. AUN reduced the viability of GIST-882 in a dose-dependent manner. GIST-882 cells were treated with different concentrations of AUN (50, 100, 200 µg/mL). Cell viability is expressed in % ± Standard deviation (SD) with respect to Control. The viability was calculated based on the number of viable cells estimated through Guava® ViaCount™ staining and flow cytometry. Adjusted p-value * <0.05, *** <0.001 (One-way ANOVA-Dunnett's Multiple comparison test with respect to Control). A representative experiment among three replicates is shown.
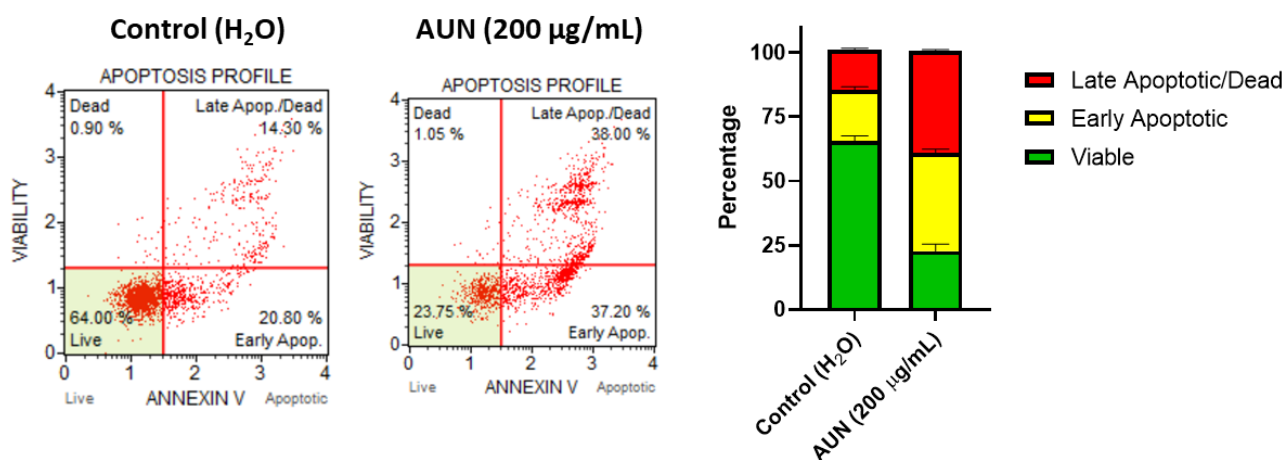
3.1.2. AUN promotes the rise of early and late apoptotic cells

According to the d_t, if AUN had only inhibited cell proliferation in GIST-882, cell viability should have decreased by a maximum of 50%. However, the higher reduction suggested that 200 µg/mL could have also induced cell death. Flow cytometry data displayed two similarly represented cell populations in the AUN treated sample (Figure 2 – lower panels). In contrast, a single population was only observed in Control (Figure 2 – upper panels). The first in both samples is defined by a cell size index of around 3 and a viability staining of less than 1. Instead, the second, exclusively in the AUN treated sample, is characterized by a lower cell size index and a slight increase in viability staining. Interestingly, the lower-size cellular events are less stained with the nucleated dye, a fluorescent DNA binder that can diffuse through the membranes of viable cells (Figure 2 – right panels). This supports the concept that cellular events with a lower size could contain degraded DNA. Both features, less size and degraded DNA, suggested that AUN could stimulate cell death in GIST-882 by triggering apoptosis.
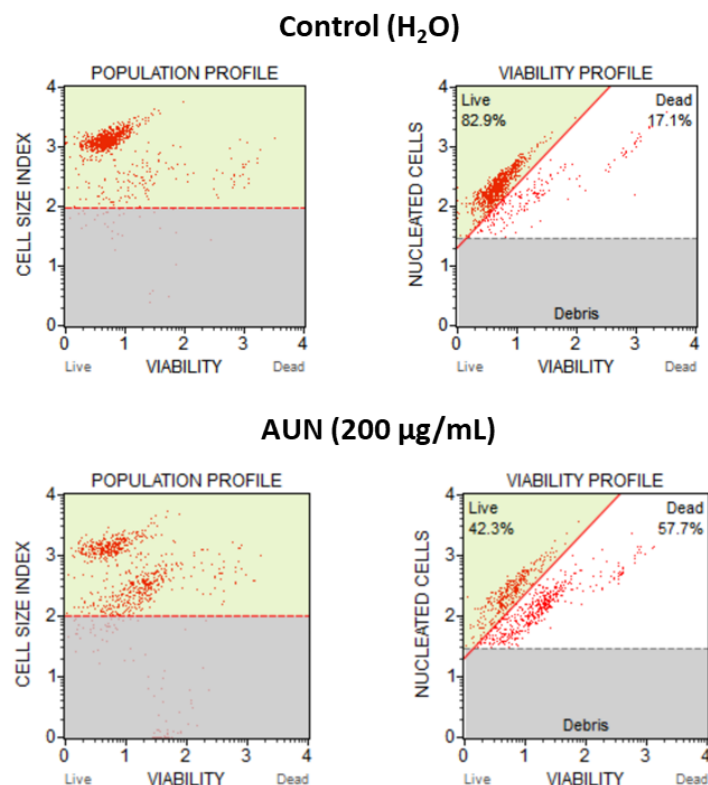
Figure 2. AUN promoted the origin of smaller cellular events with less nuclear-related DNA staining. GIST-882 cells were treated with AUN at 200 µg/mL. Each red point in the graphs represents a cellular event detected by the flow cytometer. The analysis was performed after the staining with Guava® ViaCount™. The graphs on the left define the "Population profiles" and classify cellular events by the "cell size index" (x-axis) and the positivity to the "viability" dye (y-axis). Instead, the "viability profile" on the right defines the events based on the positivity to the "nuclear dye" (y-axis) and "viability" dye (x-axis). A representative experiment among three replicates is shown.

To test this hypothesis, the exposure of phosphatidylserine (PS), typically on the membranes of early apoptotic cells, was investigated using an Annexin-V and 7-amino actinomycin D (7-AAD) dual staining 24h after treatment. AUN induced an increase in cellular events with a high Annexin-V signal (intensity higher than 2) and no 7-AAD related signal (viability staining less than 1.1) in GIST-882, a marker of early apoptosis (Figure 3 – left panel). Moreover, a further population with Annexin-V and 7-AAD high signals (higher than 2), commonly classified as late apoptotic/dead cells, was also detected. Hence, data indicated a significant increase of early (mean=38%, p-value <0.01) and late (mean=41%, p-value P <0.01) apoptotic cells as a consequence of AUN treatment compared to Control (the mean of early and late apoptotic cellular events was 21% and 13%, respectively) (Figure 3 – right panel). Despite different kinetics, similar findings were reported in GIST-T1 after 6h treatment (Supplementary Figure 1B). Indeed, the percentage of early (31% vs. 15%) and late (15% vs. 3%) apoptotic cells were higher in the AUN-treated sample with respect to Control, indicating that AUN similarly triggered apoptosis in imatinib-sensitive GIST cells.

Figure 3. AUN promoted the rise of early and late apoptotic cells in GIST-882. GIST-882 cells were treated with AUN (200 µg/mL) for 24h. The "apoptosis profiles" are defined by 7-AAD signal ("viability on the y-axis) and "Annexin-V" (y-axis). Representative "apoptosis profiles" are shown. The percentage ± SD of viable (Annexin-V (-)/7-AAD (-)), early apoptotic (Annexin V (+)/7-AAD (-)), and late apoptotic/dead (Annexin V (+) and 7-AAD (+)) cell populations are displayed in the graph on the right. The average values are reported in the columns. A representative experiment among three experimental replicates is shown.

3.1.3. Bio-guided fractionation of AUN and isolation of FR2-A

Since AUN was associated with an interesting pharmacological activity in imatinib-sensitive GIST cells, it was subjected to bio-guided fractionation to identify the bioactive compounds. The first step was a liquid-liquid partitioning starting from AUN initially suspended in water. Chloroform and ethyl

acetate were in series used to extract phytochemicals with high and mild/low hydrophobicity. Hence, three fractions were obtained: FR1, containing phytochemicals extracted in chloroform (yield approximately 0.33% w/w); FR2, those that were successively extracted in ethyl acetate (8.8% w/w); FR3, harboring the more hydrophilic phytochemicals that remained in the water. They were then tested in GIST-882 to identify the fraction in which active phytochemicals were mainly distributed. As shown in Figure 4A, cell viability was impaired primarily by FR2, approximately 90% (p-value < 0.0001). FR2 activity was even more intense than the progenitor AUN, suggesting that active phytochemicals were collected and enriched in FR2. About 30% reduction was observed in the FR3-treated sample (p-value < 0.05), while FR1 promoted no effect. No significant differences were present between the control samples (untreated and solvent-treated). Consistent with the results in Figure 2, a decrease in cell size and shape alteration because of AUN and FR2 treatment was observed by brightfield microscopy (Figure 4B). In agreement with the proapoptotic effect of AUN in GIST-882, the rise of an Annexin (+)/7-AAD (-) cell population was also detected after FR2 treatment with respect to Control, confirming that promising proapoptotic phytochemicals were fractionated in FR2 (Figure 4C). A similar result was also observed in GIST-T1, where FR2 remained the most active AUN-derived fraction (Supplementary Figure 2).

A.
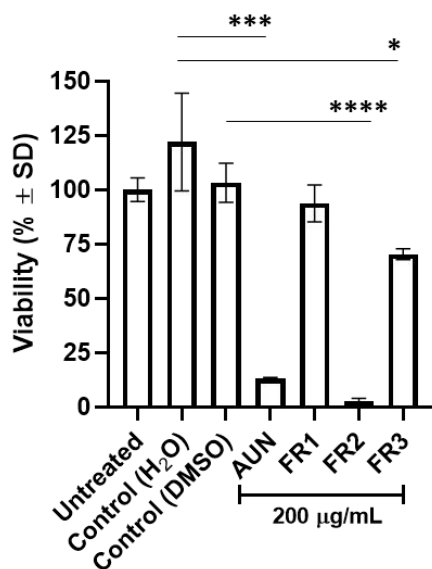
B.
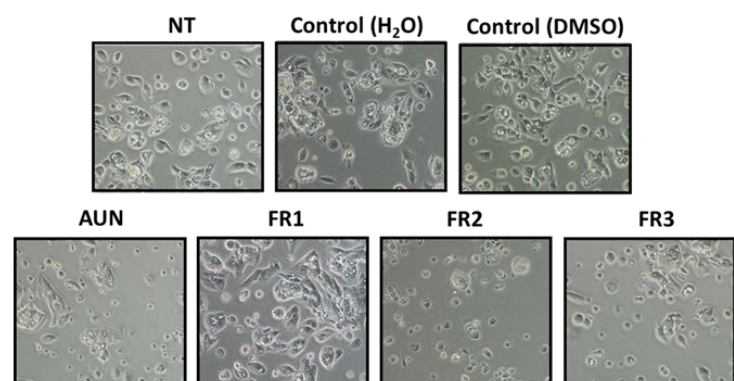
C.
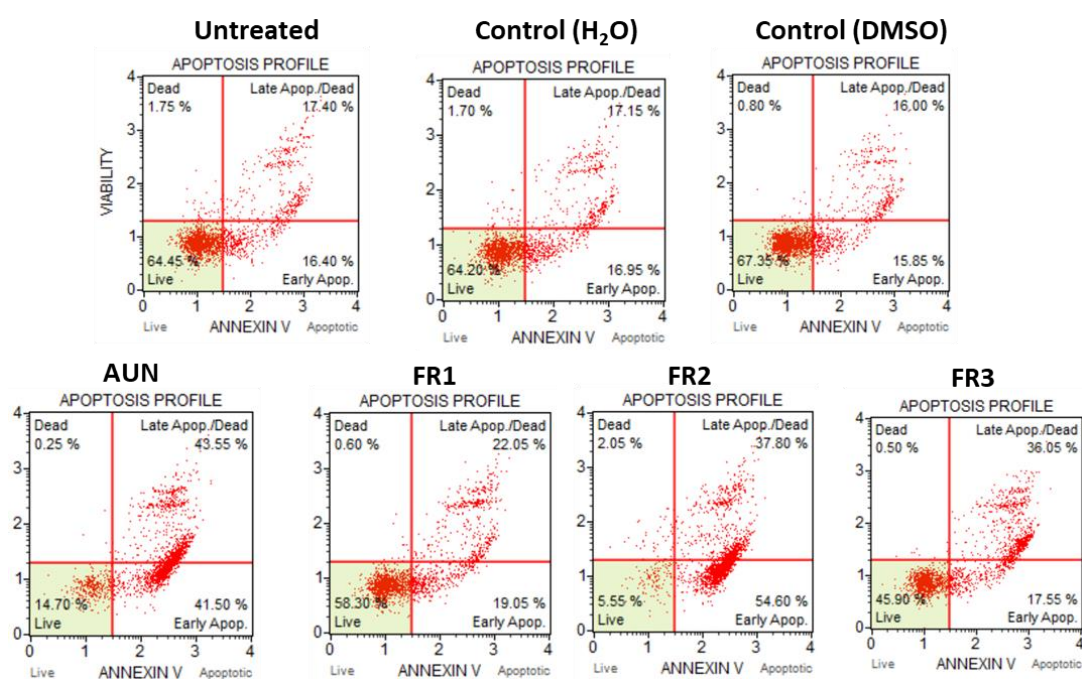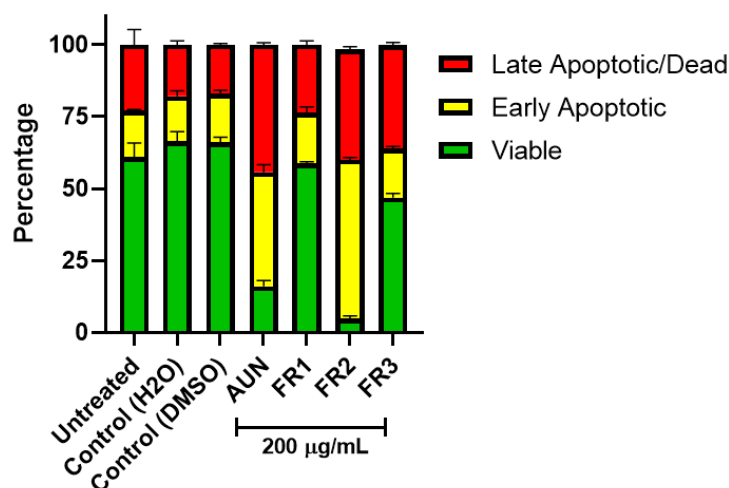
Figure 4. AUN fractions in GIST-882 A. Cell viability after the treatment with AUN or derived fractions (FR1-FR2-FR3) at 200 µg/mL. Cells were treated for 24h. Cell viability is expressed in % ± SD with respect to Untreated. The viability was calculated based on the number of viable cells estimated through Guava® ViaCount™ staining and flow cytometry. Adjusted p-value * <0.05, *** <0.001, ****<0.0001 - One-way ANOVA-Tuckey's Multiple comparison test with respect to the corresponding solvent-treated control sample (Control H_2O in the case of AUN and FR3, Control DMSO for FR2 and FR3). **B.** Brightfield microscopy pictures of each experimental sample before performing the staining and flow cytometry analysis are shown at 10X magnification. **C.** The % ± SD of viable (Annexin-V (-)/7-AAD (-)), early apoptotic (Annexin V (+)/7-AAD (-)), and late apoptotic/dead (Annexin V (+) and 7-AAD (+)) cell populations are displayed. A representative "apoptosis profile" of each sample is shown.

Harboring phytochemicals of potential interest, FR2 underwent the second step of the bio-guided fractionation. A reverse-phase medium-pressure chromatography (MPLC), associated with a detector in the spectrum of ultraviolet and visible ranges, was used to separate phytochemicals with

different polarities (Figure 5). Four main absorbance peaks were observed during the elution induced by an increasing methanol gradient in the mobile phase. Thus, these main peaks guided FR2 fractionation into four subfractions named FR2-A, FR2-B, FR2-C, and FR2-D. The effect of FR2 subfractions on GIST-882 viability was assessed 24h after treatment with respect to Control and the progenitor FR2 (Figure 6). Treatment with FR2-A at 50 µg/mL induced a 90% impairment of cell viability (p-value < 0.0001), similar to that observed with the highest dose of FR2, 200 µg/mL. Despite significant (p-value < 0.001), only a fainter viability reduction (about 40%) was observed with FR2-B and FR2-C at 50 µg/mL. Therefore, the result stated that FR2 fractionation mainly collected active phytochemicals in FR2-A. FR2-A was more potent than FR2 since it showed higher activity at 50 µg/mL. This supported the efficient proceeding of the bio-guided approach and the enrichment of bioactive compounds in FR2-A. Consistent with data reported for FR2, FR2-A similarly impaired the viability of imatinib-sensitive GIST-882 and GIST-T1. Indeed, the calculated IC_{50} was around 33 µg/mL in both cellular models, indicating that a different mutational pattern in KIT does not influence the FR2-A mechanism of action (Supplementary Figure 3). As the more potent FR2 subfraction, FR2-A was the object of further studies to decipher its mechanism of action and chemical composition.
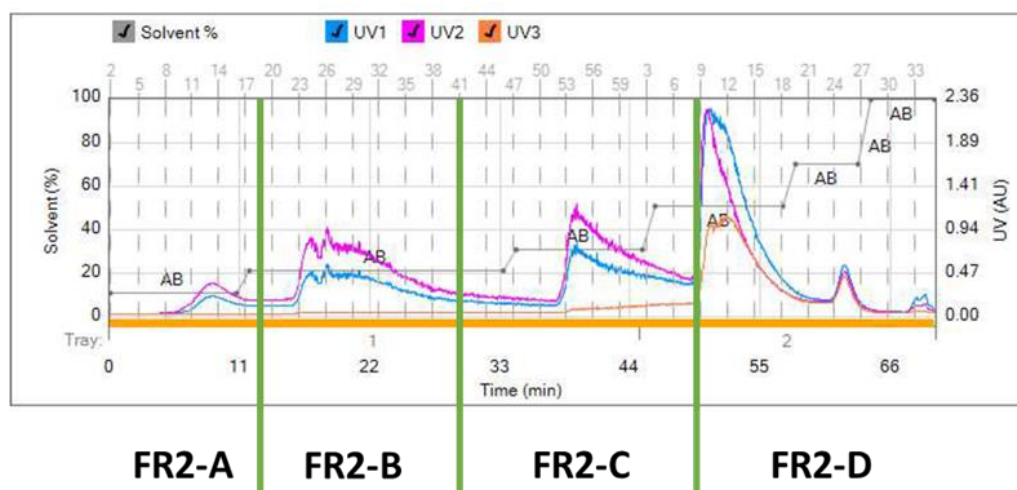
Figure 5. Establishment of FR2 subfractions. FR2 was further fractionated through reverse-phase MPLC chromatography (the 2nd step of bio-guided fractionation). Phytochemicals were eluted with different retention times by an increasing gradient of CH_3OH. The evolution of the UV absorbance at three different wavelengths (UV1=254 nm, UV2=270 nm, and UV3=340 nm) was used to differentiate phytochemicals with different solubility. Thus, FR2 was divided into FR2-A, FR2-B, FR2-C and FR2-D (green lines).
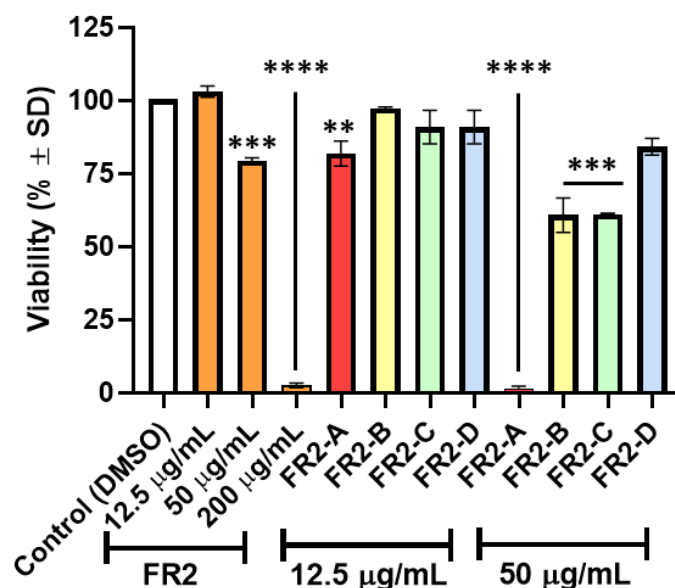
Figure 6. Active phytochemicals in FR2 were fractionated in FR2-A. GIST-882 cells were treated with FR2 or derived fractions for 24h at the indicated final concentration (µg/mL). Cell viability is expressed in % ± SD with respect to Control sample. The viability was calculated based on the number of viable cells estimated through Guava® ViaCount™ staining and flow cytometry. Adjusted p-value **<0.01, *** <0.001, **** <0.0001 (One-way ANOVA-Dunnett's Multiple comparison test with respect to Control). A representative experiment among three replicates is shown.

3.1.4. FR2-A is more efficient than imatinib in GIST-882

The pharmacological effect of FR2-A was compared to imatinib in a time course experiment up to 48h since it represents the gold standard for GIST therapy. FR2-A affected GIST-882 viability in a dose and time-dependent manner (Figure 7A). 66 µg/mL (a dose two times higher than the IC_{50}) reduced the viability by about 50% 4h after treatment (p-value < 0.001), while 33 µg/mL (IC_{50}) required about 6h (p-value < 0.05). 66 µg/mL FR2-A almost entirely impaired the viability within 24h, while no more than 50% reduction was observed with 33 µg/mL between 6 and 48h. Compared with imatinib, FR2-A quickly affected the viability of GIST-882, while imatinib only reduced it at 48h faintly (p-value < 0.05). FR2-A treatment promoted more apoptotic cells than imatinib (Figure 7B). In detail, focusing on 48h, the time in which imatinib significantly reduced the cell viability with respect to Control, imatinib faintly increased the percentage of early apoptotic cells from about 16%, observed in Control, to about 23%. On the contrary, 33 µg/mL and 66 µg/mL of FR2-A induced the rise of early apoptotic cells 48h after treatment to about 40 and 50%, respectively (Figure 7B and Figure 7C).
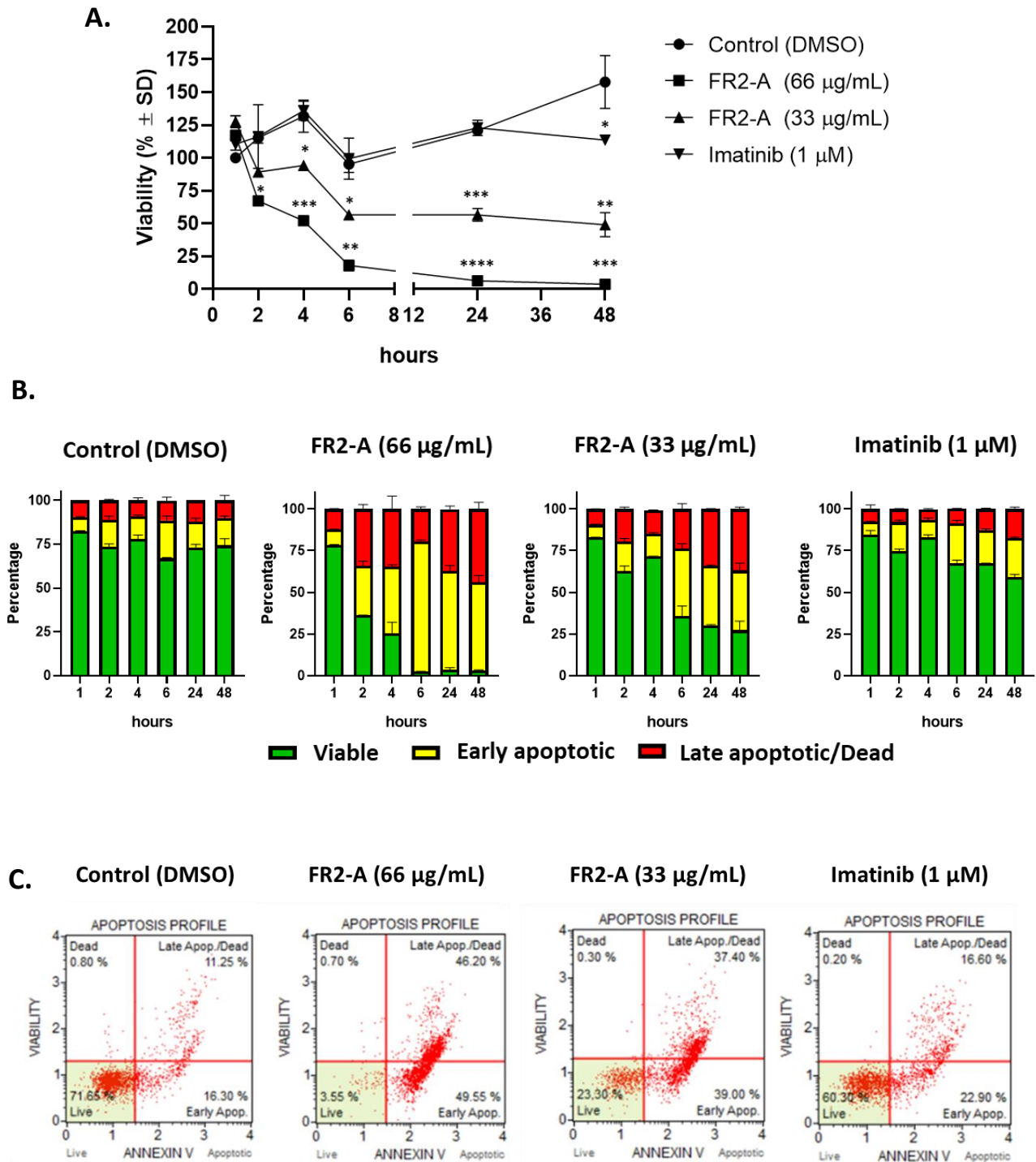
Figure 7. Comparison between FR2-A and imatinib in GIST-882. GIST-882 cells were treated with FR2-A and imatinib in a time-course experiment within 48h. **A.** The viability was measured through Guava® ViaCount™ staining and flow cytometry. The viability is expressed in % ± SD with respect to the Control sample. Adjusted p-value * < 0.05, **<0.01, *** <0.001, **** < 0.0001 (One-way ANOVA-Dunnett's Multiple comparison test with respect to Control). **B.** The percentage (±SD) of viable (Annexin-V (-)/7-AAD (-)), early apoptotic (Annexin V (+)/7-AAD (-)), and late apoptotic/dead (Annexin V (+) and 7-AAD (+)) cell populations induced by FR2-A or imatinib are displayed. **C**. A representative "apoptosis profile" of the indicated samples at 48h. A representative experiment among two experimental replicates is shown.

3.1.5. FR2-A leads to PARP1 downregulation

Activation of traditional apoptotic pathways based on the cleavage of caspase-3 or caspase-9 was evaluated. Although FR2-A promoted the increase of Annexin V (+) and 7-AAD (-) population, no caspase activation was observed (data not shown). Thus, the cleavage of PARP1 was also monitored since it is a well-known downstream target of caspase-3. However, no cleavage was detected, confirming the absence of traditional caspase-3 activation. Interestingly, even if no PARP1 cleavage was observed since the non-caspase-3 dependent apoptosis, downregulation of PARP1 was similarly observed because of 66 µg/mL FR2-A treatment. Indeed, a 50% reduction in PARP1 expression level was already present 2h after treatment (fold change 0.47), even reaching a downregulation of about 85% after 3h (fold change 0.15). This supported the fact that the pharmacological effect of FR2-A was strictly related to PARP1 downregulation (Figure 8).
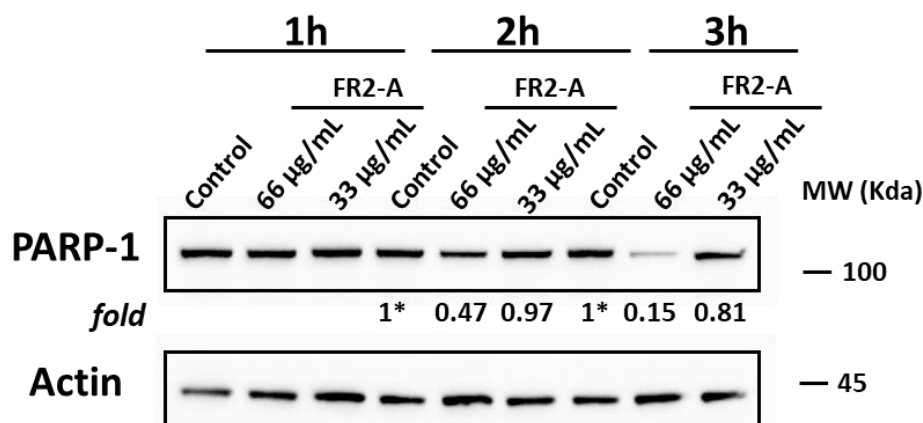
Figure 8. FR2-A led to PARP-1 downregulation in GIST-882. The expression level of PARP-1 after FR2-A treatments at 1h, 2h, and 3h is shown. Normalization was performed using the intensity of the corresponding actin band in each lane. Fold change was then calculated by dividing the normalized level of PARP1 in the FR2-A treated sample by those in the corresponding control sample. The molecular weight (MW) is reported.

3.1.6. FR2-A also targets imatinib-resistant cells

Since the remarkable effect of FR2-A in imatinib-sensitive cells, the effect in imatinib-resistant cells was investigated. Therefore, GIST-48 and GIST-48b were treated with FR2-A, and IC_{50} was calculated. Despite a higher IC_{50}, FR2-A also targets GIST-48 (IC_{50}= 46.4 µg/mL) and GIST-48b (IC_{50}= 58.6 µg/mL), indicating a wide-spectrum capability of targeting, which also included imatinib-resistant cells (Figure 9A). Interestingly, as already stated in the literature, in contrast to GIST-882, GIST-T1, and GIST-48, GIST-48b cells did not express detectable levels of KIT protein. This indicated that the mechanism of action of FR2-A was KIT-independent (Figure 9B).
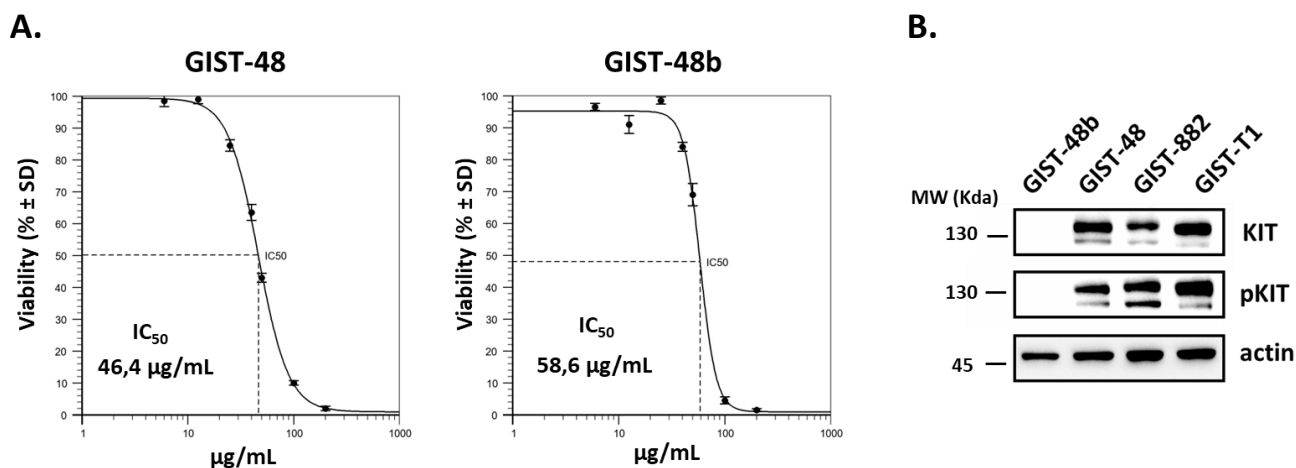
Figure 9. FR2-A IC$_{50}$ in imatinib-resistant GIST-48 and GIST-48b. A. GIST-48 (graph on the left) and GIST-48b (on the right) were treated with different concentrations of FR2-A, and the viability was measured through Guava® ViaCount™ staining and flow cytometry. Cell viability is expressed in percentage with respect to Control ± SD. The calculated IC$_{50}$ is reported at the bottom of the corresponding graph. A representative experiment among two experimental replicates is shown. **B.** Total and phosphorylated KIT expression levels in GIST cell lines are shown. The expression level of actin was used as a reference. The molecular weight (MW) is reported.

3.1.7. β-arbutin is not the active compound in FR2-A

The analysis of the ^{1}H NMR spectrum of FR2-A revealed that the most intense signals were ascribable to arbutin, a compound already reported in the literature as a constituent of Arbutus unedo L. leaves (Martins et al., 2021). The protons responsible for the identification are detailed in Figure 10A. Notably, arbutin is in the β anomeric form because the coupling constant of the doublet related to the anomeric proton at δ 4.87 was 7.7 Hz. Therefore, since β-arbutin is the main component of FR2-A and was already associated with a proapoptotic activity in melanoma cells (L. Jiang et al., 2017), it was hypothesized that β-arbutin could promote the pharmacological effect observed with FR2-A treatment. Hence, GIST-882 cells were treated with pure β-arbutin at 200 μg/mL (Figure 10B). However, no significant effect was detected on cell viability nor in apoptosis stimulation up to 72h after treatment, indicating that β-arbutin is not the compound responsible for FR2-A activity.
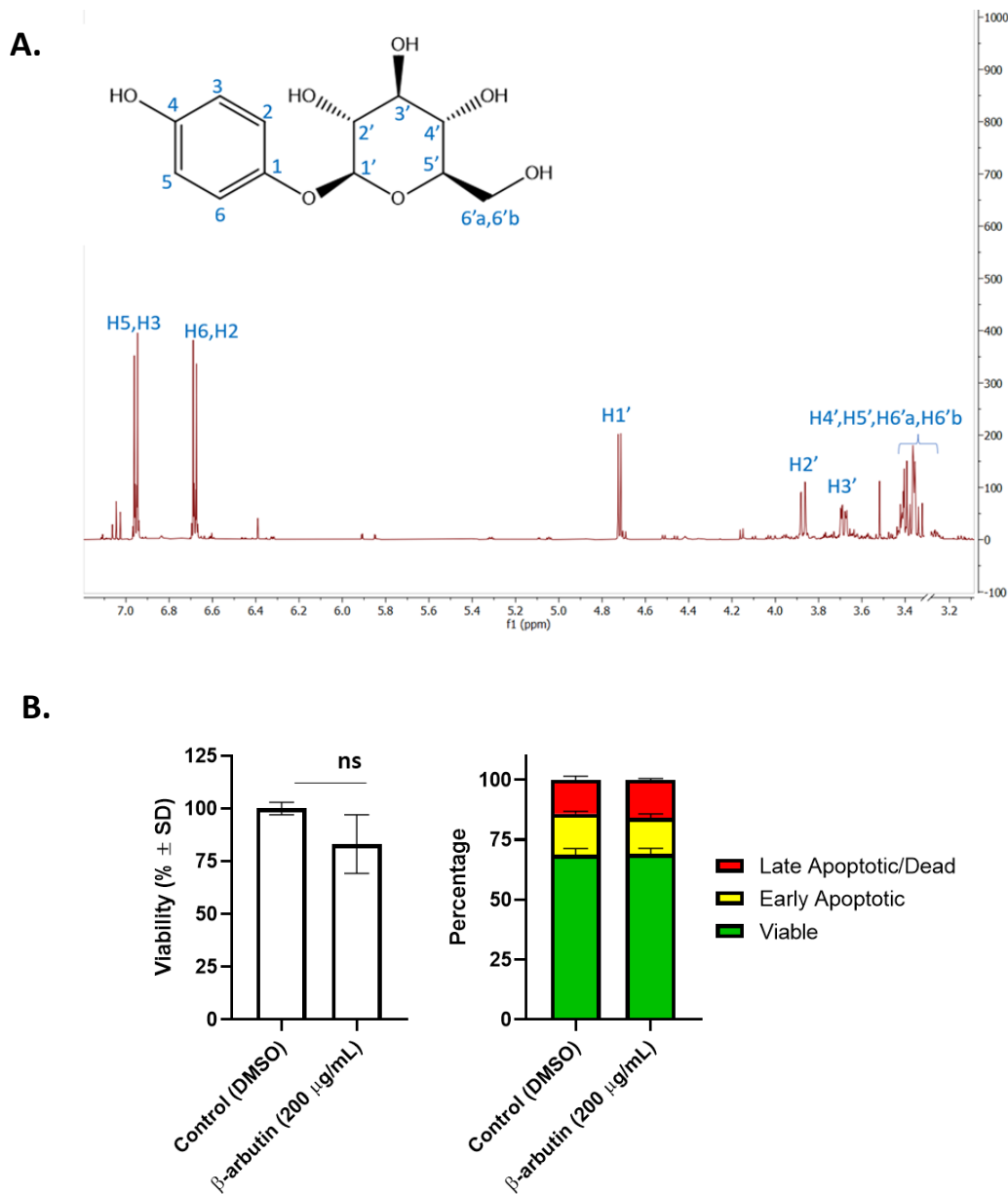
Figure 10. A. ^{1}H NMR spectrum in MeOH-*d4* of FR2-A containing as main compound β-arbutin. The β-arbutin molecule and the identified hydrogens are reported at the top of the spectrum. **B.** The graph on the left shows the viability of GIST-882 after β-arbutin treatment (200 µg/mL). The length of the treatment was 72h. Cell viability is expressed in % ± SD with respect to the control sample. The viability was calculated based on the number of viable cells estimated through Guava® ViaCount™ staining and flow cytometry. Ns means "not significative" using the unpaired t-test. The percentage ±SD of viable (Annexin-V (-)/7-AAD (-)), early apoptotic (Annexin V (+)/7-AAD (-)), and late apoptotic/dead (Annexin V (+) and 7-AAD (+)) cell populations are displayed in the right panel. A representative experiment among two experimental replicates is shown.

3.1.8. Bio-guided fractionation of FR2-A through size exclusion chromatography

FR2-A was further fractionated using Size-exclusion chromatography[(d)] (SEC), obtaining over two hundred subfractions. A small amount of each was then analyzed using Thin-layer chromatography[(d)] (TLC), and subfractions with an analogous TLC profile were combined to constitute 84 FR2-A derived

subfractions. Only 61 were tested in GIST-882 and GIST-T1 cells due to insufficient material of certain for the viability assays (<1 mg). Among them, nine subfractions maintained the pharmacological activity in GIST-882 and GIST-T1, suggesting that more than one phytochemical was responsible for the FR2-A effect. In detail, 30 µg/mL of 2A-29, 2A-30, 2A-31, 2A-35,2A-36, 2A-60, and 2A-61 reduced the viability of both cell lines up to the limit of assay detection (LOD) defined by the sample named CNTRL w/o MTT, a control sample in which no MTT reagent was added and, for this reason, representing the assay LOD (Figure 11 – upper graph). Instead, about 60% viability reduction was observed in treated cells with 2A-48 and 2A-49. Interestingly, only 2A-35 and 2A-36 subfractions were active at 6 µg/mL, thus representing the most potent subfractions (Figure 11 – lower graph). To make them more easily visible, the graphs only include the nine active subfractions delimitated by the adjacent weakly- or non-active. Notably, the adjacent weakly- or non-active subfractions in the graphs could not be precisely the subfraction numerically contiguous. Indeed, as indicated before, the absent subfractions, which would be numerically adjacent, were not tested due to unsuitable starting material. For this reason, the adjacent subfractions were considered the first available for performing the *in vitro* testing.
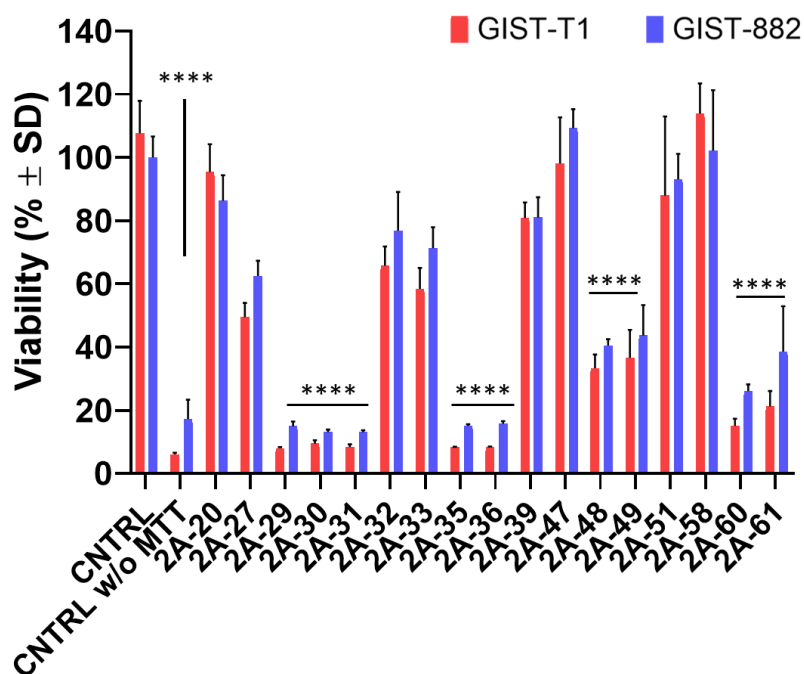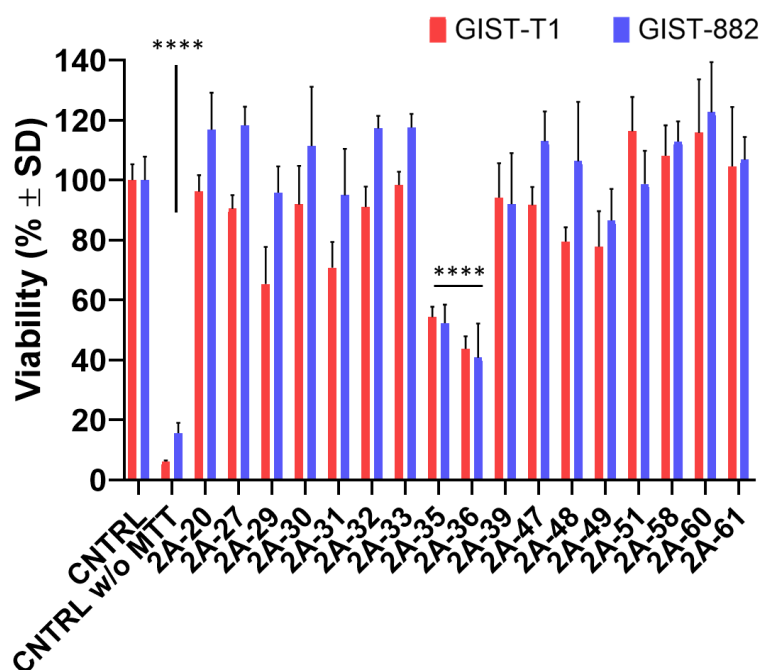
Figure 11. Among 61 FR2-A derived subfractions, only nine impaired the viability of GIST-T1 and GIST-882 cells. The graphs show the effect promoted by seventeen subfractions. They include all active subfractions and the adjacent weakly or non-active. Cell viability was assessed 24h after treatment using the MTT assay. The viability is expressed in % ± SD with respect to Control. The graph at the top of the figure includes 30 µg/mL treatments, while the graph at the bottom shows that at 6 µg/mL. CNTRL (Control) means 0.1% DMSO treated sample. CNTRL w/o (without) MTT means the CNTRL sample in which no MTT reagent was added, representing, for this reason, the assay limit of detection (LOD). Adjusted p-value **** <0.0001 compared to CNTRL (one-way ANOVA and Dunnett's Multiple comparison test). A representative experiment among three experimental replicates is shown.

3.1.9. FR2-A active subfractions target both GIST cells and lymphocytes

Notably, the nine active FR2-A derived subfractions constitute four groups of in-series active subfractions, suggesting that, despite such differences in TLC profiles, they could harbor the same bioactive compound. Based on this assumption, we combined active contiguous subfractions to constitute 4 clusters (C.2A-29-31/C.2A-35-36/C.2A-48-49/C.2A.60-61). The toxicity of FR2-A derived clusters was evaluated in lymphocytes from the peripheric blood (PBMCs), a healthy cellular model. Thus, PBMCs and GIST-T1 were treated with the established clusters at 30 µg/mL, while 2A-20 was used as a negative control since it was not active in GIST cells (Figure 12A). Clusters similarly affected the viability of resting lymphocytes and GIST-T1, suggesting that phytochemicals in the clusters could target via a non-specific mechanism of action. Despite the highlighted cytotoxicity, clusters showed a chemotherapeutic-like activity since traditional chemotherapy is commonly non-specific. For example, doxorubicin, a chemotherapeutic successfully used in clinics to treat numerous solid tumors, is frequently associated with myelosuppressive side effects in clinics. In agreement with this statement, doxorubicin also impaired PBMC viability, similar to that shown for 2A clusters (Figure

12B). This supports the concept that phytochemicals in the 2A clusters could belong to the class of chemotherapeutics.
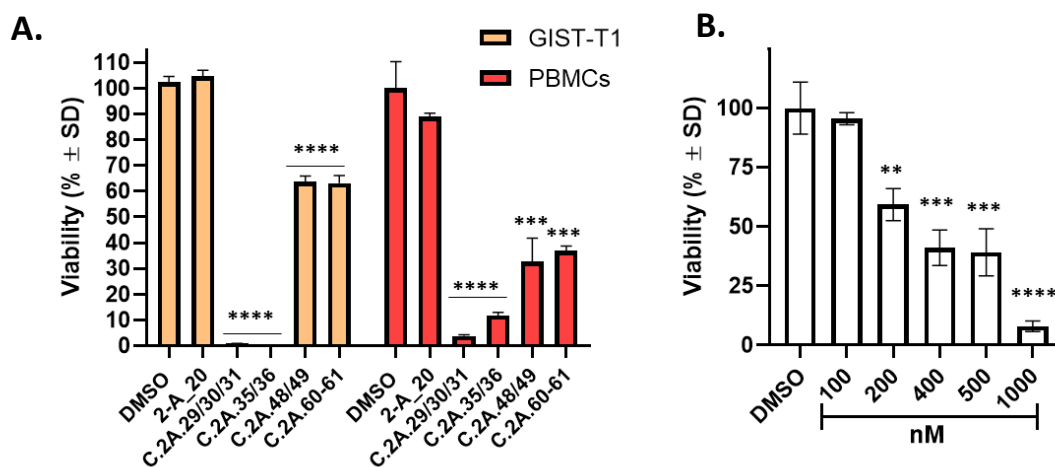
Figure 12. *In vitro* **toxicity of FR2-A derived clusters A.** Evaluation of the viability of GIST-T1 cells and PBMCs after the treatment with 2A clusters (30 μg/mL). 2A-20 fraction was used as a negative control. Cells were treated for 24h. The viability was calculated based on the number of viable cells estimated through Guava® ViaCount™ staining and flow cytometry. The viability is expressed in % ± SD with respect to GIST-T1 DMSO **B.** PBMCs were treated with different doses of doxorubicin, and viability was assessed after 24h through Guava® ViaCount™ staining and flow cytometry. The viability is expressed in % ± SD with respect to DMSO. For both Adjusted p-values compared to DMSO: ** <0.01, *** <0.001, and **** <0.0001 (one-way ANOVA and Dunnett's Multiple comparison test).

3.1.10. FR2-A active subfractions harbor pyrogallol-bearing compounds

The nine active subfractions were individually analyzed through ^{1}H NMR to identify the phytochemicals responsible for the pharmacological activity. The adjacent weakly- or non-active subfractions were also included in the analysis. ^{1}H NMR revealed that all active subfractions exclusively harbored pyrogallol-bearing phytochemicals that could be the bioactive compounds. In detail, the most potent subfractions, 2A-35 and 2A-36, which constituted C.2A-35-36, analogously contained gallic acid and the flavonoid myricetin hexoside (Figure 13A). Instead, the presence of galloyl arbutin characterized the adjacent weakly-active 2A-39. The galloyl moiety could promote the weak activity observed since 2A-20, the fraction used as a negative control, contained β-arbutin as a prevalent compound and was, according to our result, non-active. Despite lower concentration, 2A-33 also contained gallic acid, which could explain its weak activity. Regarding C.2A-60-61, a further pyrogallol-bearing compound, trigalloyl-glucose, was detected in 2A-60 and 2A-61 (Figure 13B). Neither trygalloyl-glucose nor additional pyrogallol-bearing compounds were identifiable in the adjacent non-active 2A-58. In line with these observations, both 2A-48 and 2A-49 harbored gallocatechin, while the adjacent non-active 2A-47 contained catechin, an analogous molecule without the pyrogallol moiety, supporting the critical role of the pyrogallol moiety again (Figure 13C).

Interestingly, different from the adjacent non-active fractions, 2A-29, 2A-30, and 2A-31 exclusively contained fumaric acid and a pyrogallol-bearing compound, of which the entire structure remains unknown (Figure 13D).

A.
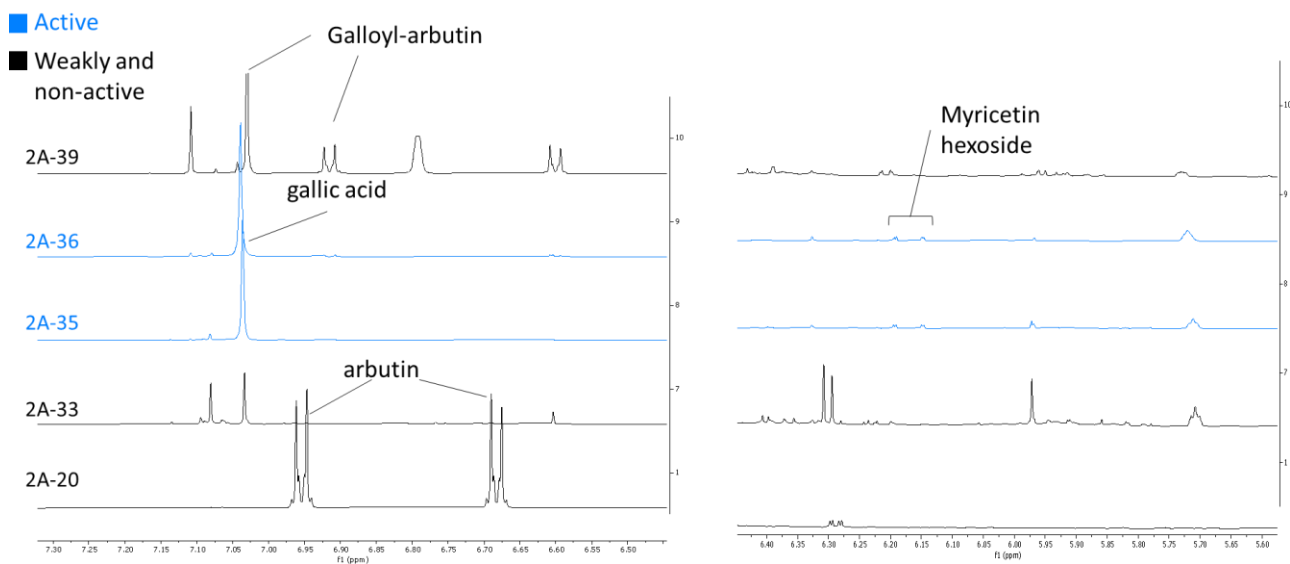
B.
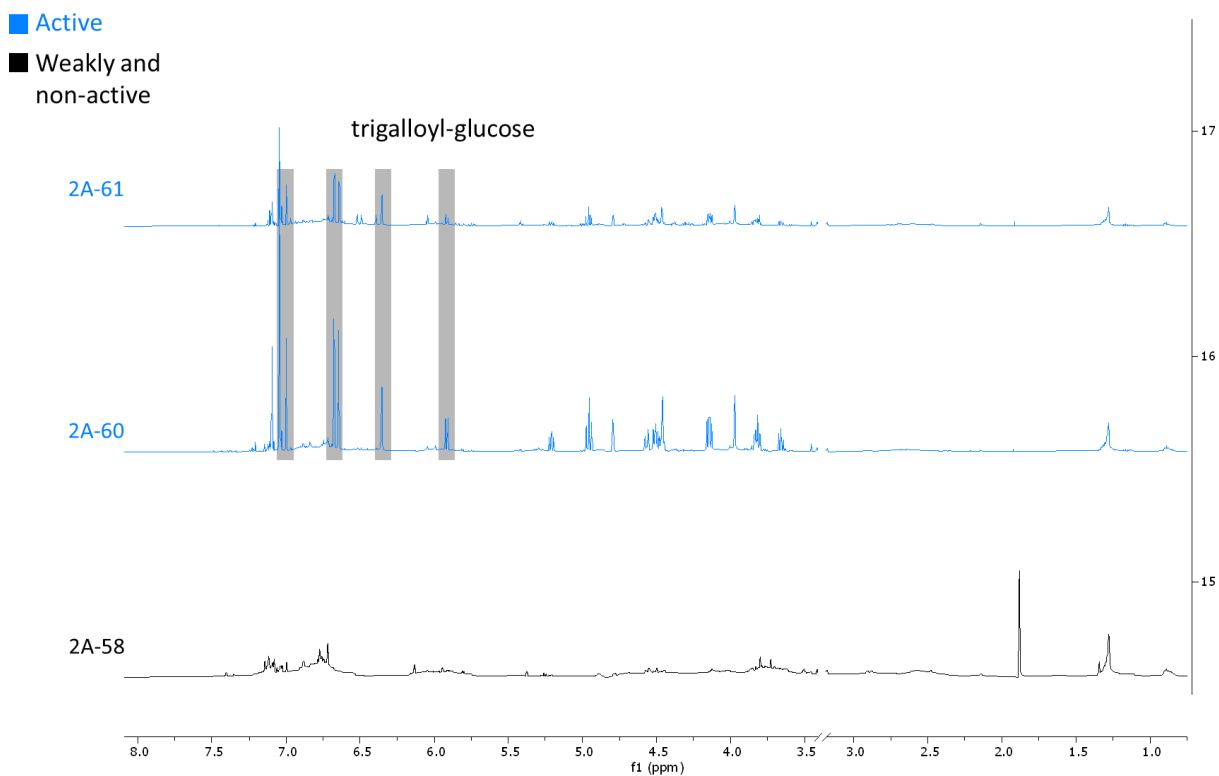
C.
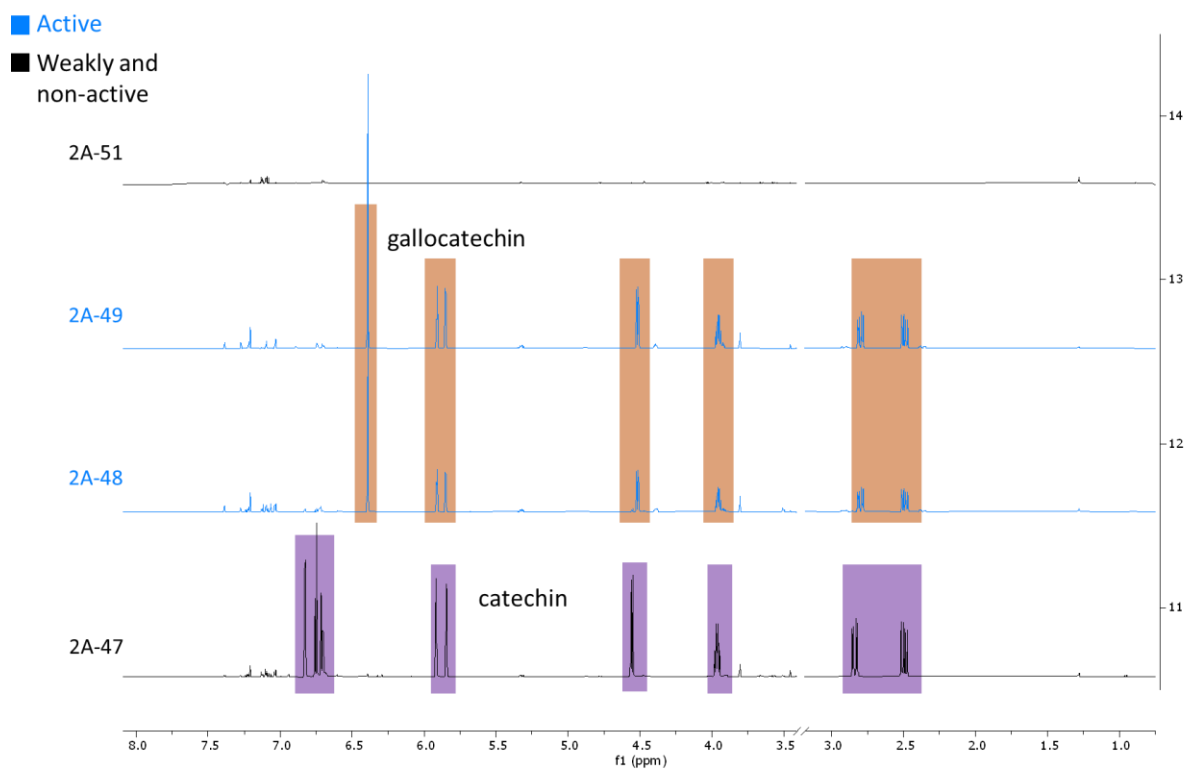
D.
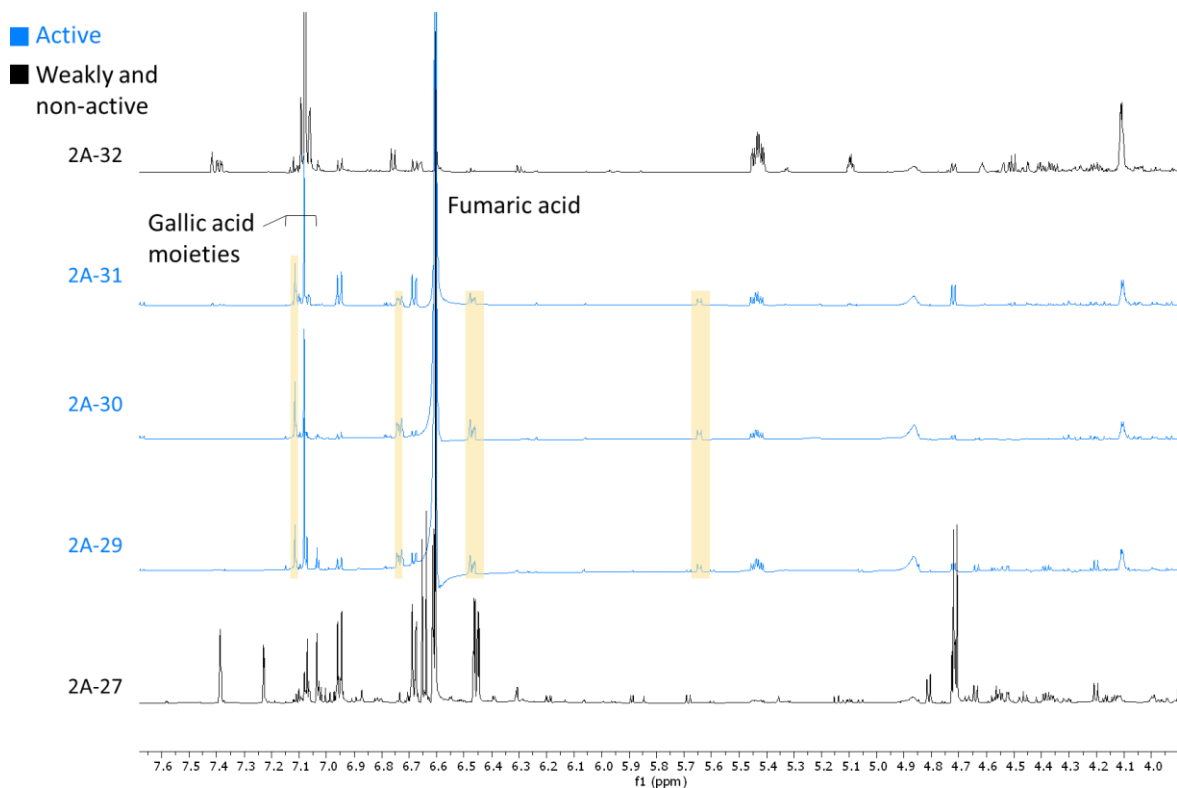
Figure 13. ^{1}H NMR spectrum of the active subfractions (in blue) with respect to those weakly- or non-active (in black) in each cluster. **A.** The spectra of 2A-35 and 2A-36 compared to 2A-33, 2A-39, and 2A-20 **B.** The spectra of 2A-60 and 2A-61 compared to 2A-58 **C.** The spectra of 2A-48 and 2A-49 compared to 2A-47 and 2A-51. **D.** The spectra of 2A-29,2A-30,2A-31 with respect to adjacent 2A-27 and 2A-32.

3.1.11. Gallic acid contributes to the pharmacological activity promoted by 2A-35

With myricetin hexoside, gallic acid characterized the most active subfractions derived from FR2-A, 2A-35, and 2A-36. In addition, it was reported to promote apoptosis in pancreatic cancer models (Kim et al., 2023). For this reason, we tested gallic acid as mono-treatment with respect to 2A-35 in both GIST-T1 and GIST-882. Although gallic acid and 2A-35 showed a similar effect at 30 µg/mL, a significant difference was observed at 6 µg/mL (Figure 14). GIST-882 viability was not impaired by gallic acid at 6 µg/mL, and it is only faintly (about 25%), but not significantly, reduced in GIST-T1. Differently, 2A-35 affected the viability of both GIST-882 and GIST-T1 by about 50% (p-value < 0.0001), indicating a higher activity in GIST cells than gallic acid. Therefore, considering that the tested concentration of gallic acid was arguably higher than that currently present in 2A-35, data supported the statement that acid gallic could promote an effect in concert with other phytochemicals in 2A-35.
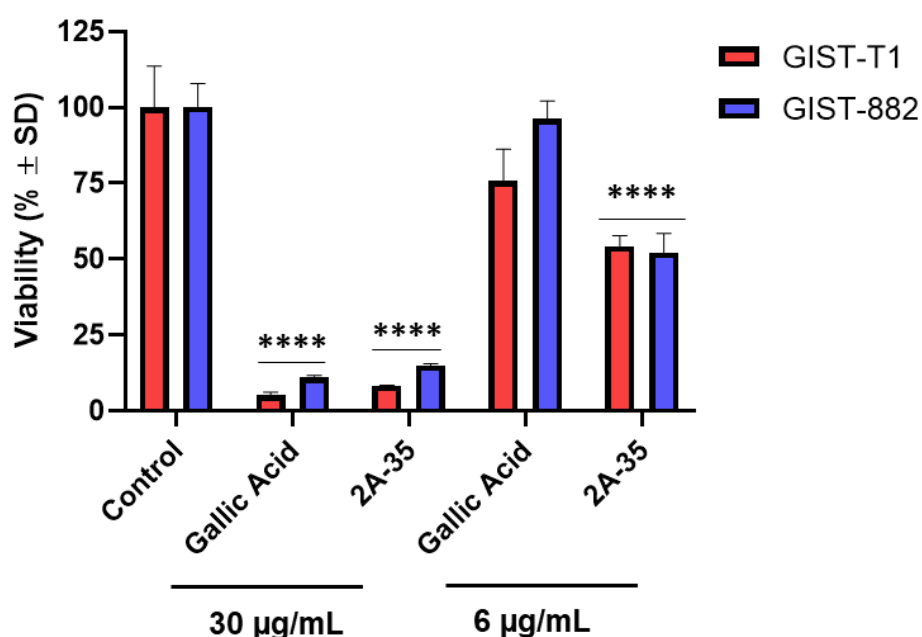
Figure 14. The gallic acid in GIST-882 and GIST-T1 cells. The cell viability after gallic acid and 2A-35 treatments was measured by MTT assay. Cells were treated for 24h. Both gallic acid and 2A-35 were used at 30 and 6 µg/mL. Viability is expressed in % ± SD with respect to the Control. Adjusted p-value *** <0.001, ****<0.0001 (One-way ANOVA-Dunnett's Multiple comparison with respect to Control). A representative experiment among two experimental replicates is shown.

3.2. An *in vitro* model for the study of metastasis in GISTs

3.2.1. GIST-T1 cells spontaneously give rise to viable cells in suspension

As reported by Vargas-Accarino and co-authors, certain adherent cells can spontaneously detach from the surface of a cell culture plate, survive in suspension, and re-attach if seeded in a new one, thus mimicking specific steps of the metastatic cascade *in vitro* (Vargas-Accarino et al., 2021). Therefore, to identify an analogous model for metastasis in GISTs, we investigated if a GIST cell line could recapitulate this behavior. Experiments were first focused on GIST-T1, an adherent cell line established from a metastasis related to a primary GIST (Taguchi et al., 2002). Since numerous cellular elements were observed in suspension during cell culture, we hypothesized that certain viable cells could colonize a new culture plate. Interestingly, a few adherent circular cells were observable among elongated, the canonical phenotype of these mesenchymal cells *in vitro* (Figure 15A). Hence, we speculated that the attached circular cells could derive from the elongated, be weakly attached to the plate surface, and represent the progenitor of viable cells in suspension. To validate our hypotheses, GIST-T1 cells were divided into three subpopulations: i) "Suspension", consisting of viable cells suspended in the culture medium; ii) "Semi-Adherent", which included circular cells that could be collected with a culture medium rinse; iii) "Adherent", consisted of elongated cells which were firmly attached to the plate surface and require Trypsin-EDTA solution for detaching (Figure 15B). The same division was performed in GIST-882 and GIST-48 cells as non-metastatic GIST models.
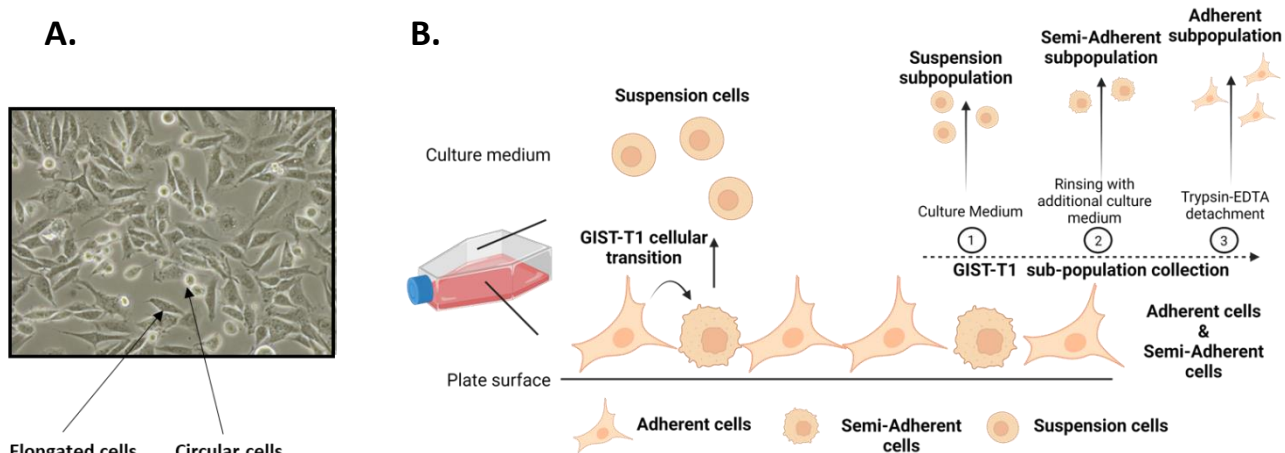
Figure 15. Evaluation of GIST-T1 as a model of *in vitro* metastasis A. GIST-T1 gave rise to circular-shaped cells during cell culture. Pictures were taken 72h after cell seeding (10X brightfield microscopy picture). **B.** The proposed model of

transition between GIST-T1 adherent and suspension cells. As detailed in the picture, GIST-T1 cells were divided into three different sub-populations: 1) "Suspension"; 2) "Semi-Adherent"; 3) "Adherent".

The number of viable cells was estimated in each subpopulation up to 72h after seeding (Figure 16). Viable cells in GIST-T1 Suspension subpopulation gradually increased over time, while no increase was highlighted in those collected from GIST-882 and GIST-48. According to the cell doubling times (d_t), GIST-T1 and GIST-882 Adherent subpopulations proliferated (d_t between 48h and 72h). As expected, no complete cellular replication was observed in GIST-48 Adherent (d_t=96h). Even though GIST-T1 adherent cells proliferated, the number of viable cells in the Semi-Adherent subpopulation was stable along the experimental time points. This indicated that adherent cells didn't accidentally lose contact with the plate surface due to the rinsing with the culture medium.
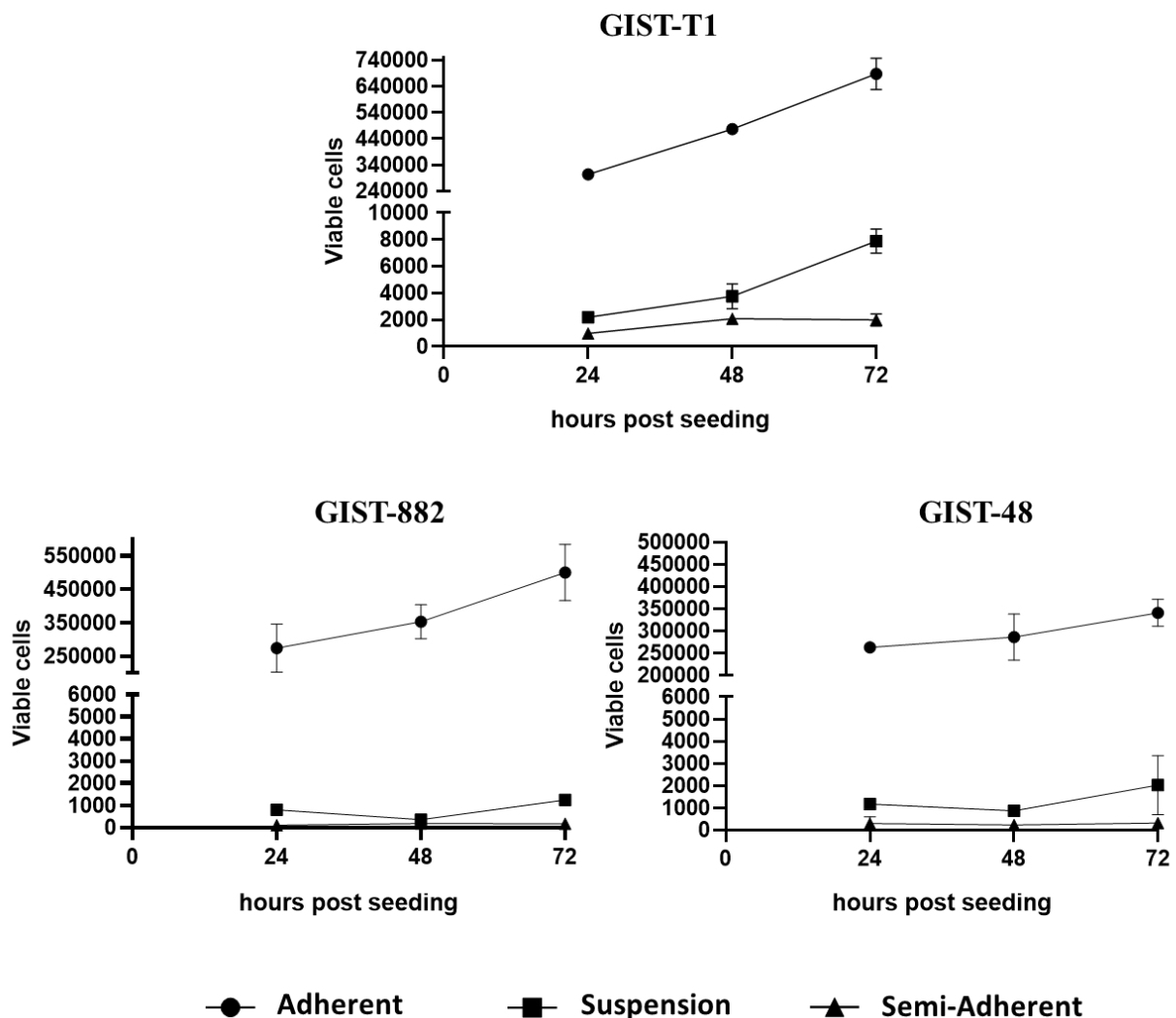
Figure 16. A. Adherent, Suspension, and Semi-Adherent subpopulations in GIST-T1, GIST-882, and GIST-48. The number of viable cells was monitored between 24h and 72h post-seeding in each subpopulation. Viable cells were estimated through Guava® ViaCount™ and flow cytometry. As indicated, this reagent uses a viability dye, which selectively labels dead cells due to altered membrane permeability and excludes them from the count of viable cells.

The number of viable cells ± Standard deviation (SD) is shown in each graph. A representative experiment among an experimental triplicate is shown.

Suspension and Semi-Adherent subpopulations represented a small percentage compared to the corresponding Adherent measured at 24h (Supplementary Figure 4). Indeed, GIST-T1 Suspension subpopulation represented approximately 2.5%, while the percentage of GIST-T1 Semi-Adherent remained stable at around 0.5-1% in all investigated time points. Suspension and Semi-Adherent from GIST-882 and GIST-48 were much less detected than GIST-T1 counterparts, not exceeding a percentage of about 0.5%.

Since the exclusion of dead cells led to the estimation of "viable" cells, the possibility that cells classified as viable could be apoptotic was examined. Therefore, each subpopulation was labeled with fluorescent Annexin V and 7-AAD, a method to differentiate early apoptotic from viable or dead cells. The "death profile" of Suspension and Semi-Adherent subpopulations, both collected 72h after GIST-T1 seeding, showed the presence of cellular events with an analogous size to viable cells in the Adherent subpopulation, but an Annexin-V (+) /7-AAD (-) staining (Figure 17). Thus, these data indicated that the previously calculated number of viable cells was partially overestimated. Despite this consideration, the percentage of viable cells in GIST-T1 Suspension subpopulation remained high, at about 42%. This percentage was lower in GIST-882 and GIST-48, reaching about 10% and 28%, respectively (Supplementary Figure 5).
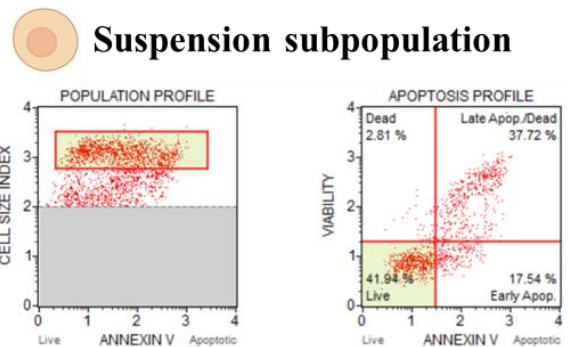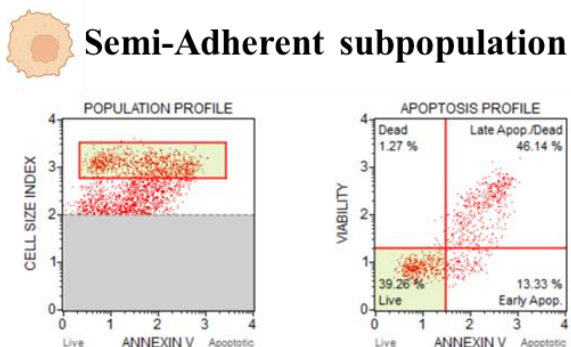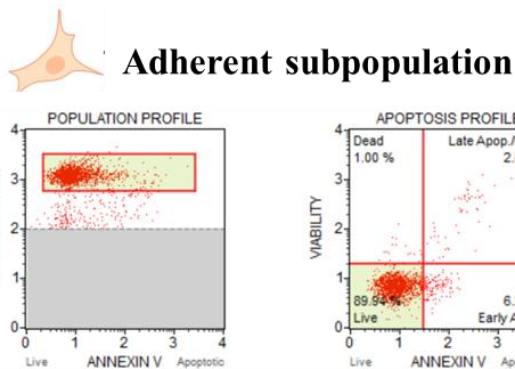
3.2.2. Viable cells in suspension re-attach and colonize a new cell culture plate

Consistent with Vargas-Accarino et al., GIST-T1 viable cells in suspension could settle down and grow again if seeded in a new cell culture plate. However, despite the lower number, viable cells in suspension were also collected from non-metastatic GIST-882 and GIST-48. Therefore, Suspension subpopulations from each cell line were moved in a new 24-well cell culture plate with fresh medium (Figure 18). Notably, to seed an analogous number of viable cells from each cell line, two dilutions of GIST-T1 Suspension subpopulations (1:6 and 1:36) were also tested. As testified by crystal violet staining and brightfield microscopy pictures (10 days after seeding), viable cells in suspension from GIST-T1, named for convenience "suspension cells" from now on, re-attached and proliferated. Interestingly, growing colonies were also observed in both diluted samples, suggesting that a smaller GIST-T1 Suspension subpopulation could similarly lead to colonizing a new cell culture plate. No attached cells and growing colonies were observed when GIST-882 and GIST-48 Suspension subpopulations were seeded, corroborating their non-metastatic origin. Thus, although viable cells could be observed in suspension from GIST-882 and GIST-48, they could be only transiently viable, already directed towards cell death, or unable to re-attach and complete *the in vitro* metastatic-like process.
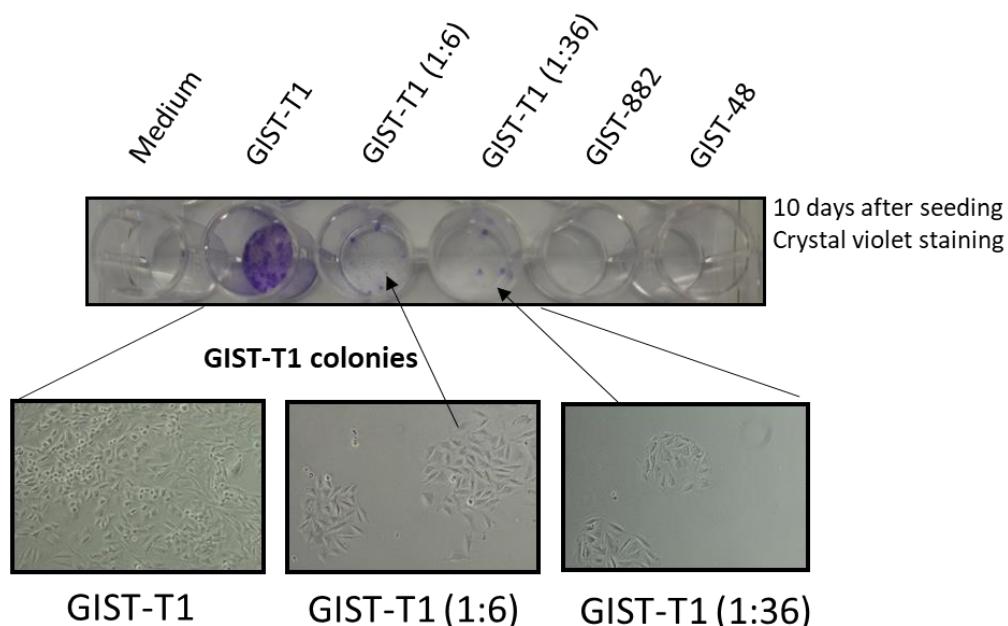
Figure 18. GIST-T1 viable cells in suspension can colonize a new cell culture plate. The re-attachment of suspension cells and their growth as adherent were evaluated. Colonies were identified by crystal violet staining and brightfield

microscopy pictures 10 days after seeding. Pictures (10X magnification) were taken immediately before crystal violet staining was performed. Medium, the control sample, means fresh medium without cells. A representative experiment is shown among three experimental replicates.

3.2.3. Suspension cells originate from a small clonal population in GIST-T1

Since suspension cells represented a small percentage compared to adherent (Supplementary Figure 4), we hypothesized that they could originate from a small clonal population in GIST-T1, classified as "metastatic-like". In addition, we also supposed that newly adherent cells, derived from the re-attachment and colonization of suspension cells, could give rise to novel suspension cells in turn. If both hypotheses were confirmed, harvesting and seeding suspension cells could enrich the "metastatic-like" population, leading to a subline with an improved capability to produce suspension cells and sustain the *in vitro* metastasis model.

To evaluate this hypothetical scenario, GIST-T1 Suspension population was collected 72h after seeding and moved into a new cell culture plate. We then grew the re-attached cells up to confluency and named them Adherent-F1-GIST-T1 (Adh-F1-T1). As shown in Figure 19A, seeding of suspension cells from Adh-F1-T1 led to more intense crystal violet staining than the progenitor GIST-T1, indicating a higher number of re-attached cells. Moreover, the result showed that Adh-F1-T1 preserved the capacity to originate suspension cells.

Applying an analogous workflow, we attempted to establish a subline with the maximum ability to recapitulate the *in vitro* metastatic model. Thus, through the serial collection and seeding of suspension cells, further sublines were established up to the genesis of Adh-F4-T1. Seeding of suspension cells from Adh-F3-T1 and Adh-F4-T1 led to an analogous crystal violet-related signal, suggesting the achievement of a plateau (Figure 19B). Moreover, the signals were higher than those from GIST-T1 and Adh-F1-T1, indicating a further increase in re-attached cells. We then evaluated if the increase of re-attached cells was ascribable to a higher number of suspension cells in the culture medium of Adh-F4-T1 or a slower re-attachment of those derived from progenitor GIST-T1. In response to this question, 4 times more viable cells were detected in the Suspension subpopulation from Adh-F4-T1 with respect to GIST-T1 (Figure 19C). In contrast, the seeding of an equal number of viable cells in suspension only led to a faint increase in crystal violet staining (<25%) (Figure 19D). Therefore, both results confirmed that the increase of re-attached cells was mainly related to the capacity of Adh-F4-T1 to originate more suspension cells than the progenitor GIST-T1. Thus, "metastatic-like" cells were enriched by serial collection and seeding of suspension cells. This corroborated the statement that only a few subclones give rise to suspension cells in GIST-T1.
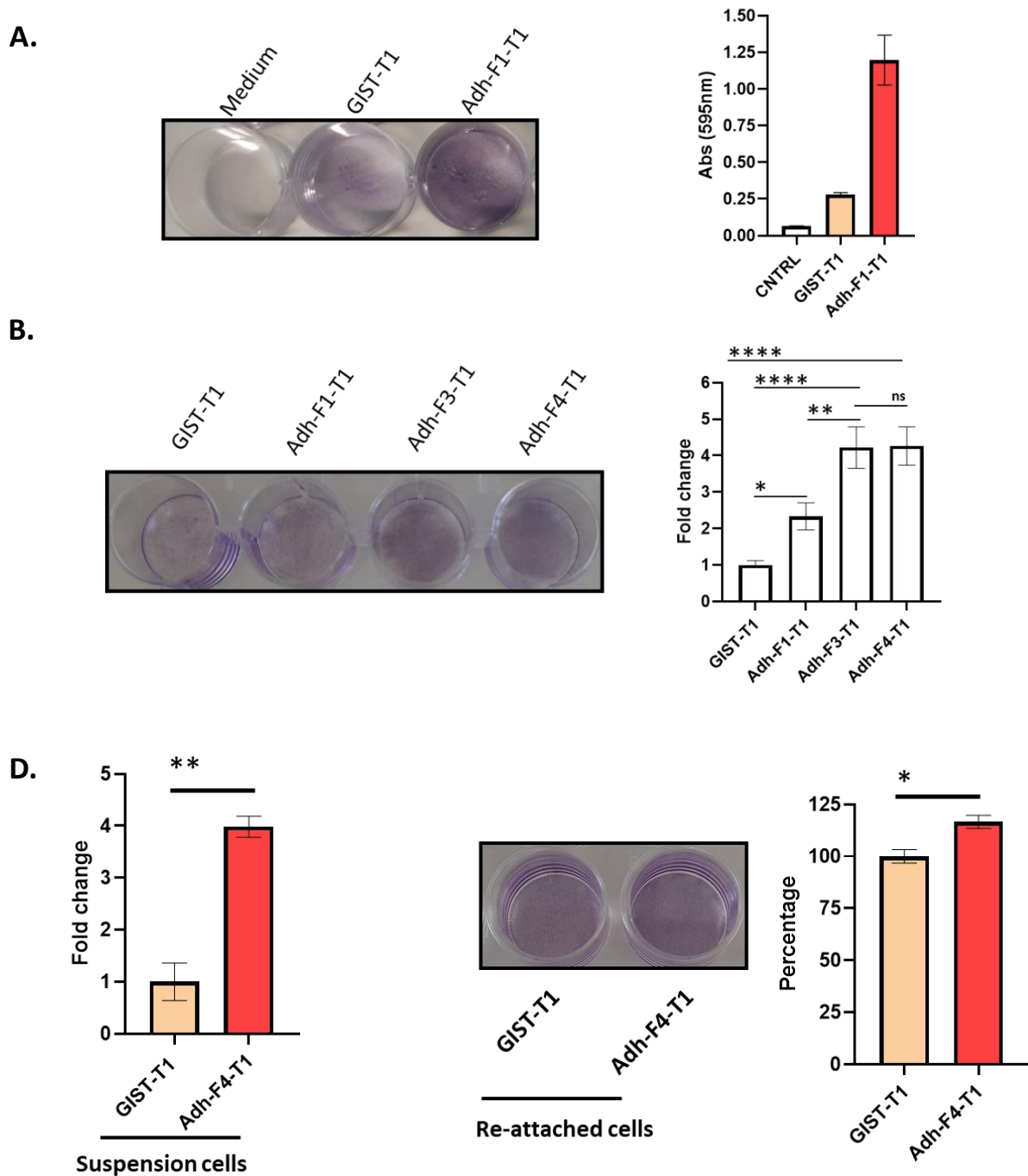
Figure 19. Serial collection and seeding of suspension cells lead to establishing sublines with a higher propensity to originate suspension cells A. Suspension cells were collected from progenitor GIST-T1 or Adh-F1-T1 72h after seeding. They were then seeded, and the capability to re-attach was measured through crystal violet staining the day after seeding. Crystal violet signal was measured after its solubilization and reading the absorbance at 595 nm. Absorbance at 595 nm ± SD is shown in the graph. Medium represents a negative control in which no cells were seeded **B.** Evaluation of the number of suspension cells from GIST-T1, Adh-F1-T1, Adh-F3-T1, or Adh-F4-T1 that can newly re-attach. Fold change with respect to GIST-T1 progenitor ± SD is shown. Adjusted p-value *<0.05, ** <0.01, ****<0.0001; "ns" means non-significative (One-way ANOVA-Tuckey's Multiple comparison test). **C.** Viable cells in suspension from GIST-T1 and Adh-F4-T1 were estimated through Guava® ViaCount™ and flow cytometry 72h after seeding. Fold change with respect to GIST-T1 ± SD is reported. Unpaired t-test; p-value * <0.05, ** <0.01 **D.** Seeding equal viable cells from GIST-T1 or Adh-F4-T1 Suspension subpopulations. The graph shows the fold change (± SD), calculated starting from the crystal violet-related absorbance. Unpaired t-test; p-value ** <0.01.

3.2.4. Suspension cells originate from circular-shaped cells

The brightfield pictures of GIST-T1 and the derived sublines, taken 72h after seeding of an analogous cell number, revealed the presence of more circular-shaped cells in sublines, especially in Adh-F3-T1 and Adh-F4-T1, with respect to GIST-T1 (Figure 20A). This was in line with the hypothesis of the circular phenotype as the progenitor of suspension cells since there was a correlation between the number of circular cells and the capacity to originate suspension cells, supporting the concept that detaching could involve cells with this phenotype. Notably, the cell viability of Adherent subpopulations, including that we initially classified as Semi-Adherent, was analogous among GIST-T1 and derived sublines (>90%), indicating that circular-shaped status was not linked to phenomena associated with cell death (data not shown).

To confirm the hypothesis that the spontaneous detachment of cells involved circular-shaped cells, we monitored what occurred in Adh-F4-T1 by time-lapse microscopy. The time-lapse microscopy showed numerous circular-shaped cells that lost the attachment to the plate surface, moving to suspension immediately after a quick step in which cells started to vibrate, probably because of Brownian water movement in the presence of shallow attaching properties. Noteworthy, cells were not in a confluent state, indicating that the phenomenon was not stimulated by the absence of space for cell growth. An example is shown in Figure 20B. Three photograms, taken at the beginning, the middle, and the end of a 90-minute monitoring, display a circular cell (above the asterisk in the figure) that lost contact with the plate surface. The arrow in the last photogram highlights the cell, now in suspension, before leaving the microscope objective.

A.

GIST-T1	Adh-F1-T1
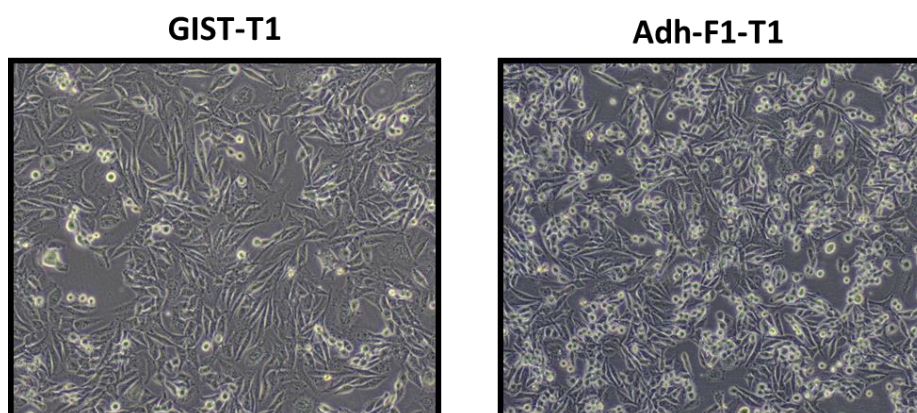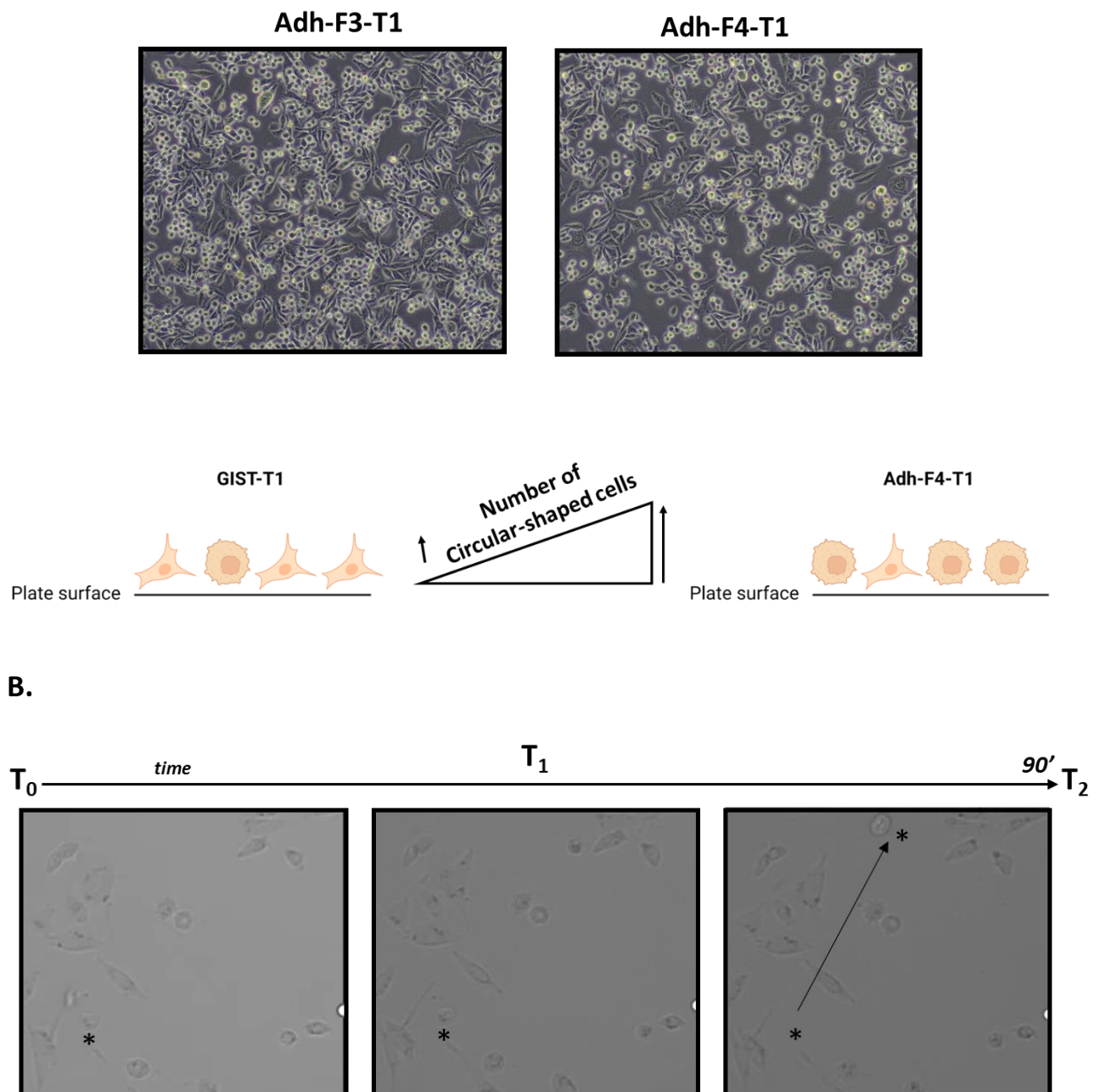
Figure 20. A. Brightfield microscopy picture of GIST-T1 and derived sublines. Pictures were taken 72h after seeding using 10X magnification. A representative area is shown. **B.** An example of circular cell detachment. The photograms show a circular cell (above the asterisk) that loses contact with the plate surface. The arrow indicated the movement of the cell, now in suspension, before leaving the microscope objective (10X magnification).

3.2.5. Re-attachment of suspension cells newly leads to elongated-shaped cells

The re-attachment of suspension cells from Adh-F4-T1 was similarly investigated through time-lapse microscopy. Suspension cells were observed in dynamic and free movement in the culture medium. They remained as single cells up to interaction with the surface of the cell culture plate. Indeed, the re-attachment of the first cells promoted the re-attachment of other cells, leading to colony constitution. Notably, once re-attached, they newly appeared in an elongated shape, confirming the

plasticity of these cells that could transiently modify the interaction with the plate surface passing through the circular and elongated states. An example is highlighted with the hash in Figure 21. No cells are initially present in the first photogram, but a colony of elongated cells can be observed 6h after the seeding of suspension cells. Moreover, a circular cell (indicated by the asterisk) is also present in the second photogram but not in the first, testifying the movement of suspension cells in the culture medium, which can still proceed even 6 hours after the beginning of the monitoring. This indicated that the attachment occurred with different kinetics and suggested that suspension cells needed to acquire specific properties to attach newly. Overall, the last photogram, taken 16h after the seeding of suspension cells, shows a preponderance of elongated-shaped cells with respect to those circular. Notably, this differs from the picture shown in Figure 20A, where more circular-shaped cells were observed. The difference between the two pictures is the experimental time point. Picture of Adh-F4-T1 in Figure 20A was taken 72h after seeding, while the photogram in Figure 21 was taken after 16h only. This suggested that cells acquire an elongated phenotype and then become available for a new transition toward the suspension status, passing through a circular-intermediate step.
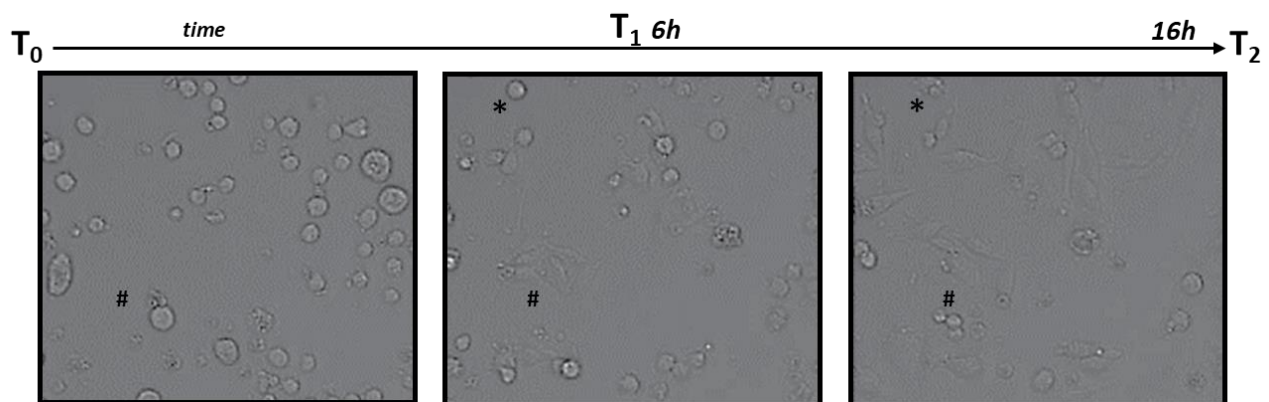
Figure 21. Reattachment of circular-shaped cells and transition toward an elongated phenotype. * highlights a circular-shaped cell in movement, absent in the first photogram. Instead, # indicates an area of the cell culture plate surface that is initially empty. This area is then colonized by cells with an elongated phenotype.

3.2.6. Adh-F4-T1 cells are still dependent on KIT oncogenic deregulation

Once the novel cell sublines were established, we wondered if they could still be KIT-dependent as reported for progenitor GIST-T1 (Noma et al., 2005; Tarn et al., 2006). Hence, we evaluated the effect of imatinib in Adh-F4-T1 with respect to the progenitor GIST-T1 (Figure 22). As shown, imatinib similarly impaired the viability of Adh-F4-T1 and GIST-T1 at 100 nM or 1 µM, suggesting that KIT continued to be the primary driver of Adh-F4-T1 cells. Moreover, this supported the concept that Adh-F4-T1 and GIST-T1 cells derive from the same ancestral progenitor.
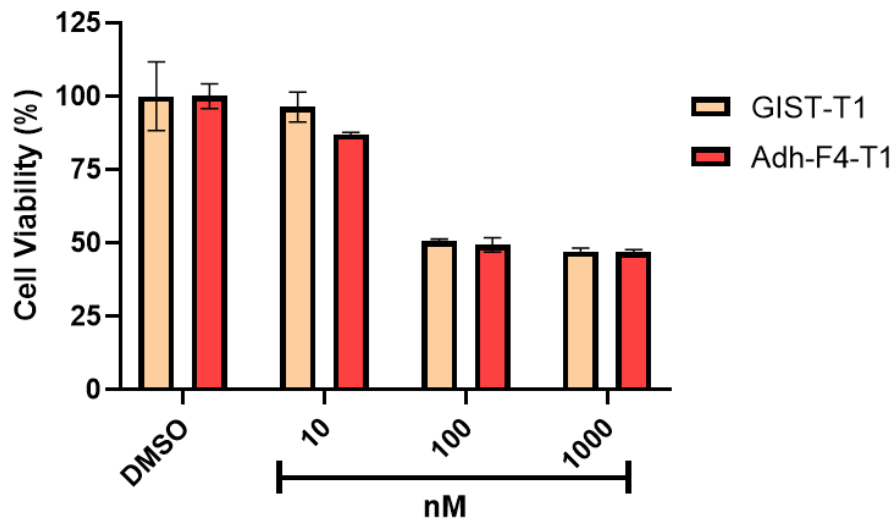
Figure 22. Imatinib similarly impairs viability in GIST-T1 and Adh-F4-T1. The drug treatment was maintained for 48h, and viability was measured with CCK-8. Cell viability (%) ± SD with respect to solvent-treated (DMSO 0.1%) cells. A representative experiment is shown among two experimental replicates.

3.2.7. A Poly-L-Lysine plate coating partially inhibits the rise of suspension cells

The "metastatic-like" cells in GIST-T1 and in the sublines spontaneously gave rise to suspension cells that re-attached in a new cell culture plate. However, the described model took place on the surface of standard cell and tissue culture-treated plates (TC plate), consisting of hydroxyl and carboxyl groups induced by the treatment of polystyrene hydrophobic plastic to be more hydrophilic. Hence, the surface could not correctly represent the extracellular matrix, thus promoting an artificial phenomenon of detaching. Therefore, the transition between adherent and suspension was evaluated in three experimental conditions: i) TC plate; ii) Gelatin-coated TC plate; iii) Poly-L-Lysine-coated TC plate.

Gelatin is a heterogeneous mixture of water-soluble and average/high molecular weight proteins derived from collagen. It is usually used to improve the attachment of various cell lines and is considered a better representation of the extracellular matrix. The Poly-L-Lysine coating is a nonspecific and artificial attachment factor for cells that weakly attach to the plate surface by enhancing electrostatic interaction between negatively charged ions of the cell membrane and the positive charge of L-Lysine amino acids on the plate surface. The last is widely recognized as among the stronger conditions to promote *in vitro* cell attachment.

Hence, Adh-F4-T1 cells were seeded in TC, Gelatin-coated TC, or Poly-L-Lysine-coated TC plates. As shown in Figure 23A, contrary to cells in the TC plate, the brightfield pictures taken 72h after the seeding revealed that the Poly-L-Lysine coating remarkably changes the phenotype of cells,

primarily in the elongated shape. Instead, no differences can be reported between the TC and Gelatin-coated TC plates, whose cells are mainly circular. Consistent with the brightfield pictures, which indicated a higher confluent state, the count of viable cells in the Adherent subpopulations confirms that more cells are attached in the presence of Poly-L-Lysine coating compared to those that were seeded in TC and Gelatin-coated TC plates (Figure 23B). At the same time, no differences were observed between these two. Notably, the percentage of viable cells in Adherent subpopulations was similar independently on the different plate surfaces (≈90%), indicating that no change in viability was induced by the coatings (data not shown).

Moreover, Suspension subpopulations were collected 72h after the seeding of Adh-F4-T1 on the three different cell culture surfaces. Estimating the viable cell number indicated a reduction of suspension cells when applying a Poly-Lysine coating. The reduction agreed with the higher number of attached cells, suggesting that this condition could partially counteract their spontaneous detachment. Accordingly, the seeding of suspension cells and crystal violet staining showed that the Poly-L-Lysine coating remarkably reduced, but did not prevent, the rise of suspension cells with respect to using a TC plate (Figure 23C). On the contrary, the seeding of Adh-F4-T1 in the TC or the Gelatin-coated TC plate led to the rise of an analogous number of suspension and re-attached cells (Figure 23B and 23C). This result indicated that Gelatin-based coating did not affect the rise of suspension cells, supporting the concept that spontaneous detachment could similarly occur in a more accurate extracellular matrix model.

A.
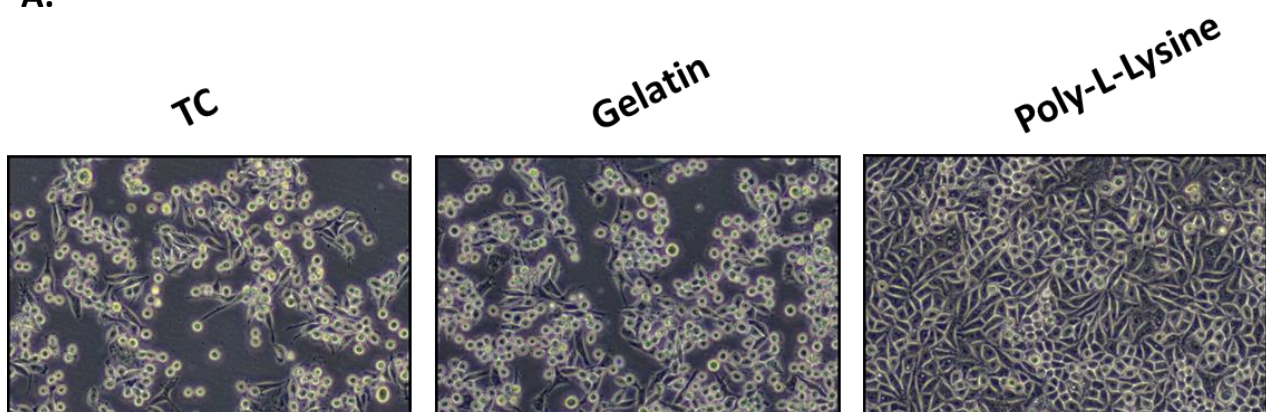
B.
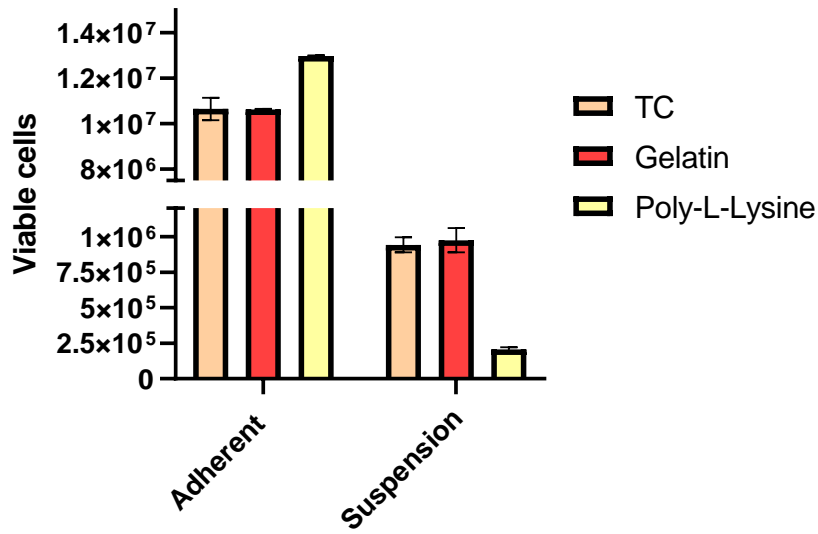
C.
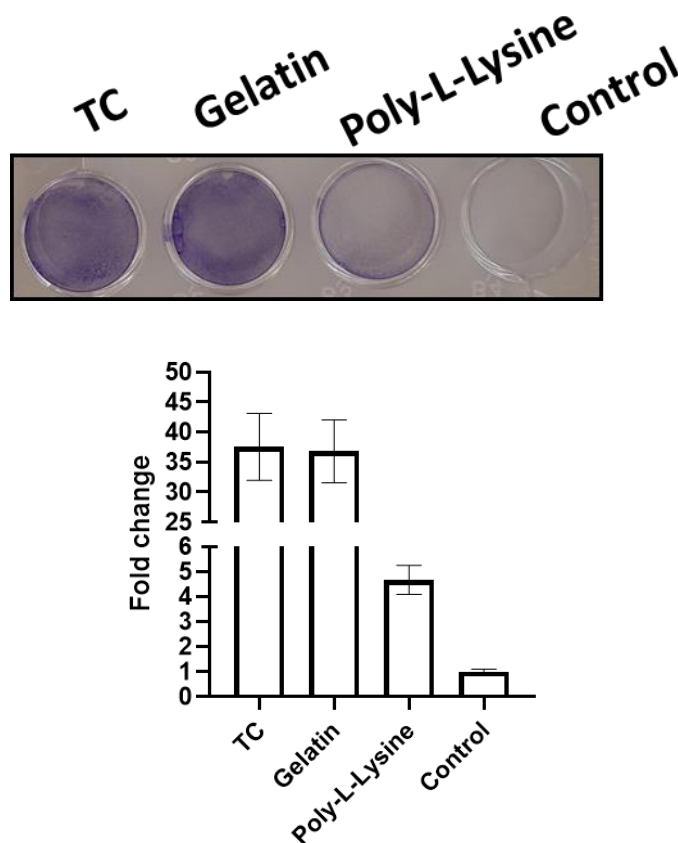
Figure 23. The Poly-L-Lysine coating could reduce but not prevent the rise of suspension cells. A. Brightfield pictures of Adh-F4-T1 cells seeded in standard TC, Gelatin-coated TC, and Poly-L-Lysine-coated TC plates. Pictures were taken 72h after seeding (10x magnification). **B.** Viable cells in Adherent and Suspension subpopulations from each experimental condition (± SD). **C.** The number of re-attached cells was estimated using Crystal violet staining (the day after seeding). Suspension cells were first collected from the medium of Adh-F4-T1 in TC, Gelatin-coated TC, or Poly-L-Lysine-coated TC plates and then seeded in a 12-well standard TC plate. The graph shows the fold change calculated from the crystal violet-related absorbance with respect to the Control sample (± SD).

3.2.8. Suspension cells survive in a forcibly suspended condition

Resistance to anoikis (detachment-induced cell death) is a widely recognized feature of metastatic cells that can survive without interactions with the extracellular matrix and surrounding cells (Buchheit et al., 2014).

Therefore, we evaluated if suspension cells from Adh-F4-T1 could survive in these conditions. Suspension cells were collected 72h after seeding and equally split in TC or 2% agar-coated TC plates (Figure 24A).

The agar-based coating impeded the re-attachment of suspension cells, maintaining them in a forcibly suspension condition and mimicking the absence of extracellular interactions. Indeed, only a few cells were observed as adherent in the presence of the agar-based coating. Non-treated cell culture plates, typically used for the growth of suspension cells, were inefficient because numerous floating cells could likewise adhere to the surface of the non-treated TC plate (data not shown).

Suspension cells immediately seeded in the TC plate were stained with crystal violet the day after seeding. On the contrary, those seeded in the 2% agar-coated TC plate were forcibly maintained in suspension for 72 hours. Cells were then harvested and seeded in the TC plate, and crystal violet was analogously performed the day after seeding. As shown in Figure 24B, no significant differences were observed between crystal violet-related signals, indicating that a similar number of both suspension subpopulations could re-attach. Therefore, cells forcibly maintained in suspension survived without interacting with the plate surface for 72 hours.

Interestingly, the survival of suspension cells for 72 hours suggested that the increasing number of viable cells in the Suspension subpopulation (previously shown in Figure 2) could also be related to an accumulation in the culture medium. Hence, we evaluated whether viable cells in suspension, capable of colonizing a new cell culture plate, were present 24h and 48h after GIST-T1 seeding. As shown in Supplementary Figure 6, certain suspension cells collected 24h and 48h after GIST-T1 seeding could already settle down and grow as colonies, supporting the concept that the genesis of suspension cells was a continuously activated process. Similar results were obtained with Adh-F4-T1 (data not shown)
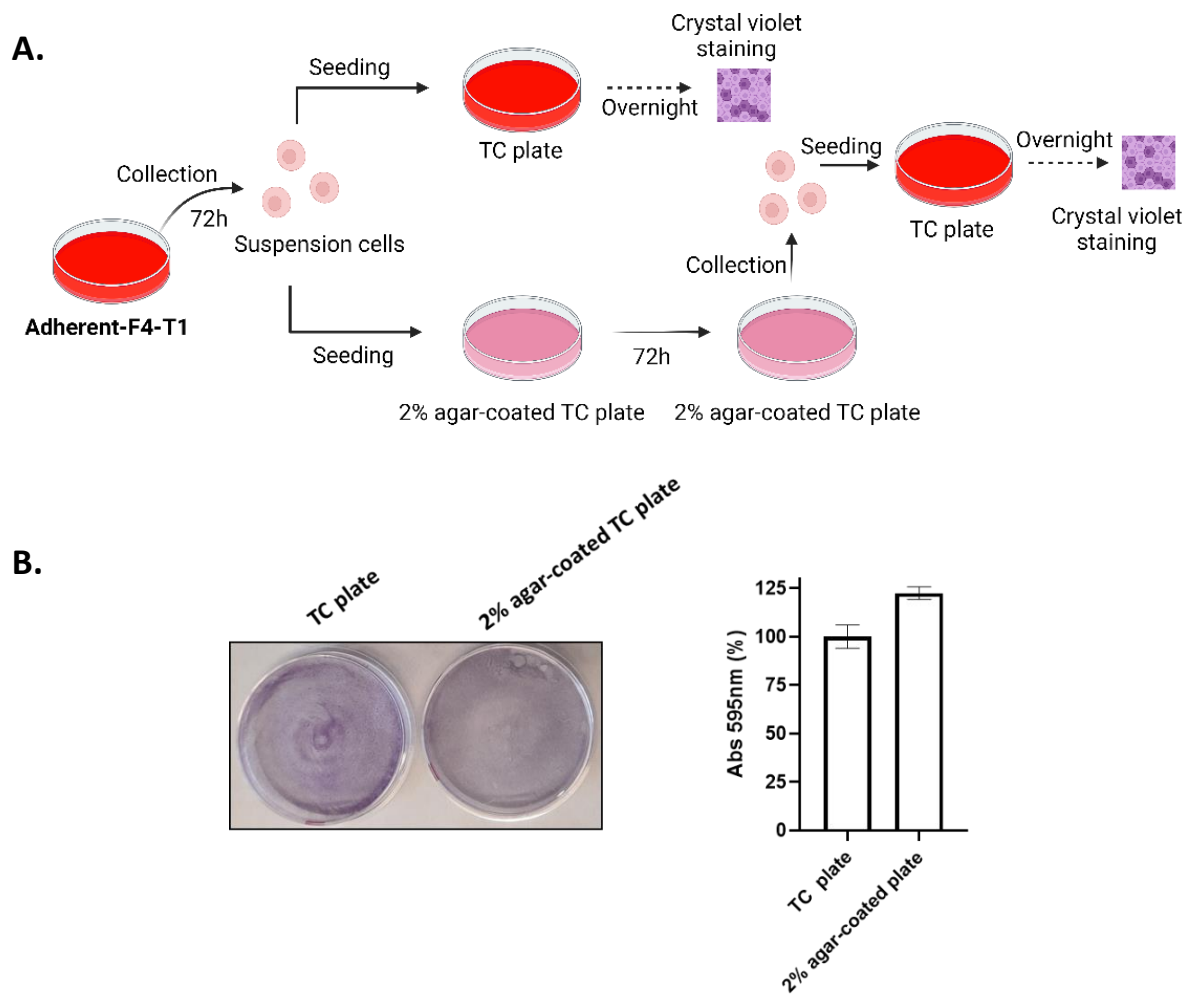
Figure 24. Suspension cells survived without contact with the TC plate A. Suspension cells were collected 72h after Adh-F4-T1 seeding, equally split, and seeded in two different p60 TC plates, with a 2% agar coating or without (TC plate). In the case of suspension cells immediately seeded in the TC plate, re-attached cells were revealed the day after using crystal violet staining. On the contrary, suspension cells in the 2% agar-coated TC plate were forcibly maintained in suspension for 72h. Cells were then harvested and seeded in a TC plate. Crystal violet staining was similarly performed the day after. Created with BioRender.com. **B.** A representative picture of crystal violet staining is shown (left panel). The absorbance at 595 nm of solubilized crystal violet is expressed in percentage ± SD with respect to the TC plate sample (graph on the right). A representative experiment is shown among two experimental replicates.

3.2.9. Conditioned medium has no role in the rise of suspension cells

To investigate the mechanisms that promoted the origin of suspension cells, we hypothesized that adherent cells could be affected by chemical or physical changes in the culture medium (conditioned medium) facing a transient "omic" reprogramming. For example, it was supposed that mediators could be released into the medium during cell culture, acting as autocrine or paracrine factors. Analogously, some nutrients could be consumed or degraded, triggering adaptive mechanisms to seek better microenvironmental conditions for cellular growth. This hypothesis could explain why suspension cells were newly attached and grew in a new cell culture plate in a fresh medium, which lacked mediators excreted by growing cells and was richer in nutrients. To validate this thesis, the

number of suspension cells originating in the presence of conditioned or fresh medium was assessed (Figure 25A). Fresh medium was replaced every 24h, while the conditioned was left for 72h. No statistical differences were observed in cell number among the Suspension and Adherent subpopulations, indicating that the conditioned medium did not increase the number of viable cells in suspension or affect the viability of adherent cells. Consistent with this conclusion, the seeding of suspension cells collected in the conditioned medium and those in the fresh originate an analogous number of growing colonies (Figure 25B).

Despite the absence of an effect on the transition between adherent and suspension cells, we wondered if the conditioned medium could have a role in maintaining cells in suspension, thus negatively regulating the opposite transition, that from suspension to adherent. Therefore, suspension cells were collected 72h after seeding and split into two TC plates in fresh or 72h conditioned medium. Interestingly, as shown in Figure 26 (left panels), crystal violet staining displays that suspension cells that re-attached were remarkably less if they were seeded in the conditioned medium than in the fresh medium. Moreover, brightfield microscopy revealed that re-attached cells in the fresh medium appeared mainly to be elongated, in line with the expected shape of Adh-F4-T1 (previously shown in Figure 21), suggesting that the transition between suspension and adherent is proceeding (panels in the middle). On the contrary, attached cells in the conditioned medium are predominantly circular. Hence, data support that fresh medium could promote a stronger re-attachment to the plate surface or accelerate the transition toward adherent cells. On the other hand, the 72h conditioned medium could prevent their re-attachment, maintaining cells in suspension.
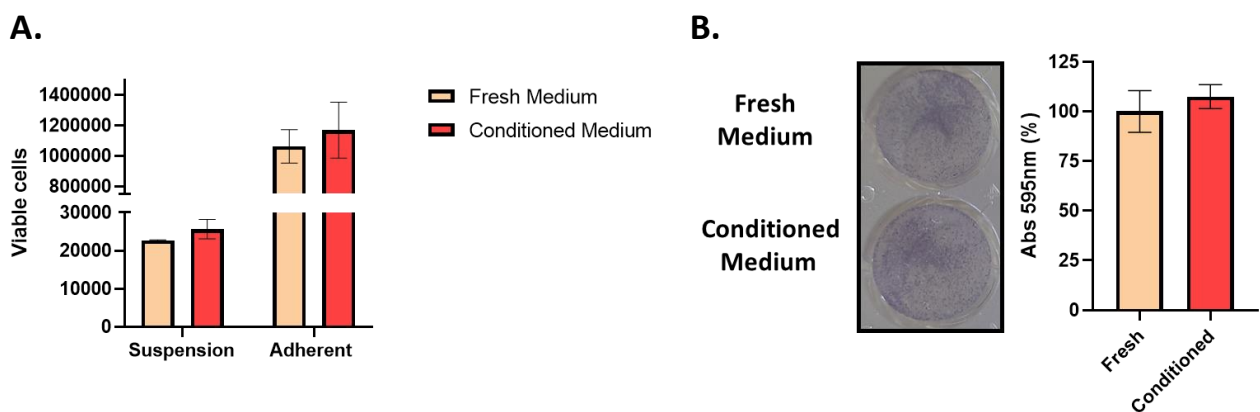
Figure 25. A. The conditioned medium did not stimulate the rise of floating cells. Suspension cells were collected 72h after Adh-F4-T1 seeding in the presence of the conditioned or fresh medium. This last was replaced every 24h. "Conditioned medium" means the culture medium in which Adh-F4-T1 cells grew during the experimental procedure.

The number of viable cells (± SD) in Suspension and Adherent subpopulations is shown. **B. An analogous number of suspension cells are re-attached independently if they originate in the conditioned or fresh medium**. Suspension cells were collected from Conditioned and Fresh Medium samples and seeded in a 24-well plate. Growing colonies were then evaluated 12 days after seeding through crystal violet staining. An example of crystal violet staining among a technical triplicate is shown. Absorbance at 595 nm (%) ± SD with respect to the Fresh sample is reported in the graph on the right. A representative experiment is shown among two experimental replicates.
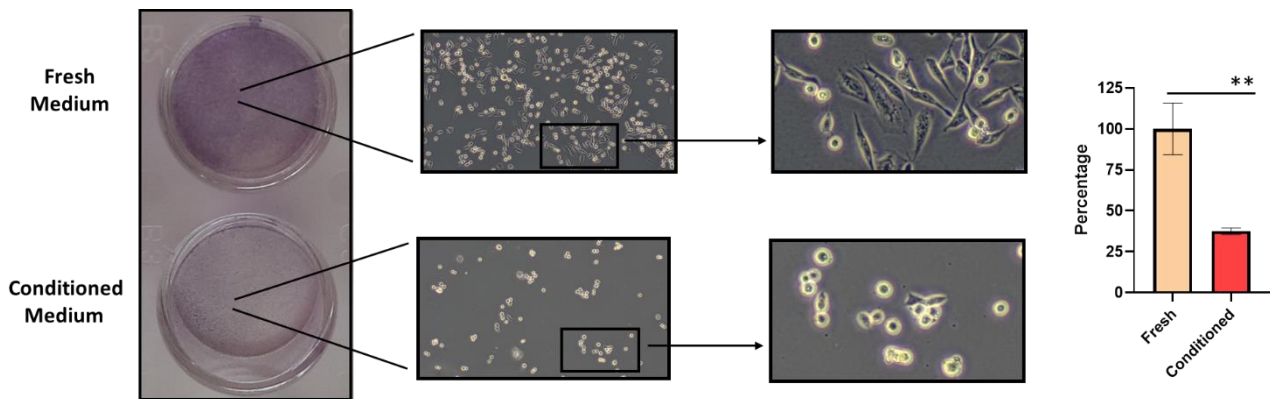
Figure 26. The conditioned medium prevented the re-attachment of suspension cells and the transition between circular and elongated cells. The left panel shows the crystal violet staining of re-attached cells seeded with fresh (top) or conditioned medium (bottom). In the middle are shown the brightfield microscopy pictures of representative areas. The pictures were taken immediately before crystal violet staining. A magnification of the regions included in the black boxes is shown. Crystal violet-related signal was measured at 595 nm (right graph). The percentage with respect to the Fresh Medium sample is indicated. Unpaired t-test with respect to the Fresh; p-value ** <0.01. A representative experiment is shown among three experimental replicates.

3.2.10. The entry into the cell cycle is associated with the origin of suspension cells

The fact that GIST-T1 sublines can similarly give rise to suspension cells indicated that the transition between the adherent and suspension states could be experienced numerous times by the cells. We hypothesized that it could be strictly related to the cell cycle, a process continuously activated in cancer cells. To confirm the reliability of our hypothesis, we analyzed the cellular DNA content, a widely recognized marker of the different cell cycle stages. As shown in Figure 27, about 60% of adherent cells were characterized by a DNA content index of around 2, thus thought to reside in the G_0/G_1 phases. On the contrary, suspension cells mainly displayed a DNA content index of about 4, predominantly G_2/M cells. A significant difference was also observed among S phase cells (DNA content index between 2 and 4). The differences suggested that the transition could occur because of the entry into or during the cell cycle. Notably, this result again confirmed the different biological properties of adherent and suspension cells. If suspension cells were caused by a simple detachment of adherents, the distribution in the cell cycle phase would have been analogous.
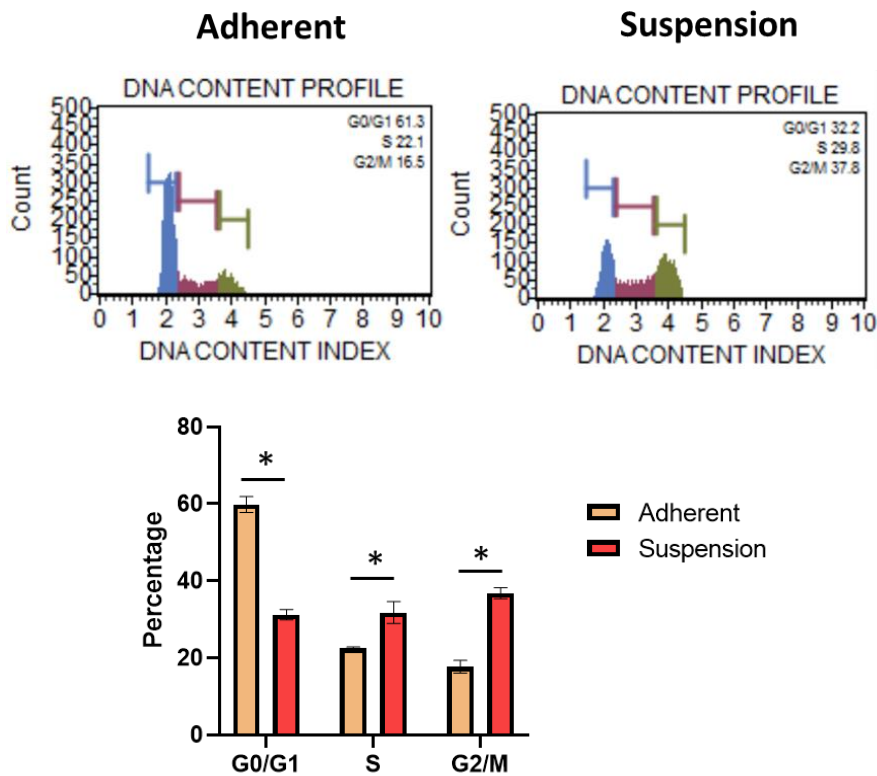
Figure 27. Suspension cells are primarily in the G_2/M phase. Analysis of DNA content in GIST-T1 Adherent or Suspension subpopulations and classification into cell cycle phases. A representative output of the flow cytometry analysis is shown at the bottom. Blu, violet, and green curves are related to the G_0/G_1, S, and G_2/M phases. Compared to the Adherent subpopulation, a reduction of cells in the G0/G1 phase in favor of an increase in the G2/M phase is observed in the Suspension. Multiple t-test statistical analysis was used; p-value *<0.05. A representative experiment is shown among three experimental replicates.

As the gold standard of GIST therapy, imatinib was widely tested in GIST cell lines, including GIST-T1 cells, since they are commonly classified as imatinib-sensitive. In particular, Gupta and colleagues demonstrated that imatinib promoted quiescence in GIST-T1, a mechanism activated to escape apoptosis (Gupta et al., 2010). Hence, imatinib mainly affects the viability of GIST-T1, impeding cell proliferation rather than stimulating apoptosis. We first confirmed the reproducibility of this finding in Adh-F4-T1, which is, as previously demonstrated, analogously imatinib-sensitive. Consistent with quiescence induction, we observed the increase of cells classified in G0/G1 and a concomitant reduction in those in S or G_2/M because of imatinib treatment (Figure 28A). Thus, to decipher the cell cycle role in the origin of suspension cells, we induced quiescence in Adh-F4-T1, treating cells with imatinib the day after seeding from 48h. Suspension cells were collected 72h after seeding as described until now and then seeded with a fresh medium in which imatinib was newly added for a short treatment (overnight). Acting by this, imatinib was present in all phases of the *in vitro* model (about 72h), including the rise of suspension cells (detachment), their viability in suspension (surviving), and re-attachment (Figure 28B). As shown by crystal violet staining (Figure 28C), the

number of cells that completed the colonization of a TC was more than 90% less when treated with imatinib than the control sample, indicating that imatinib remarkably impaired the entire biological process. An analogous experiment was performed in GIST-T1 cells, leading to the same conclusion (data not shown). Noteworthy, no effect was instead reported in C33a and SW-620, two cell lines reported to origin suspension cells in an analogous manner we demonstrate for GIST-T1 and derived sublines (Supplementary Figure 7) (Vargas-Accarino et al., 2021). This indicated that the *in vitro* "metastatic-like" process, despite being mechanistically similar, was likely guided by different oncogenic drivers in C33a and SW-620.

A.

B.

C.
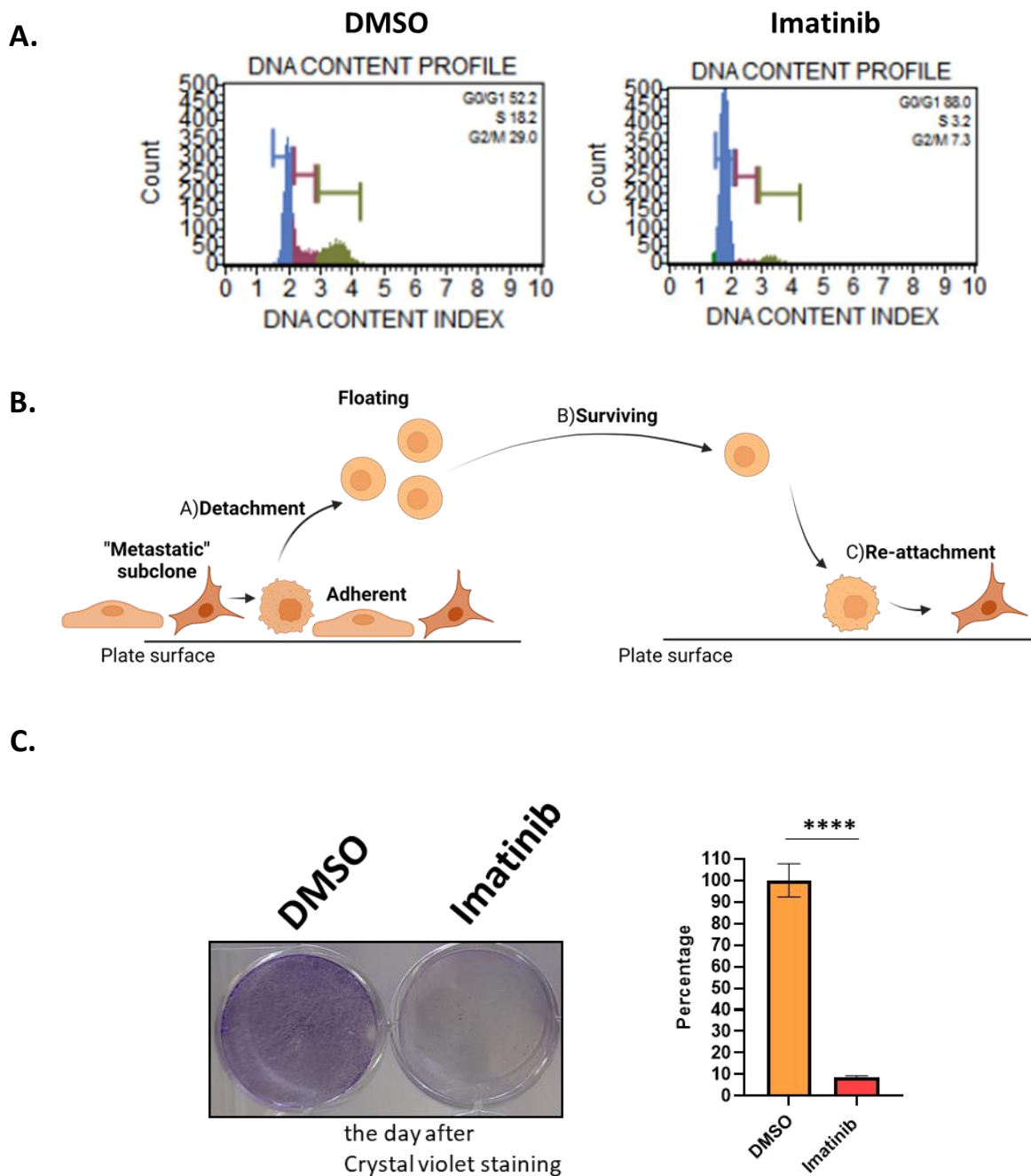
Figure 28. **Imatinib impaired the *in vitro* model, reducing the number of cells that completed the colonization of a new TC plate. A.** Imatinib can promote quiescence in Adh-F4-T1. Analysis of DNA content and classification into cell cycle phases after DMSO (0.01%) or imatinib treatment (100 nM) is shown. Blu, violet, and green curves are related to G_0/G_1 – S and G_2/M phases. An increase of the G_0/G_1 phase is observed in favor of a remarkable decrease of the S and G2/M phases. **B.** Summary of the *in vitro* "metastatic-like" process. "Metastatic-like" cells spontaneously detach (detachment). Then, as demonstrated, they can survive (surviving) as suspension cells and re-attach in a new TC plate in the presence of the fresh medium (re-attachment). Created with BioRender.com. **C.** Effect of imatinib on the entire *in-vitro* process. Adh-F4-T1 cells were treated with imatinib (100 nM) the day after seeding and maintained for 48h. Then, suspension cells were collected and newly seeded in the presence of imatinib (100 nM) or only solvent (DMSO). Crystal violet staining was performed the day after the re-seeding (left panel). Absorbance at 595 nm (% with respect to DMSO) ± SD is shown in the graph. Unpaired t-test with respect to the DMSO (right panel); p-value ****<0.0001. A representative experiment is shown among three experimental replicates.

According to the *in vitro* model and the performed experiment, the result could be a consequence of the inhibition of detachment, reduction of the viability of suspension cells, inhibition of the re-attachment, or a combination of them. To identify at which stage of the *in vitro* model imatinib acted, we performed an experiment in which we included a sample that was initially treated with the solvent and then, only in the re-seeding step (overnight), was shortly treated with imatinib (DMSO+Imatinib) (Figure 29A). As shown, the crystal violet-related signal of DMSO+Imatinib is faintly lower but not statistically different from DMSO+DMSO (Figure 29B). In agreement with that detailed in Figure 28C, the long-term treatment with Imatinib (Imatinib+Imatinib) remarkably reduced the crystal violet-related signal. Therefore, short-term imatinib treatment did not significantly affect the re-attachment, indicating that imatinib could mainly act on the detachment of adherent and viability of suspension cells.
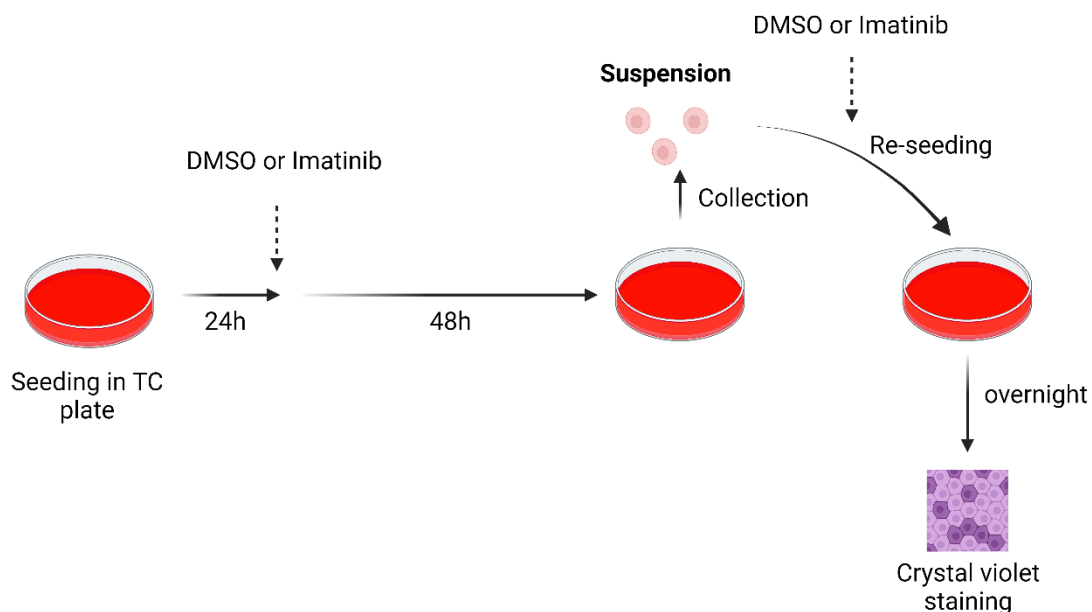
B.
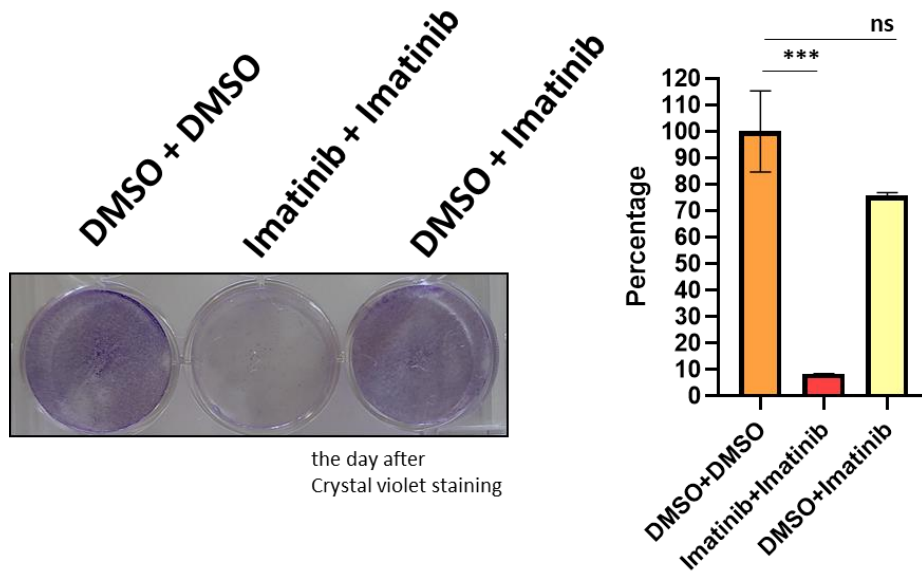
Figure 29. **Short-term imatinib-based treatment did not significantly inhibit the re-attachment of suspension cells A.** Summary of the experimental workflow. Adh-F4-T1 was treated with imatinib (100 nM) or solvent (DMSO) the day after seeding. Cells were then incubated for 48h. Suspension cells were collected and seeded in the presence of imatinib (100 nM) or solvent (DMSO). Created with BioRender.com. **B.** Crystal violet staining was performed the day after the seeding of suspension cells. The absorbance at 595 nm was measured, and the percentage (with respect to DMSO+DMSO) ± SD is shown in the graph. Adjusted p-value ***<0.001 (One-way ANOVA- Tuckey's Multiple comparison test with respect to DMSO+DMSO). A representative experiment is shown among three experimental replicates.

We then focused on the long-term effect of imatinib in cells already in suspension (surviving). Thus, suspension cells were collected and seeded in a 2% agar-coated TC plate in the presence of imatinib or the solvent for an additional 72h (Figure 30A). The length of the treatment was set to mimic the treatment applied in the workflow in Figure 29A. This experiment followed the same method previously indicated but started with the collection of suspension cells, thus excluding the effect that imatinib could have on adherent cells and their detachment. Imatinib was not added during the re-attachment phase in this experiment, having already demonstrated the short overnight treatment has no effect. As the crystal violet-related signal testified, the long-term imatinib treatment did not significantly reduce the number of re-attached cells (Figure 30B). Although a faint reduction of crystal violet signal was observed, this was not consistent with the impairment previously shown in Figure 28C (Imatinib) and Figure 29B (Imatinib+Imatinib). Thus, data indicated that the main targets of imatinib are adherent cells and their detachment rather than the viability of suspension cells. The induction of quiescence impeded the entry into the cell cycle, confirming its crucial involvement in acquiring the cell plasticity needed for the transition between adherent and suspension cells.

A.
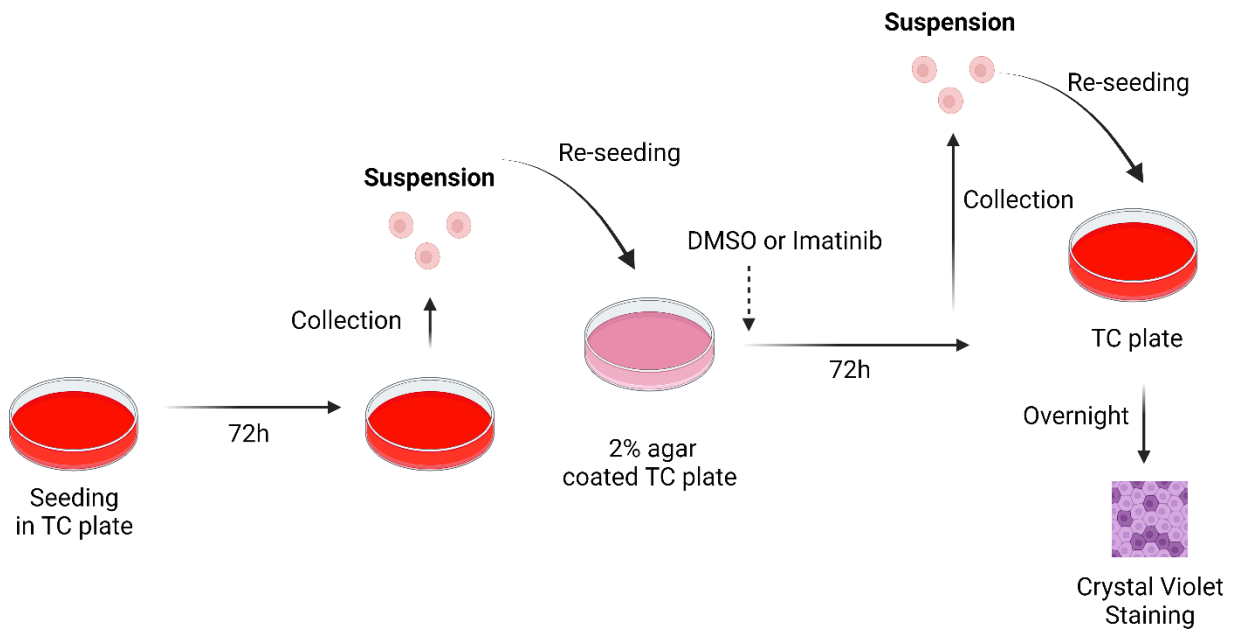
B.
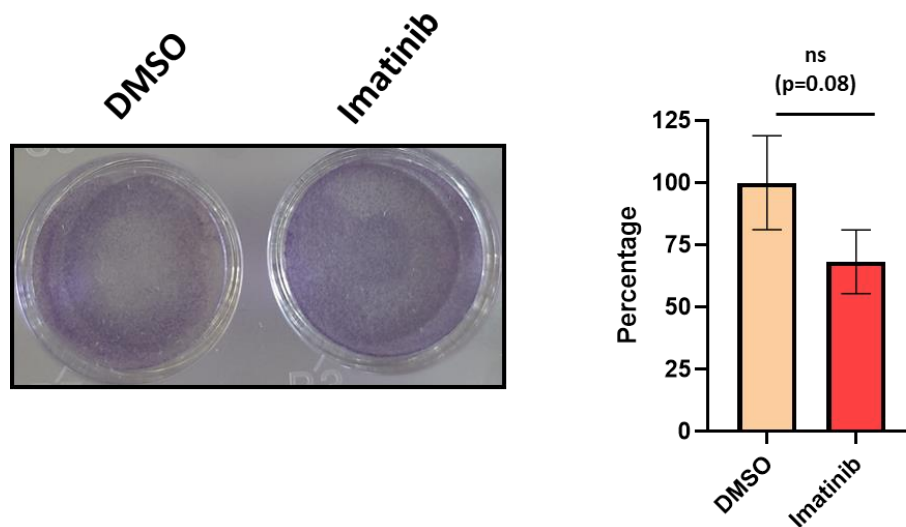
Figure 30. **Quiescence inhibited the rise of suspension cells. A.** Suspension cells were collected from Adherent-F4-T1 72h after seeding and seeded in the presence of solvent (DMSO) or imatinib (100 nM) in a 2% Agar-coated TC plate (forcibly suspension condition). Treatment was maintained for 72h. Then, suspension cells from both experimental samples were individually collected and re-seeded in a TC plate. Cell re-attachment was measured the day before through crystal violet staining. Created with BioRender.com. **B.** Effect of imatinib long-term treatment on the re-attachment of suspension cells. A representative Crystal violet staining is shown in the left panel. Absorbance at 595 nm (% with respect to DMSO) ± SD is shown in the graph on the right. T-test with respect to the DMSO (right panel). Ns means "not significative". A representative experiment among three experimental replicates is shown.

3.2.11. Suspension cells fulfill the cell cycle in suspension

Even if the effect promoted by the long-term imatinib treatment on suspension cells was not significant, the low p-value (p=0.08), close to the standard threshold, suggested that imatinib could also influence cells that were in suspension. Having demonstrated that suspension cells were actively involved in the cell cycle, we hypothesized that they could progress through the cell cycle phases and were still targetable by imatinib. To validate these hypotheses, we seeded the suspension cells in a 2% agar-coated TC plate and monitored the number of forcibly maintained in suspension cells up to 96h after seeding. The number of cells was measured at 24h (considered as T_0 time point) and 96h post-seeding (T_1). As shown in Figure 31A, the percentage of viable cells increased, indicating that suspension cells can fulfill the cell cycle as suspended cells, becoming around double that initially seeded. The long-term imatinib treatment (96h) of forcibly maintained suspension cells showed a 50% viability reduction by CCK-8 assay. Nevertheless, no apoptosis and cell death induction were detected (data not shown). This finding indicated that suspension cells are still targetable, and the different viability observed was linked to the proliferation of suspension cells in the DMSO-treated sample rather than the death of those that were imatinib-treated, suggesting that imatinib can likely slow down the cell cycle progress of cells in the suspension (Figure 31B).
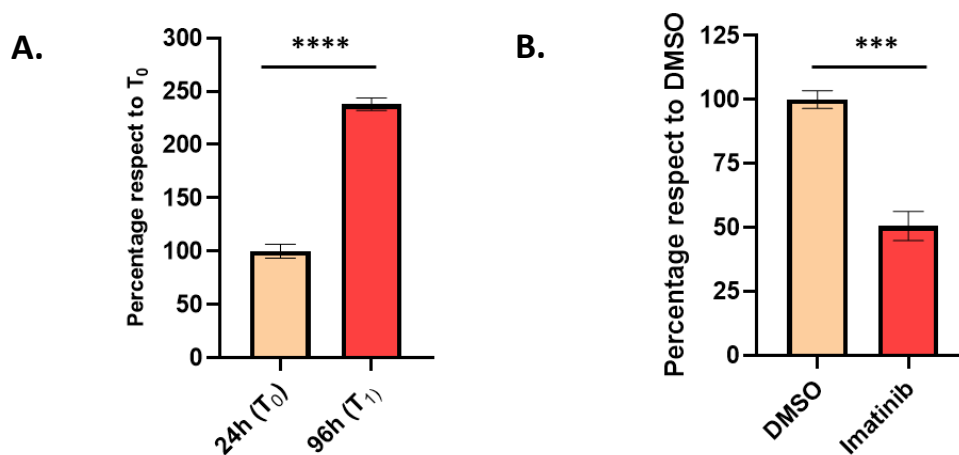
Figure 31. Suspension cells can fulfill the cell cycle even if they are in suspension **A.** Suspension cells from Adh-F4-T1 were seeded in a 2% agar-coated TC plate, and the number of viable was first estimated 24h after seeding (T_0). The number of suspension cells was newly measured 72h after the first observation, named T_1 (96h after seeding). Unpaired t-test with respect to the T_0. p-value *** 0.001, **** <0.0001. **B.** Evaluation of cell viability after long-term imatinib treatment (100 nM for 72h) by CCK-8 assay. Suspension cells were collected from Adh-F4-T1 and seeded in a 2% agar-coated 96-well plate in the presence of DMSO or imatinib (100 nM). CCK-8 assay was performed 72h after seeding. The percentage of the CCK-8-related signal (calculated from the absorbance at 450 nm) with respect to the solvent ± SD is shown. A representative experiment is shown among two experimental replicates.

3.2.12. Isolation of viable cells in suspension through cell sorting

As already shown in the apoptosis profile in Figure 17, viable cells in the Suspension Subpopulation, for convenience, named "suspension cells", resided in the culture medium with cellular debris, apoptotic, and dead cells, which can represent most of the subpopulation. Therefore, the molecular study of suspension cells by omics-science approaches could not be straightforward due to the contamination of death-related cellular elements that make the result unreliable. Consequently, we set up a method to overcome this drawback, isolating suspension cells from the culture medium through TO-PRO™-3 Iodide-based cell sorting. TO-PRO™-3 Iodide is a fluorescent dye that selectively labels dying and dead cells, including those in early apoptotic stages (L. Jiang et al., 2016). We collected the culture medium 72h after GIST-T1 seeding and labeled non-viable cellular elements with TO-PRO™-3 Iodide. An example of the applied workflow is shown in Supplementary Figure 8. The Adherent subpopulation was used to draw the gates enclosing viable cells. Hence, the Forward/Side Scattering (FSC/SSC) parameters and the fluorescence related to TO-PRO™-3 Iodide negativity were properly defined (top panels). These parameters were then similarly applied to the Suspension subpopulation. As supposed, different grades of TO-PRO™-3 Iodide positivity were observed, suggesting that numerous death statuses were present among cellular elements in suspensions (low panels). In agreement with what was thought, only a small percentage of viable cells was present in the Suspension subpopulation from GIST-T1 (≈12%), corroborating the necessity to isolate viable cells to pursue an analysis through omics-sciences (Supplementary Figure 9). To confirm that the isolated cells were responsible for the colonization of new TC plates previously shown, sorted cells were newly seeded, and the capability to re-attach was evaluated by crystal violet staining. As shown in Supplementary Figure 9, sorted cells completed the colonization of a new TC plate, indicating that the designed approach was suitable for isolating suspension cells successfully. Noteworthy, applying this method to Adh-F4-T1, a percentage of viable cells of about 75% was observed, corroborating our finding related to the enrichment of "metastatic-like" cells (Supplementary Figure 9).

The designed FACS-based approach was used to obtain a reliable protein extract from suspension cells and to assess the expression level of CDK4, a well-recognized player of G_1 progression. As expected by the lower percentage of cells in G_0/G_1, suspension cells expressed less CDK4 than adherent, confirming the distribution in the cell cycle phases and corroborating our finding about the involvement of the cell cycle (Figure 32).
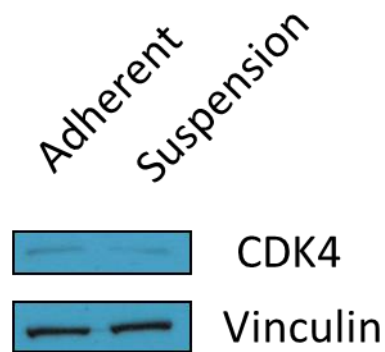
Figure 32. The expression level of CDK4 in adherent and suspension cells. The expression level of Vinculin was used as a reference control.

3.2.13. Proteomics-based comparison between adherent and suspension cells

Numerous proteins could be differentially expressed because of the transition from adherent to suspension cells. Therefore, after the design of a method to isolate suspension cells from debris, dying, and dead cells, a proteomics-based comparison between GIST-T1 adherent and suspension cells was performed. C33a and SW-620, two epithelial cancer cell lines (cervical and colorectal, respectively), were also included since they give rise to a similar *in vitro* transition between adherent and suspension cells. Analysis of an experimental triplicate was performed for each sample. The proteome study of a mesenchymal and two epithelial-derived tumor cell lines could elucidate which players are similarly deregulated and crucial in the biology of suspension cells, independently from the origin and tumor type. The principal component analysis (PCA) in Figure 33 showed a remarkable difference between adherent and suspension proteomes. Interestingly, the proteomes of all suspension cells are in the right panel of the graph (PCA1<0), suggesting the presence of common deregulated players. The mesenchymal origin of GIST-T1, which is different with respect to the epithelial of C33a and SW-620, was also highlighted, being both GIST-T1 adherent and suspension in the lower panel of the graph (0<PCA2<-0.5). As expected, more similarity between floating C33a and SW620 cells was observed. Overall, the analysis revealed that among 5914 proteins successfully quantified by proteomics, around 2500 were differentially expressed between adherent and floating samples.
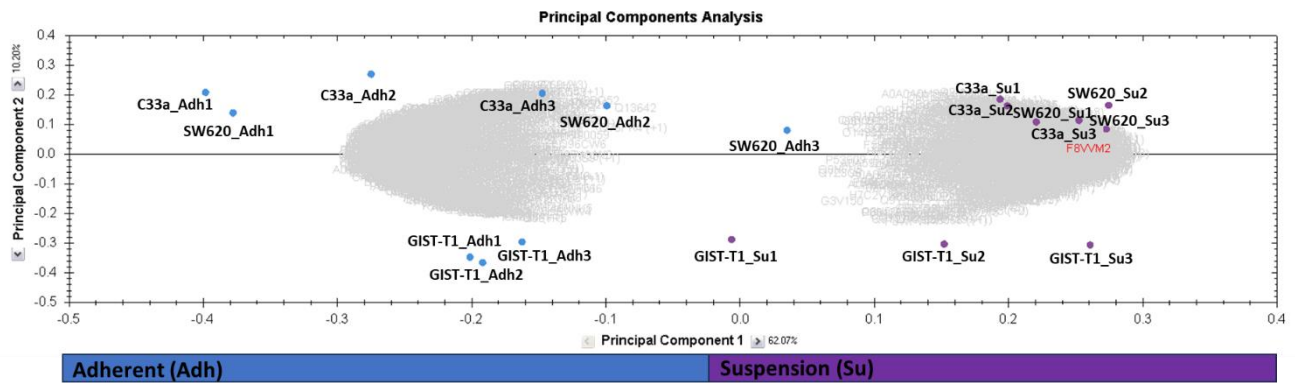
Figure 33. **PCA revealed a different protein expression between adherent and suspension cells.** Proteins were extracted from adherent and suspension cells obtained from GIST-T1, C33a, and SW-620. Experimental triplicates are reported in the graph. "Adh" means adherent, while "Su" means Suspension. PCA was performed exclusively, including deregulated proteins with a fold change > 2 and an adjusted p-value < 0.05. P-value was obtained using One-way ANOVA between adherent and suspension samples. Blue spots indicate adherent samples, while purple spots identify suspension ones.

Focusing on proteins differently expressed between GIST-T1 adherent and suspension cells, our attention was immediately oriented on proteins well recognized as fundament players of S and G_2/M cell cycle phases. Proteomics also revealed upregulation of CDK2, CDC123, CDK1, CDC23, CDC27, and ANAPC7, corroborating the finding that most cells are in the S and G_2/M phases (Figure 34). ANAPC7 was also upregulated in C33a and SW-620 suspension cells.
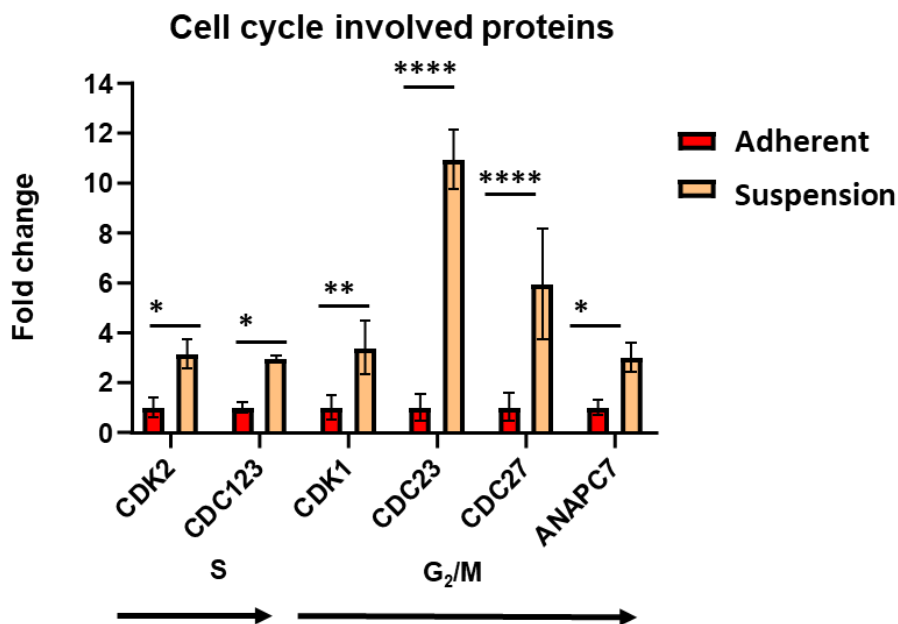
Figure 34. **Up-regulation of S and G_2/M cell cycle proteins in GIST-T1 suspension cells compared to adherent.** Proteomics displays the upregulation of crucial proteins in the S and G_2/M phases. Differential expressions of CDK2, CDC123, CDK1, CDC23, CDC27 and ANAPC7 are shown. Fold change calculated on relative abundance expression (based on quantification of unique peptides) ± SD. Multiple unpaired t-test; Adjusted P Value *<0.05; ** <0.005; ****<0.00005.

The analysis was then oriented on identifying proteins commonly deregulated between suspension and adherent samples, independently from the type and origin of cell lines. In detail, among the successfully identified and quantified proteins (N=5914), around 2645, 1353, and 1321 were deregulated between suspension and adherent in C33a, SW-620, and GIST-T1. 180 and 171 were similarly up-regulated and down-regulated in GIST-T1, C33a, and SW-620, respectively (Figure 35 – left and right panels). All similarly deregulated proteins are reported in Supplementary Tables 1 and 2.
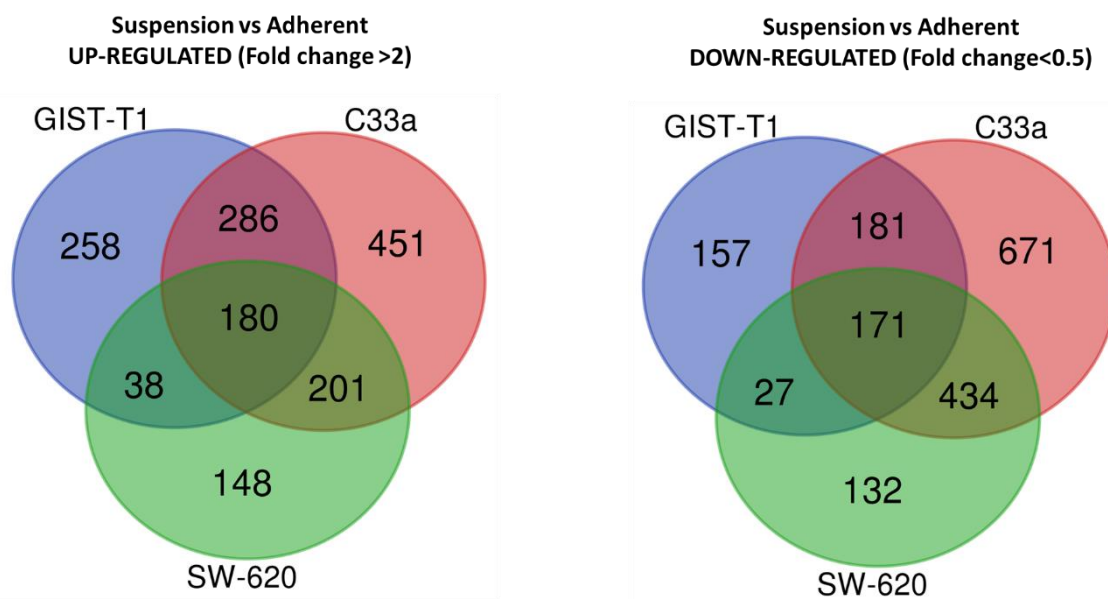
Figure 35. **The Venn diagram summarizes deregulated proteins that are common between suspension cells.** Deregulated proteins in GIST-T1 are in the blue circle, while those deregulated in C33a and SW-630 are in red and green, respectively. Included proteins are only those identified with a Mascott score >20. The Venn diagram on the left gathers all upregulated proteins in suspension cells (Fold change <2), while that on the right gathers downregulated proteins (Fold change <0.5). Proteins are considered deregulated when the statistical analysis is associated with a p-value<0.05 (calculated using an unpaired t-test comparing suspension and adherent). The intersection areas between the circles mean the elements that are commonly deregulated. The number of upregulated proteins in the Venn diagram are 1118, 762, and 567 for C33a, GIST-T1, and SW-620, respectively. Instead, the included downregulated proteins are 1457, 537, and 764. Proteins that are similarly upregulated in GIST-T1, C33a, and SW-620 are 180, while 171 proteins are downregulated.

To identify the most interesting players involved in the biology of suspension cells, we decided to increase the stringency of our analysis, including only proteins that were characterized by a higher Mascot score (>50), quantified using the relative abundance of at least three unique peptides, and differently expressed with a more robust statistic (p-value < 0.01). This stringent cutoff increased the grade of confidence of the identified proteins, thus only highlighting proteins that were more deregulated in suspension and showed less variability between experimental replicates. Acting this

way, four upregulated and five downregulated proteins in suspension cells were identified (Figure 36). Cln Three Requiring 9 (CTR9), Replication Factor C Subunit 5 (RFC5), Branched-chain amino acids transferase 2 (BCAT-2), and Importin 9 (IPO9) seem to be the most promising upregulated players. The TATA element modulatory factor 1 (TMF1, also known as ARA160), Translocase of Inner Mitochondrial Membrane 8 Homolog B (TIMM8B), Activated RNA Polymerase II Transcriptional Coactivator P15 (SUB1), Small Ribosomal Subunit Protein US14 (SUB1), and Metastatic Lymph Node Gene 50 Protein (LASP1), could be instead interesting among the downregulated players.
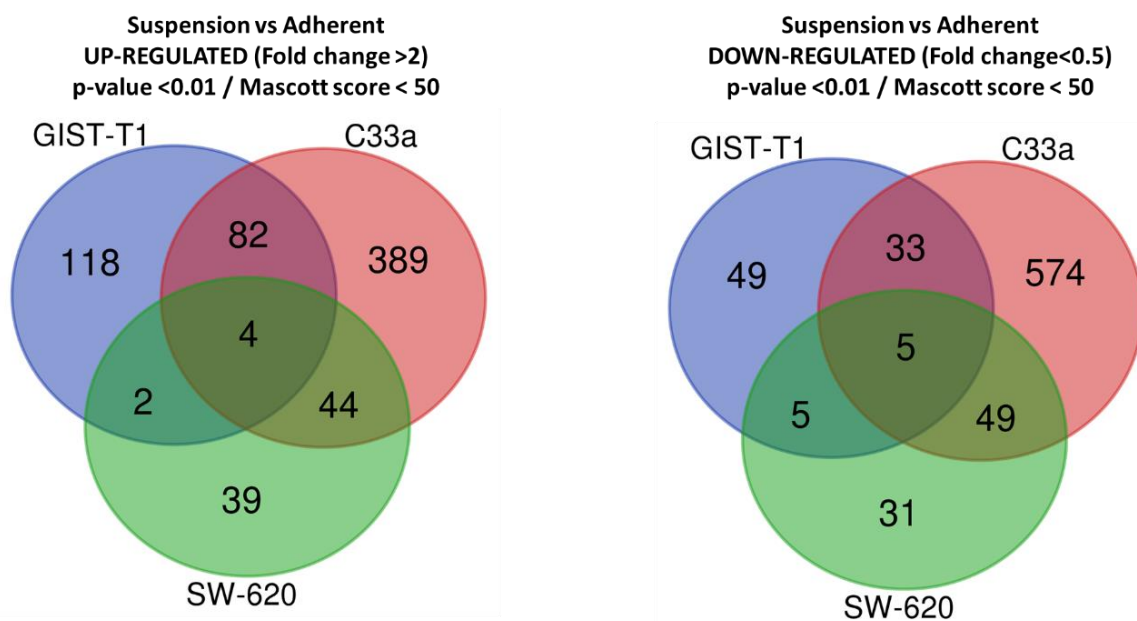
Figure 36. **Venn diagram only includes proteins that respect the higher stringency cutoff.** Included proteins are only those identified with a Mascott score >50 and quantified using the relative abundance of at least three unique peptides. In addition, the higher stringency cutoff applies a more robust statistic. Indeed, only differences associated with a p-value < 0.01 were considered statistically significant (calculated using an unpaired t-test comparing suspension and adherent samples). This approach identified only 4 upregulated and 5 deregulated proteins in common.

4. MATERIAL AND METHODS

4.1. Bio-guided fractionation of AUN to identify chemotherapeutics for GIST treatment

4.1.1. Cell lines and culture conditions

GIST-882 and GIST-T1 cell lines harbor gain of function primary mutation in KIT and are imatinib-sensitive. They are characterized by exon 9 (K642E) homozygous mutations and an exon 11 heterozygous mutation (V560-Y579 deletion) in c-kit, respectively. GIST-882 and GIST-T1 were grown in RPMI-1640 supplemented with 15% FBS. GIST-48 is instead reported as an imatinib and sunitinib-resistant cell line harboring a primary homozygous gain of function mutation on KIT exon 11 (V560D) and an additional secondary heterozygous mutation in exon 17 (D820A). This latter promotes resistance to both imatinib and sunitinib. GIST-48b was established *in vitro,* starting from GIST-48 after HSP-90 inhibitor (17-AAG) drug pressure selection, which resulted in a subline characterized by nearly undetectable KIT transcript and protein. GIST-48 and GIST-48b were grown in Iscove's Modified Dulbecco's Medium (IMDM) supplemented with 15% FBS. All indicated cell lines were routinely tested to avoid mycoplasma contamination (MycoBlue Mycoplasma Detector – Vazyme). Fletcher JA, MD (Harvard Medical School) kindly provided GIST cell lines.

4.1.2. Extraction of phytochemicals from the leaves of *A. unedo*

Leaves from *A. unedo* (harvested in Sardinia in 2018) were dried and powdered. Phytochemicals were then extracted from 30mg of powdered material by sonication for 30 minutes using 1.5 mL of MeOH/H_2O (1:1). After centrifugation at 1700 × g for 20 minutes, the supernatant was dried in vacuum concentrators (speedVac SPD 101b 230). For biological assays, stock solutions were prepared solubilizing extracts in H_2O at 10 mg/mL and centrifuged twice (13200 rpm) to remove no resuspended elements if present.

4.1.3. Cell viability and apoptotic profile by flow cytometry

10^5 GIST cells were seeded in a 24-well cell culture plate the day before treatment. Cells were treated with AUN or derived fractions at indicated final concentrations in the culture medium (FBS included) for indicated time points. The analysis of cell viability and the presence of apoptotic cells were evaluated on the entire cellular population, including cells that were in suspension due to the treatment. For this reason, the culture medium, and the phosphate-buffered saline (PBS) used to rinse cells before trypsinization, were also collected. Adherent cells were harvested by trypsinization

and combined with cells in the culture medium and PBS. The entire sample was then centrifugated and resuspended in 500µL of fresh medium. Samples were stained with Guava® ViaCount™ or Guava® Nexin Reagent according to the manufacturer's instructions. Guava® Muse® Cell Analyzer was used for flow cytometry analysis. The Guava® ViaCount™ differentiates viable and non-viable cells based on differential permeabilities of two fluorescent DNA binders. The nuclear dye distinguishes between nucleated cells and cellular debris, while the viability dye brightly stains dying cells. The number of total cells in the sample was defined starting from cell concentration (cells/µL) calculated by the flow cytometer instrument. Guava® Nexin Reagent enables evaluating apoptosis activation. The reagent combines a fluorescent Annexin V (Annexin V-PE) and 7-Aminoactinomycin D (7-AAD). Annexin V-PE is a calcium-dependent phospholipid-binding protein with a high affinity for phosphatidylserine, a membrane component selectively exposed on the surface of apoptotic cells or bodies. On the other hand, 7-AAD is a fluorescent DNA intercalator excluded from living and early apoptotic cells since their membrane is impermeant; for this reason, it only recognizes late apoptotic/dead cells.

4.1.4. Bio-guided fractionation of AUN (I, II, and III steps)

1ˢᵗ step (liquid-liquid partitioning): 500 g of dried and powdered material from *A. unedo* leaves were extracted using 2L of CH_3OH 80% v/v. The extraction procedure was repeated four times on the same plant material (estimated yield of about 12%). The produced extract (AUN) was filtered and dried in a rotary evaporator. For the first step of the bio-guided fractionation, AUN was suspended in 700 mL of water and subjected to liquid-liquid partition using in-series chloroform ($CHCl_3$) or ethyl acetate (EtOAc). Each solvent-based extraction was performed three times using each solvent. Thus, three AUN-derived fractions were produced: $CHCl_3$ (FR1; yield: 0.33% w/w), EtOAc (FR2; yield: 8.8% w/w), and H_2O (FR3). The stock solutions for the biological assay were prepared as follows: FR3 was prepared by solubilizing dried extracts in distilled and sterile H_2O at 20 mg/mL initial concentration; FR2 and FR3 were instead solubilized in DMSO 10% at the same initial concentration of FR3. FR1, FR2, and FR3 fractions were then diluted (1:1000) during the biological assays, leading both H_2O and DMSO to a final concentration of 0.1% in the medium supplemented with FBS 15%. **2ⁿᵈ step (reverse phase MPLC)**: 4g of FR2 were suspended in 5 mL of water and injected in a Medium-Pressure Liquid Chromatography (MPLC) instrument (Reveleris®, Büchi, Switzerland) associated with a reverse phase stationary matrix (40g of C_{18} column). A gradient of water (solvent A) and methanol (solvent B) was used as eluent. The gradient was composed of an isocratic phase of 10 min (90% A and 10% B), a gradient from 90% A to 80% A in 1.1 min, an isocratic phase of 20 min (80% A and

20% B), a gradient from 80% A to 70% A in 1.1 min, an isocratic phase of 10 min (70% A and 30% B), a gradient from 70% A to 50% A in 1.1 min, an isocratic phase of 10 min (50% A and 50% B) a gradient from 50% A to 30% A in 1.1 min, an isocratic phase of 5 min (30% A and 70% B), a gradient from 30% A to 0% A in 1.1 min, an isocratic phase of 5 min (0% A and 100% B). The flow rate was 20 mL/min, and the run length was 70 min. Based on the chromatogram and the UV absorbance, eluted fractions were divided into four and dried, obtaining four FR2 fractions (FR2-A, FR2-B, FR2-C, and FR2-D). Stock solutions for biological assay were prepared analogously to that indicated before for FR2. **3rd Step (size-exclusion chromatography):** 879.8 mg of FR2-A were suspended in a minimum amount of methanol and then subjected to a size exclusion chromatography using a chromatography column (1800 mm × 25 mm) filled with 220 g of Sephadex (LH-20) and, as eluent, methanol. The flow rate was 0.4 mL/min. The eluate in each tube was concentrated in a rotary evaporator, while a small quantity was analyzed through thin-layer chromatography (TLC). The stationary phase of the TLC used a silica gel matrix with florescent indicator 254 nm (Sigma-Aldrich), while EtOH: MeOH: H2O (10: 1.35: 1) was used as the mobile phase. TLC was applied to acquire information on fraction chemical composition, enabling us to group the equal ones and to define the end of the running. Acting by this, 84 fractions were obtained.

4.1.5. Western blot

Whole-cell protein lysates were prepared using NP40 buffer containing protease inhibitors (Halt protease and phosphate-inhibitor cocktail; Thermo Fisher Scientific) and 1mM of phenylmethylsulfonyl fluoride (Sigma-Aldrich). Proteins were separated in SDS-PAGE (12%) and transferred onto nitrocellulose membranes. Nonspecific binding sites in the membrane were blocked with a 5% skimmed milk in tween-tris-buffered saline (T-TBS). Primary antibodies against KIT (A4502; Dako), phospo-KIT (3391; Cell Signaling), PARP-1 (9542, Cell-Signaling), and actin (A1978; Sigma-Aldrich) were incubated at 4°C overnight. After rinsing, membranes were incubated with horseradish peroxidase–conjugated secondary antibody (Thermo Fisher Scientific) at room temperature for 2 hours. After further rinsing, immunoreactive bands were visualized by enhanced chemiluminescence (BioRad), and signals were captured and quantified using ChemiDoc (BioRad). The intensity of PARP1 and actin bands was measured using Image Lab software. Normalization was then performed using the corresponding actin band in each lane. Fold change was calculated by dividing the normalized expression level of PARP1 in FR2-A treated samples by the corresponding control sample at each time point.

4.1.6. NMR spectra measurement

^{1}H NMR spectra, J-resolved (J-res), ^{1}H-^{1}H homonuclear (COSY), and inverse detected ^{1}H-^{13}C correlation experiments (HMBC, HSQC) were recorded at 25 °C on a Varian Inova instrument (equipped with a reverse triple resonance probe). Each ^{1}H NMR spectrum consisted of 256 scans (corresponding to 16 min) with a relaxation delay (RD) of 2 s, acquisition time of 0.707 s, and spectral width of 9595.8 Hz (corresponding to δ 16.0).

The reference spectral data of all the detected compounds are reported in Sanna et al., 2023, except for galloylarbutin and trigalloylglucose, which are reported below.

Galloylarbutin 1H NMR spectral data (600 MHz, CD3OD): δ 7.10 (2H, s, H-2'', H-6''), 6.95 (2H, d, J = 9.12 Hz, H-3, H-5), 6.60 (2H, d, J = 9.12 Hz, H-2, H-6), 4.69 (1H, d, J = 7.4 Hz, H-1'), 4.56 (1H, dd, J1 = 11.8, J2 = 2.14 Hz, H-6'a), 4.42 (1H, ov, H-6'b) 3.66 (1H, td, H-5') 3.48–3.40 (3H, ov, H-2', H-3', H-4'); Negative ESI-MS m/z: 423.34 [M − H] − calculated as 424.1 for C19H20O11.

Trigalloylglucose 1H NMR spectral data (600 MHz, CD3OD): δ 7.08 (2H, s, H-2', H-6'), 7.04 (ov), 7.00 (2H, s, H-2''', H-6'''), 5.9 (1H, d, J = 8.4 Hz, H-1 glucose) 5.18 (1H, t, H-2 glucose); Negative ESI-MS m/z: 635.27 [M − H] − calculated as 636.1 for C27H24O18.

4.1.7. Chemical compounds

Sigma-Aldrich supplied β-arbutin, while imatinib was supplied by Selleckchem.

4.1.8. MTT viability assay

$2,5*10^4$ GIST-882 or GIST-T1 cells were seeded in a 96-well culture plate the day before the treatment. Cells were treated with FR2-A derived fractions, and viability was analyzed 24h after treatment. Treatment was removed, and cells were incubated with MTT reagent (0.5 mg/mL) in the medium without serum for 2h. At the end of the incubation, the MTT solution was carefully removed completely, and formazan crystals were dissolved in DMSO. Absorbance was read at 492 nm using a TECAN spectrophotometer.

4.1.9. PBMC isolation

PBMCs were isolated as described in Panda, S. K. and Ravindran, B. (2013) (Panda & Ravindran, 2013).

4.1.10. Statistical analysis and software

Statistical analysis was performed using GraphPad Prism software, applying the indicated statistical test. Details are shown below each figure. IC_{50} was instead calculated with the free "aatbioquest" tool (https://www.aatbio.com/tools/ic50-calculator-v1).

4.2. An *in vitro* model for the study of metastasis in GISTs

4.2.1. Cell lines and culture conditions

Details about GIST cells are already indicated in the 4.1.1 paragraph. C33a (colorectal cancer) and SW620 (cervical cancer) were supplied by ATCC (American Type Cell Collection) and grown in Dulbecco's Modified Eagle Medium High Glucose (DMEM) supplemented with 10% FBS.

4.2.2. Collecting of GIST cell subpopulations

GIST-T1, GIST-882, and GIST-48 were seeded at $1.2*10^5$ cell/cm^2 density in a 24-well cell culture plate. Each cell line was then divided into three subpopulations: Suspension, Semi-Adherent, and Adherent. The culture medium was collected to harvest suspension cells. Semi-Adherent subpopulation was harvested through a single and gentle rinse with culture medium. Instead, the Adherent subpopulation was collected using a trypsin-EDTA solution after PBS washing. Each subpopulation was collected after the time point indicated in the graph or below each picture. The collected subpopulations were centrifuged for 7 minutes at 900 rpm, and the supernatant was almost entirely removed. Cell pellets were then resuspended based on the assay of interest.

4.2.3. Cell viability and apoptotic profile by flow cytometry

Cell pellets obtained by collecting Suspension and Semi-adherent subpopulations were resuspended in 30µL of culture medium. Instead, the Adherent subpopulations, which were the most represented in terms of cell number, were resuspended in 1000uL. The volumes were set to be compatible with the sensitivity limit and the working range of the Guava® Muse® Cell Analyzer and assays. The entire Suspension and Semi-adherent subpopulation (30µL) and 30µL of Adherent were then stained with Guava® ViaCount™ according to the manufacturer's instructions and analyzed by Guava® Muse® Cell Analyzer. The number of cells/ µL and the volume of the cellular suspension were used to calculate the number of viable cells. The "apoptotic profile" was instead obtained using Guava® Nexin Reagent. Further details about the assay principles are reported in 4.1.3. paragraph.

4.2.4. Attachment assay and crystal violet staining

Cell pellet of suspension cells was resuspended in fresh medium and seeded in a 24-well plate. Newly adherent cells were then rinsed with PBS and fixed with formaldehyde 3.7-4.0 w/v buffered to pH 7 and stabilized with methanol (PanReac Applichem). Fixed cells were subsequently rinsed with PBS and stained with 1% crystal violet solution (in methanol 20%). The excess crystal violet was removed

by rinsing with PBS, and the absorbance of methanol-solubilized crystal violet was measured at 595 nm (The Spark® Multimode Reader).

4.2.5. Establishment of GIST-T1 sublines

$5*10^6$ GIST-T1 cells were seeded in a 10cm TC plate, and suspension cells were collected 72h after seeding. Suspension cells were then resuspended in fresh medium and newly seeded in a new 10cm TC plate. The re-attached cells were grown up confluency and named Adh-F1-T1. F1 means the first generation established from GIST-T1. Subsequently, an analogous workflow was applied to Adh-F1-T1 to originate Adh-F2-T1. The procedure was then serially repeated up to the genesis of Adh-F4-T1 (Figure below).
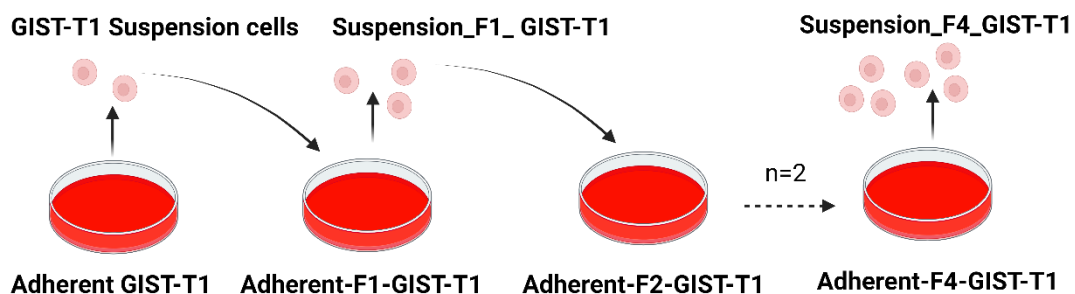
4.2.6. Time-lapse microscopy

Live cell imaging studies were evaluated by brightfield microscopy using the Thunder widefield microscope (Leica Microsystems) set at 37ºC and 5% CO2. Images from each sample were acquired using an HC PL FLUOTAR 10x/0.32 DRY objective and a Leica-DFC9000GTC-VSC12324 sCMOS camera with a 2x2 pixel binning and a 16-bit resolution. The stage was slowed to ensure proper stage displacement during acquisition with minimal or no effect on the position of suspension cells. For detachment experiments, image fields were photographed every minute for 18h. For attachment experiments, fields were photographed every three minutes for 16h.

4.2.7. Effect of different plate surface coatings on the rise of suspension cells

10cm TC plates were coated using 0.1% Gelatin (Sigma-Aldrich) or 100ug/mL Poly-L-Lysine (Merck Millipore) solutions. In detail, 0.1% Gelatin solution was left in contact with the plate surface for 1h at room temperature. The excess Gelatin was removed, and the coated plates were left until dry. Instead, Poly-L-Lysine coated TC plates were prepared the day before incubating the Poly-L-Lysine solution overnight at 37°C. The Poly-L-Lysine coated TC plates were then rinsed twice with sterile water and dried for at least two hours. Both coated TC plates were rinsed twice with PBS before

experimental use. $6*10^6$ Adh-F4-T1 cells were seeded in the differently coated plates. Brightfield pictures were taken 72h after seeding. Suspension and Adherent subpopulations were then collected as previously described, and the number of viable cells was calculated using Countess Cell Counter (Thermo Fisher Scientific) in association with Trypan Blue staining. The capacity to sustain the *in vitro* model (detachment, surviving, and re-attachment) was evaluated by seeding suspension cells and measuring the re-attachment by crystal violet staining. This last was performed as already detailed.

4.2.8. Survival of suspension cells in a suspension forcibly condition

$5*10^6$ Adh-F4-T1 cells were seeded in a 10cm TC plate. Suspension cells were collected after 72h hours and filtered through a 40μm cell strainer. Cells were then split into two p60 TC plates, with or without a 2% agar coating. Cells seeded in the p60 TC plate without the agar-based coating were stained the day after with crystal violet solution as previously indicated. Instead, cells seeded in the 2% agar-coated TC plate were left in the suspension forcibly condition for 72h. Cells were harvested and seeded in a p60 TC plate with a fresh medium. The crystal violet staining was similarly performed the day after.

4.2.9. Effect of the conditioned medium on the origin of suspension cells

$4*10^5$ Adh-F4-T1 cells were seeded in 24-well plates. The medium was replaced every 24h with fresh or conditioned medium for 72h. Indeed, to avoid experimental artifacts related to the replacement of fresh medium, samples that were designed to be incubated with the conditioned medium also underwent a mimicked renewal of the conditioned medium. An analogous conditioned medium deriving from a further experimental well, with equal seeded cells and after the same experimental time, was used to mimic the renewal. Acting this way, a 72h persistent conditioned medium was simulated. Noteworthy, since suspension cells would be present in the added conditioned medium, this was filtered using a 0.4μm filter at each time point. Fresh medium was then similarly filtered every 24h to replicate the same procedure applied to the conditioned medium. Viable cells in the Suspension subpopulation and the Adherent were counted 72h after seeding using Countess Cell Counter (Thermo Fisher Scientific) and Trypan Blue staining. Suspension cells derived from Conditioned or Fresh Medium samples were isolated and newly seeded in a TC plate with fresh medium. Crystal violet staining was performed the day after seeding, as previously described.

4.2.10. Effect of the conditioned medium on the attachment of suspension cells

Suspension cells from Adh-F4-T1 were collected from a 10cm TC plate 72h after seeding, isolated by centrifugation, and resuspended in the fresh medium in high cellular concentration. Then, they were equally split into two p60 TC plates with fresh or conditioned medium. The percentage of fresh medium in the Conditioned Medium sample was less than 3% since added suspension cells were at high cell concentrations. Conditioned medium was collected 72h after Adh-F4-T1 seeding ($5*10^6$ cells) and filtered using a 0.4μm filter. Brightfield microscopy pictures were taken using 10x and 20x objectives the day after seeding before the Crystal Violet staining.

4.2.11. Cell cycle analysis

10^6 cells were seeded in a 6-well cell culture plate. Suspension, semi-adherent, and adherent subpopulations were collected as indicated before and fixed in 70% Ethanol. Fixed cells were rinsed once with PBS and stained with Muse® Cell Cycle Kit as indicated by the supplier. Different cell cycle phases were defined based on DNA content.

4.2.12. CCK-8 viability assay

$2*10^4$ GIST-T1 or Adh-F4-T1 cells were seeded in a 96-well plate the day before drug treatment. Imatinib (Sigma-Aldrich) was before resuspended in DMSO at 10mM final concentration. Then, 1mM - 100μM and 10 μM dilutions were prepared in DMSO. These dilutions were further diluted 1:1000 in 15% FBS RPMI-1640 to treat the cells with the same amount of DMSO (0.01%). Cells were treated with the indicated dilution or the negative control (0.01% DMSO) for the indicated time window. Viability was measured by adding Cell Counting Kit 8 (CCK-8) (APExBIO) for 2h and reading the absorbance at 450 nm.

4.2.13. Western Blotting

Western Blot was performed as indicated in paragraph 4.1.5. Primary antibodies against CDK4 (D963E; Cell Signaling) and Vinculin (V9131; Sigma-Aldrich) were used.

4.2.14. Fluorescence-activated Cell Sorting (FACS)

$10*10^6$ GIST-T1 cells were seeded in a 10cm TC plate, and the culture medium was collected 72h after seeding. The Suspension subpopulation was then isolated by centrifugation and concentrated to have a final concentration of about $1-2*10^6$ cells/mL. The concentration of viable cells in suspension was obtained by counting cells using a Countess Cell Counter (Thermo Fisher Scientific). The cellular suspension was filtered using a 40μm cell strainer and stained with TO-PRO™-3 Iodide (Thermo Fisher Scientific) at 500 nM final concentration, a fluorescent dye used to label apoptotic

and dead cells. Stained samples were sorted using FACS (BD FACSAriaTM sorter), and viable cells, unstained with TO-PRO™-3 Iodide, were selectively collected from the Suspension subpopulation.

4.2.15. Proteomics

Proteomics was performed on the Adherent subpopulation (viability > 95%) and viable cells in the Suspension subpopulations. As indicated in the previous paragraph, viable cells in Suspension subpopulations were isolated through TO-PRO™-3 Iodide-based FACS. Cell pellets were obtained by centrifugation and rinsed with PBS to remove FBS contaminants. Cell pellets of the Adherent subpopulation and viable cells in suspension from GIST-T1, C33a, and SW620 were obtained. Proteins were then extracted and used as follows. A) **Cell lysis and protein extraction**: Cells were resuspended in 100 µl lysis buffer (7M urea, 2M thiourea, 30mM Tris HCl, CHAPS buffer 4%, pH 8.5) by sonication (VCX 150; Sonics & Materials Inc. USA). In detail, five cycles of 20 seconds of ultrasound bursts were applied, keeping the tube ice-cooled. Then, lysed samples were centrifuged for 5 min at 16000g, and the supernatants were collected. Protein extracts were purified by a modified TCA-acetone precipitation (2D-CleanUp Kit, GE Healthcare) and resuspended in 20µL of 6M urea and 50 mM ammonium bicarbonate buffer. Protein concentration was determined using the Bio-Rad RCDC Protein Assay (Bio-Rad, UK); **B) Trypsin digestion**: Samples (10mg of total protein each) were digested with trypsin. The appropriate volume of 6M urea and 50mM ammonium bicarbonate buffer was added to achieve a 20 µL final volume. Samples were first reduced with DTT (10mM) for 1h at room temperature (RT) and then alkylated with 20mM iodoacetamide for 30min at RT in the dark. The carbamidomethylating reaction was quenched by adding N-acetyl-L-cysteine at 35mM final concentration, followed by a 15' incubation at RT in the dark. Samples were diluted with 50mM ammonium bicarbonate to dilute Urea at 1M final concentration. Modified Porcine Trypsin (Promega Gold) was added in a 1:10 (w/w) ratio, and the mixture was incubated overnight at 37 °C. The reaction was stopped by adding formic acid (0.5% final concentration). Samples were kept at -20ºC until further analysis. **C) Liquid chromatography-mass spectrometry analysis (LC-MC)**: Samples were analyzed using an Orbitrap Eclipse mass spectrometer (Thermo Fisher Scientific, San Jose, CA, USA) coupled to an EASY-nLC 1200 (Thermo Fisher Scientific (Proxeon), Odense, Denmark). Peptides were loaded directly onto the analytical column and separated by a C18-based reversed-phase chromatography (50cm column with an inner diameter of 75µm, packed with 2µm C18 particles spectrometer - Thermo Scientific, San Jose, CA, USA). Chromatographic gradients consisted of 95% buffer A and 5% buffer B with a flow rate of 300 ml/min for 5 minutes, gradually changed to 75% A and 25% B in 78 min, and then to 60% A and 40% B in 12 min. After each analysis, the column was

washed for 10 min with 10% buffer A and 90% buffer B. Buffer A: 0.1% formic acid in water. Buffer B: 0.1% formic acid in 80% acetonitrile. The mass spectrometer was operated in positive ionization mode with nanospray voltage set at 2.4 kV and source temperature at 305°C. The acquisition was performed in data-dependent acquisition (DDA) mode, and full MS scans with one micro scan at a resolution of 120,000 were used over a mass range of m/z 350-1400 with detection in the Orbitrap mass analyzer. Auto gain control (AGC) was set to 'standard' and injection time to 'auto'. In each cycle of data-dependent acquisition analysis, following each survey scan, the most intense ions above a threshold ion count of 10000 were selected for fragmentation. The "Top Speed" acquisition algorithm and a dynamic exclusion of 60 seconds determined the number of selected precursor ions for fragmentation. Fragment ion spectra were produced via high-energy collision dissociation (HCD) at a normalized collision energy of 28%, and they were acquired in the ion trap mass analyzer. AGC and injection time were set to 'Standard' and 'Dynamic', respectively, and an isolation window of 1.4 m/z was used. **D)** Protein identification and quantitative differential analysis: Progenesis ® QI for proteomics software v3.0 (Nonlinear dynamics, UK) was used for MS data analysis using default settings. The LC-MS runs were automatically aligned to an automatically selected reference sample, and then alignment was manually reviewed. Only features within the 400 to 1,500 m/z range, 10 to 100 min retention time, and positive charges between 2 to 5 were considered for identification and quantification. Peak lists were generated from Progenesis and loaded to Proteome Discoverer v2.5 (Thermo Fisher Scientific) for protein identification. Proteins were identified using Mascot v2.5 (Matrix Science, London UK) to search the SwissProt database (taxonomy restricted to human proteins, 77,027 sequences). MS/MS spectra were searched with a precursor mass tolerance of 10 ppm, fragment tolerance of 0.5 Da, trypsin specificity with a maximum of 2 missed cleavages, cysteine carbamidomethylation set as fixed modification, and methionine oxidation as variable modification. The significance threshold for the identifications was set to p<0.05, with a minimum ions score of 20. Identifications were filtered at less than 1% FDR as evaluated by searching a decoy database. Label-free protein abundance quantification was based on the sum of the peak areas within the isotope boundaries of peptide ion peaks. A ratiometric median normalization of the measured MS signals was performed to compensate for small differences in sample load or MS signal during the analysis. Unique peptides were used for quantification. Statistical analysis was performed using Progenesis software. Proteins displaying greater than 2-fold change and p<0.05 (T-test) on the pairwise between adherent and floating groups were considered significantly different.

4.2.16. Statistical analysis and software

GraphPad Prism software performed statistical analysis by applying the tests indicated below each graph. GraphPad and BioRender were used for graphs and figures, respectively. Venn diagrams were drawn using the free tools available on the Bioinformatic & Evolutionary Genomics website (https://bioinformatics.psb.ugent.be/webtools/Venn/).

5. DISCUSSION

Bio-guided fractionation of AUN to identify chemotherapeutics for GIST treatment

The main obstacle in GIST clinical management is represented by the multifaceted landscape of imatinib resistance, which is not successfully targeted by multi-target TKIs (Di Vito et al., 2023). Different from these latter (Serrano et al., 2019), we observed that FR2-A, a fraction obtained from AUN through bio-guided fractionation, impairs the viability of both imatinib-sensitive and resistant GIST cells, independently from KIT expression and its mutational pattern. In detail, FR2-A targets GIST-48b, a KIT-independent cell line broadly resistant to multi-target TKIs, and GIST-48, a cellular model with a secondary KIT mutation that determines resistance to imatinib and sunitinib. FR2-A is even more efficient than imatinib in cells commonly recognized as imatinib-sensitive (Noma et al., 2005). Indeed, FR2-A induces a higher and more prompt reduction of GIST-882 viability than imatinib, promoting the rise of an Annexin V-positive cell population, a well-recognized marker of PS exposure on the extracellular membrane layer and consequently of early apoptosis, only modestly observed in imatinib-treated cells. This is consistent with literature findings that reported the capability of GIST-882 to counteract imatinib via the activation of quiescence, a mechanism of adaptive resistance that allows the escape from apoptosis (Boichuk et al., 2013; Y. Liu et al., 2008). The high percentage of Annexin V-positive cells in FR2-A treated GIST-882 suggests the absence or less efficiency of adaptive resistance towards the mechanism of action provided by FR2-A.

Unexpectedly, the reported increase of Annexin V-related signal in FR2-A treated GIST-882 is not associated with caspase activation. Since our flow cytometry data indicate that PS exposure occurs in GIST-882 before an alteration of the membrane integrity, in line with what is commonly observed in traditional apoptosis, FR2-A could promote cell death via an alternative mechanism of regulated cell death. In agreement with this hypothesis, numerous findings have indicated that PS exposure can also be observed in non-apoptotic forms of regulated cell death (Shlomovitz et al., 2019). Analogously, caspase-independent cell death (CICD) in response to intrinsic apoptotic signals has also been reported (Tait & Green, 2008). Notably, PARP1, a well-known downstream final target of the caspase-dependent cascade, is downregulated because of FR2-A treatment without the traditional pattern of cleavage induced by activated caspase-3. This result is particularly interesting since PARP1 is considered a promising target in cancer therapy, and no efficient therapeutic strategy has been developed so far (Peng et al., 2022). Additional studies are required to decipher how FR2-

A causes cell death in GIST cells and the relation between FR2-A treatment and PARP1 downregulation.

The bio-guided fractionation of FR2-A led to the identification of four groups of in-series active subfractions, revealing that a combination of bioactive NPs could be responsible for the FR2-A pharmacological effect. NMR analysis unveiled that pyrogallol-bearing compounds, such as gallic acid, myricetin hexoside, gallocatechin, and trigalloyl glucose, characterize the active FR2-A subfractions. No compounds with this moiety are observed in the non-active subfractions, highlighting the interest in pyrogallol-bearing compounds. We focused on gallic acid since it is present in the more potent fractions, 2A-35 and 2A-36, and because it has been associated with anti-cancer activity (Y. Jiang et al., 2022). However, even if similarly active at 30 µg/mL, the effect of gallic acid does not recapitulate the pharmacological activity observed with 2A-35 at 6 µg/mL, indicating that gallic acid acts in concert with further compounds in 2A-35, probably myricetin hexoside. Further preclinical investigations are required to evaluate the effect of myricetin hexoside, and other identified pyrogallol-bearing compounds in GIST cells. Moreover, since our preliminary experiments indicate a potential simultaneous activity of pyrogallol-bearing compounds, experiments to assess the pharmacological effect of their pure chemical combination could unveil the presence of additive or synergistic effects.

The broad efficacy of FR2-A is not limited to GIST cells, as testified by the similar cytotoxicity of FR2-A derived subfractions in resting PBMCs. The absence of specificity suggests a mechanism of action in line with that provided by traditional chemotherapeutics, known for their remarkable side effects in clinics. For example, doxorubicin, a conventional chemotherapeutic approved for treating many solid tumors, similarly impairs the viability of PBMCs *in vitro* and has been associated with frequent myelosuppressive side effects. Hence, data suggest that bioactive compounds in FR2-A could belong to the class of traditional chemotherapeutics by cytotoxicity analogy. Due to low PR in clinical trials, doxorubicin and the further available chemotherapeutics were not approved for GIST therapy (Dematteo et al., 2002). Indeed, according to the aforementioned clinical results, and differently the activity of FR2-A activity in GIST cellular models showed in our results, imatinib-resistant cell lines are reported to be resistant to doxorubicin (Pessetto et al., 2013). In confirmation of GIST cells' resistance to doxorubicin, a study has recently reported the improvement of doxorubicin sensitivity via the concomitant inhibition of AKT signaling (Boichuk et al., 2020). Therefore, studying FR2-A and its NPs could lead to identifying a novel chemotherapeutic for GIST therapy that could be a valid

alternative to TKIs. Despite the expected side effects in a hypothetical clinical use, FR2-A efficiently targets sensitive and resistant GIST cell lines. This supports the idea that its NPs provide a non-specific mechanism of action that could target most imatinib-resistant subclones, representing a potential positive balance between risk and benefit. In addition, since these compounds successfully affect the viability of KIT-independent GIST cells, they could also be promising for treating WT-GISTs, a therapy-orphan subclass of GISTs associated with primary imatinib resistance (Kays et al., 2018). Further *in vitro* assays in additional patients-derived cells, which better recapitulate the complexity of imatinib-resistant subclones and WT-GISTs, could strengthen the significance of these promising findings. These additional preclinical findings could pave the way for *in vivo* validations in murine models.

The cytotoxicity of FR2-A derived subfractions contrasts with the absence of AUN toxicity in HUVEC cells, a further healthy cellular model, reported by Cappadone C. and co-authors (Cappadone et al., 2019). However, this can be explained by the fact that they tested AUN as crude extract while we evaluated AUN fractions in which bioactive compounds were present in higher concentrations following bio-guided fractionation application.

The initial hypothesis that AUN could be a promising source of active NPs for GIST treatment has been corroborated. The bio-guided fractionation successfully enriched bioactive phytochemicals, unveiling a panel of pyrogallol-bearing compounds that could efficiently treat both imatinib-sensitive and -resistant GISTs. The continuation of the project to elucidate the elements that require further investigation could support the future clinical evaluation of pyrogallol-bearing compounds for GIST therapy.

In general, our project could also reinvigorate the interest in the potentiality of the vegetal kingdom for the drug discovery process. Applying a bio-guided fractionation-based approach, we successfully reduced the complexity of AUN and identified putative bioactive compounds, suggesting that exploring this research field could still be a source of outstanding hit or lead compounds. Indeed, numerous plant extracts have been associated with anti-cancer activity, but harbored bioactive compounds remain unknown (Rajabi et al., 2021).

An *in vitro* model for the study of metastasis in GISTs

Without an efficient therapy to neutralize the rise of imatinib-resistant subclones, tumor progression cannot be prevented, and metastasis remains the leading cause of GIST-related deaths. Therefore, developing drugs capable of counteracting the metastatic cascade could represent an alternative approach for ameliorating patient prognosis. However, the mechanisms behind metastasis remain unknown, and no preclinical metastasis models were available to identify promising targets.

Although GIST-T1 was established over 20 years ago, nobody has reported its use for the study of metastasis. We unveiled that GIST-T1 cells spontaneously give rise to viable cells in suspension, which can long survive in the culture medium, re-attach, and colonize a new tissue culture plate, thus mimicking certain features of the metastatic cascade *in vitro*. This behavior is not observed in GIST-882 and GIST-48 cells, suggesting that it exclusively characterizes GIST-T1. Notably, viable cells in suspension represent a minor percentage compared to the adherent cells from which they derive and reside in the culture medium with numerous cell death derivatives, such as debris, dying, and dead cells; this could explain why suspension cells in GIST-T1 have never been observed. Our findings are consistent with those published by Vargas-Accarino and co-authors, who described this metastatic-like behavior in C33a and SW-620 epithelial cancer cell lines for the first time (Vargas-Accarino et al., 2021).

We demonstrated that GIST-T1 harbors a small population of adherent cells, named metastatic-like cells, responsible for the origin of suspension cells. These cells undergo a phenotype modification during the transition between adherent and suspension cells. In detail, the canonical elongated phenotype of adherent cells is gradually modified in a circular, and, as confirmed by time-lapse microscopy, only circular-shaped cells can lose contact with the plate surface and reside in the culture medium transiently. This represents a crucial finding since it is largely recognized that metastatic cells require high plasticity to undergo the numerous steps of the metastatic cascade efficiently.

Changes in the conditioned medium are not responsible for the transition between adherent and suspension cells, but it is an intrinsic cell property. Re-attached cells, derived from suspension cells, can newly move in suspension in turn, indicating that this transition can be activated repeatedly. Hence, the involvement of the cell cycle was hypothesized since it is continuously activated by cancer cells in culture. We observed that the induction of quiescence inhibits the *in vitro* model, preventing

the detaching of cells. This represents proof that adherent cells transiently modify their adhesion property through the entry into the cell cycle, showing a time-dependent plasticity strictly related to the progression into the cell cycle. Indeed, as demonstrated, suspension cells duplicate in suspension and arguably re-attach at the end of the cell cycle, newly acquiring the canonical elongated shape. Further studies are required to decipher the differences between non-metastatic-like GIST-T1 cells that proliferate while maintaining adhesion to the plate surface and those that proliferate through an intermediate step represented by suspension cells. This could pave the way for unveiling what exclusively occurs to promote the transition in cells classified as metastatic-like.

In general, suspension cells could represent an *in vitro* model of metastatic CTCs (Eslami-S et al., 2022; Lin et al., 2021). Although numerous CTCs are commonly found in patients' blood, few can colonize a distant tissue, originating a metastasis. This is consistent with what the model has shown since suspension cells reside in the culture medium with cell death-related derivatives. In agreement, numerous CTCs could potentially represent a population of cells that detach from the tumor mass because they are directed toward cell death and not due to the activation of the metastatic cascade. Hence, studying suspension cells could identify biomarkers for characterizing real metastatic cells among CTCs. However, studying suspension cells is not straightforward due to cell death-related derivatives commonly found in the culture medium, which would make the study of suspension cells unreliable. Hence, to promote an accurate study of suspension cells, we set up a FACS-based method to collect viable cells selectively, allowing their study by omic sciences. Applying the method above, we selectively analyzed the proteome of suspension cells with respect to adherent in GIST-T1, C33a, and SW620. More than 1000 proteins were deregulated between adherent and suspension cells in the three cell lines, supporting the remarkable plasticity during this transition. Notably, 180 and 171 were found upregulated and downregulated in suspension cells independently from the cancer type, suggesting that they could be players commonly involved in the metastatic cascade. We focused our attention on CTR, RFC5, BCAT-2, and IPO9 among upregulated since they are mostly supported by statistical analysis (P-value < 0.01). Similarly, we selected TMF1, TIMM8B, SUB1, and LASP1 among the downregulated. Further studies are required to investigate the role of these proteins in the biology of suspension cells.

The primary study limitation is the absence of *in vivo* validations. Indeed, although proposed as an *in vitro* model since they recapitulate metastatic properties such as detachment, surviving in suspension, and re-attachment, no *in vivo* proof of their malignancies has been reported. The setting

of *in vivo* models based on the injection of suspension cells or evaluating the higher propensity to metastasize of Adh-F4-T1 tumors compared to that derived from progenitor GIST-T1 could show if this model also accurately recapitulates metastasis *in vivo*. Nevertheless, numerous findings corroborate its further investigation as a metastasis model. First, GIST-T1 was established from a metastasis associated with a primary GIST tumor. The origin from a metastasis supports the hypothesis that the cell line could harbor subclones that have maintained metastatic properties, even after many cell culture passages (Taguchi et al., 2002). Interestingly, consistent with the presented data, an independent study has demonstrated that mitosis is involved in the intravasation in a tissue-engineered tumor-microvessel platform, indicating that the movement of cells could be determined by the plasticity we have described (Wong & Searson, 2017). Moreover, LASP1, also named "Metastatic Lymph Node Gene 50 Protein", has drawn increasing interest for its role in malignancy and metastasis and is overexpressed in suspension cells that we have analyzed by proteomics (Chen et al., 2020). This supports the idea that the transition toward suspension cells could be associated with a more malignant profile. Lastly, confirmation of the malignant and pro-metastatic *in vivo* behavior of suspension cells has been recently confirmed (Huh et al., 2023). A comprehensive transcriptomic analysis comparing numerous adherent versus suspension cell lines identified several "Adherent-to-Suspension Transition" (AST) factors that can reprogram anchorage-dependent solid tumor cells into metastatic circulating tumor cells (CTCs). Targeting the AST factors suppresses the rise of CTCs and lung cancer metastasis dissemination in vivo. Therefore, validating this simplistic model could represent a promising approach to facilitate cheap, fast, and genome-wide screening of regulators and targets involved in GIST metastasis. Moreover, GIST-T1 suspension cells could be the basis for developing more advanced *in vitro* models, such as 3D models, and for establishing reliable *in vivo* models.

6. CONCLUSIONS

Bio-guided fractionation of AUN to identify chemotherapeutics for GIST treatment

Data presented provide evidence of the pharmacological activity of phytochemicals in AUN for targeting both imatinib-sensitive and resistant GIST cells, independently from KIT expression and its mutational pattern. These compounds show a non-specific mechanism of action, which was assimilated to doxorubicin due to an analogous cytotoxicity in PBMCs. The lack of specificity could represent an advantage, allowing the targeting of most imatinib-resistant subclones, including those resistant to TKIs, which cause progressive disease. NMR analysis unveiled the presence of pyrogallol-bearing compounds in active AUN-derived fractions, which could represent the bioactive compounds. Further studies are required to validate these compounds for GIST treatment. Moreover, our study represents an efficient application of bio-guided fractionation that could reinvigorate the interest in phytochemicals harbored in the vegetal kingdom for drug discovery processes.

An *in vitro* model for the study of metastasis in GISTs

We presented an *in vitro* model for studying metastasis in GISTs. A small population in GIST-T1 can spontaneously detach, survive in suspension without interaction with the plate surface or other cells, and re-attach if seeded in a new culture plate, mimicking metastatic-like features *in vitro*. Interestingly, metastatic-like cells show the plasticity arguably required to allow the successful completion of the metastatic cascade. When metastatic-like cells enter the cell cycle, they modify the phenotype and lose adhesion to the plate surface, moving in the culture medium as suspension cells. Suspension cells can progress into the cell cycle phases up to the division into two daughter cells. The end of the cell cycle arguably promotes the acquisition of adhesion properties to re-attach onto the plate surface. Therefore, our findings suggest a timing-dependent metastatic-like process punctuated by the cell cycle phases. Proteomic analysis between adherent and suspension cells unveiled numerous genes that are deregulated. Studying their roles in the biology of suspension cells could lead to identifying novel promising targets and improving knowledge about the mechanism behind metastasis in GISTs. Nevertheless, translating these *in vitro* findings *in vivo* is crucial to strengthen the significance of the established model.

7. REFERENCES

Abotaleb, M., Liskova, A., Kubatka, P., & Büsselberg, D. (2020). Therapeutic Potential of Plant Phenolic Acids in the Treatment of Cancer. *Biomolecules*, *10*(2), 221. https://doi.org/10.3390/biom10020221

Adeshakin, F. O., Adeshakin, A. O., Afolabi, L. O., Yan, D., Zhang, G., & Wan, X. (2021). Mechanisms for Modulating Anoikis Resistance in Cancer and the Relevance of Metabolic Reprogramming. *Frontiers in Oncology*, *11*. https://doi.org/10.3389/fonc.2021.626577

Albritton, J. L., & Miller, J. S. (2017). 3D bioprinting: improving *in vitro* models of metastasis with heterogeneous tumor microenvironments. *Disease Models & Mechanisms*, *10*(1), 3–14. https://doi.org/10.1242/dmm.025049

Amin, M. B., Greene, F. L., Edge, S. B., Compton, C. C., Gershenwald, J. E., Brookland, R. K., Meyer, L., Gress, D. M., Byrd, D. R., & Winchester, D. P. (2017). The Eighth Edition AJCC Cancer Staging Manual: Continuing to build a bridge from a population-based to a more "personalized" approach to cancer staging. *CA: A Cancer Journal for Clinicians*, *67*(2), 93–99. https://doi.org/10.3322/caac.21388

Antonescu, C. R., Besmer, P., Guo, T., Arkun, K., Hom, G., Koryotowski, B., Leversha, M. A., Jeffrey, P. D., Desantis, D., Singer, S., Brennan, M. F., Maki, R. G., & DeMatteo, R. P. (2005). Acquired Resistance to Imatinib in Gastrointestinal Stromal Tumor Occurs Through Secondary Gene Mutation. *Clinical Cancer Research*, *11*(11), 4182–4190. https://doi.org/10.1158/1078-0432.CCR-04-2245

Antonescu, C. R., Viale, A., Sarran, L., Tschernyavsky, S. J., Gonen, M., Segal, N. H., Maki, R. G., Socci, N. D., DeMatteo, R. P., & Besmer, P. (2004). Gene Expression in Gastrointestinal Stromal Tumors Is Distinguished by KIT Genotype and Anatomic Site. *Clinical Cancer Research*, *10*(10), 3282–3290. https://doi.org/10.1158/1078-0432.CCR-03-0715

Atanasov, A. G., Zotchev, S. B., Dirsch, V. M., & Supuran, C. T. (2021). Natural products in drug discovery: advances and opportunities. *Nature Reviews Drug Discovery*, *20*(3). https://doi.org/10.1038/s41573-020-00114-z

Balachandran, V. P., & DeMatteo, R. P. (2014). GIST tumors: Who should get imatinib and for how long? *Advances in Surgery*, *48*(1). https://doi.org/10.1016/j.yasu.2014.05.014

Bauer, S., Jones, R. L., Blay, J.-Y., Gelderblom, H., George, S., Schöffski, P., von Mehren, M., Zalcberg, J. R., Kang, Y.-K., Razak, A. A., Trent, J., Attia, S., Le Cesne, A., Su, Y., Meade, J., Wang, T., Sherman, M. L., Ruiz-Soto, R., & Heinrich, M. C. (2022). Ripretinib Versus Sunitinib in Patients With Advanced Gastrointestinal Stromal Tumor After Treatment With Imatinib (INTRIGUE): A Randomized, Open-Label, Phase III Trial. *Journal of Clinical Oncology*, *40*(34), 3918–3928. https://doi.org/10.1200/JCO.22.00294

Bersini, S., Jeon, J. S., Moretti, M., & Kamm, R. D. (2014). In vitro models of the metastatic cascade: from local invasion to extravasation. *Drug Discovery Today*, *19*(6), 735–742. https://doi.org/10.1016/j.drudis.2013.12.006

Bessah, R., & Benyoussef, E.-H. (2012). Essential Oil Composition of *Arbutus unedo* L. Leaves from Algeria. *Journal of Essential Oil Bearing Plants*, *15*(4), 678–681. https://doi.org/10.1080/0972060X.2012.10644105

Blanke, C. D., Demetri, G. D., von Mehren, M., Heinrich, M. C., Eisenberg, B., Fletcher, J. A., Corless, C. L., Fletcher, C. D. M., Roberts, P. J., Heinz, D., Wehre, E., Nikolova, Z., & Joensuu, H. (2008). Long-Term Results From a Randomized Phase II Trial of Standard- Versus Higher-Dose Imatinib Mesylate for Patients With Unresectable or Metastatic Gastrointestinal Stromal Tumors Expressing *KIT*. *Journal of Clinical Oncology*, *26*(4). https://doi.org/10.1200/JCO.2007.13.4403

Blay, J.-Y., Le Cesne, A., Ray-Coquard, I., Bui, B., Duffaud, F., Delbaldo, C., Adenis, A., Viens, P., Rios, M., Bompas, E., Cupissol, D., Guillemet, C., Kerbrat, P., Fayette, J., Chabaud, S., Berthaud, P., & Perol, D. (2007). Prospective Multicentric Randomized Phase III Study of Imatinib in Patients With Advanced Gastrointestinal Stromal Tumors Comparing Interruption Versus Continuation of Treatment Beyond 1 Year: The French Sarcoma Group. *Journal of Clinical Oncology*, *25*(9). https://doi.org/10.1200/JCO.2006.09.0183

Blay, J.-Y., Serrano, C., Heinrich, M. C., Zalcberg, J., Bauer, S., Gelderblom, H., Schöffski, P., Jones, R. L., Attia, S., D'Amato, G., Chi, P., Reichardt, P., Meade, J., Shi, K., Ruiz-Soto, R., George, S., & von Mehren, M. (2020). Ripretinib in patients with advanced gastrointestinal stromal tumours (INVICTUS): a double-blind, randomised, placebo- controlled, phase 3 trial. *The Lancet Oncology*, *21*(7), 923–934. https://doi.org/10.1016/S1470-2045(20)30168-6

Blomberg, O. S., Spagnuolo, L., & de Visser, K. E. (2018). Immune regulation of metastasis: mechanistic insights and therapeutic opportunities. *Disease Models & Mechanisms*, *11*(10). https://doi.org/10.1242/dmm.036236

Boichuk, S., Bikinieva, F., Nurgatina, I., Dunaev, P., Valeeva, E., Aukhadieva, A., Sabirov, A., & Galembikova, A. (2020). Inhibition of AKT-Signaling Sensitizes Soft Tissue Sarcomas (STS) and Gastrointestinal Stromal Tumors (GIST) to Doxorubicin via Targeting of Homology- Mediated DNA Repair. *International Journal of Molecular Sciences*, *21*(22). https://doi.org/10.3390/ijms21228842

Boichuk, S., Galembikova, A., Dunaev, P., Valeeva, E., Shagimardanova, E., Gusev, O., & Khaiboullina, S. (2017). A Novel Receptor Tyrosine Kinase Switch Promotes Gastrointestinal Stromal Tumor Drug Resistance. *Molecules*, *22*(12). https://doi.org/10.3390/molecules22122152

Boichuk, S., Parry, J. A., Makielski, K. R., Litovchick, L., Baron, J. L., Zewe, J. P., Wozniak, A., Mehalek, K. R., Korzeniewski, N., Seneviratne, D. S., Schöffski, P., Debiec-Rychter, M., DeCaprio, J. A., & Duensing, A. (2013). The DREAM Complex Mediates GIST Cell

Quiescence and Is a Novel Therapeutic Target to Enhance Imatinib-Induced Apoptosis. *Cancer Research*, *73*(16). https://doi.org/10.1158/0008-5472.CAN-13-0579

Bosbach, B., Rossi, F., Yozgat, Y., Loo, J., Zhang, J. Q., Berrozpe, G., Warpinski, K., Ehlers, I., Veach, D., Kwok, A., Manova, K., Antonescu, C. R., DeMatteo, R. P., & Besmer, P. (2017). Direct engagement of the PI3K pathway by mutant KIT dominates oncogenic signaling in gastrointestinal stromal tumor. *Proceedings of the National Academy of Sciences*, *114*(40). https://doi.org/10.1073/pnas.1711449114

Boussommier-Calleja, A. (2020). In vitro models of cancer. In *Bioengineering Innovative Solutions for Cancer* (pp. 273–325). Elsevier. https://doi.org/10.1016/B978-0-12-813886-1.00013-9

Brahmkhatri, V. P., Prasanna, C., & Atreya, H. S. (2015). Insulin-Like Growth Factor System in Cancer: Novel Targeted Therapies. *BioMed Research International*, *2015*, 1–24. https://doi.org/10.1155/2015/538019

Briguglio, G., Costa, C., Pollicino, M., Giambò, F., Catania, S., & Fenga, C. (2020). Polyphenols in cancer prevention: New insights (Review). *International Journal of Functional Nutrition*, *1*(2), 9. https://doi.org/10.3892/ijfn.2020.9

Buchheit, C. L., Weigel, K. J., & Schafer, Z. T. (2014). Cancer cell survival during detachment from the ECM: multiple barriers to tumour progression. *Nature Reviews Cancer*, *14*(9), 632–641. https://doi.org/10.1038/nrc3789

Cappadone, C., Mandrone, M., Chiocchio, I., Sanna, C., Malucelli, E., Bassi, V., Picone, G., & Poli, F. (2019). Antitumor Potential and Phytochemical Profile of Plants from Sardinia (Italy), a Hotspot for Biodiversity in the Mediterranean Basin. *Plants*, *9*(1). https://doi.org/10.3390/plants9010026

Cháirez-Ramírez, M. H., de la Cruz-López, K. G., & García-Carrancá, A. (2021). Polyphenols as Antitumor Agents Targeting Key Players in Cancer-Driving Signaling Pathways. *Frontiers in Pharmacology*, *12*. https://doi.org/10.3389/fphar.2021.710304

Chen, W., Li, Z., Liu, H., Jiang, S., Wang, G., Sun, L., Li, J., Wang, X., Yu, S., Huang, J., & Dong, Y. (2020). MicroRNA-30a targets BECLIN-1 to inactivate autophagy and sensitizes gastrointestinal stromal tumor cells to imatinib. *Cell Death & Disease*, *11*(3). https://doi.org/10.1038/s41419-020-2390-7

Cheng, X., Wang, J., Lu, S., Fan, W., & Wang, W. (2021). Aurora kinase A (AURKA) promotes the progression and imatinib resistance of advanced gastrointestinal stromal tumors. *Cancer Cell International*, *21*(1), 407. https://doi.org/10.1186/s12935-021-02111-7

Chompret, A., Kannengiesser, C., Barrois, M., Terrier, P., Dahan, P., Tursz, T., Lenoir, G. M., & Bressac-De Paillerets, B. (2004). PDGFRA germline mutation in a family with multiple cases of gastrointestinal stromal tumor. *Gastroenterology*, *126*(1), 318–321. https://doi.org/10.1053/j.gastro.2003.10.079

Chou, A., Chen, J., Clarkson, A., Samra, J. S., Clifton-Bligh, R. J., Hugh, T. J., & Gill, A. J. (2012). Succinate dehydrogenase-deficient GISTs are characterized by IGF1R overexpression. *Modern Pathology*, *25*(9), 1307–1313. https://doi.org/10.1038/modpathol.2012.77

Cohen, N. A., Zeng, S., Seifert, A. M., Kim, T. S., Sorenson, E. C., Greer, J. B., Beckman, M. J., Santamaria-Barria, J. A., Crawley, M. H., Green, B. L., Rossi, F., Besmer, P., Antonescu, C. R., & DeMatteo, R. P. (2015). Pharmacological Inhibition of KIT Activates MET Signaling in Gastrointestinal Stromal Tumors. *Cancer Research*, *75*(10). https://doi.org/10.1158/0008-5472.CAN-14-2564

Corless, C. L., Barnett, C. M., & Heinrich, M. C. (2011). Gastrointestinal stromal tumours: Origin and molecular oncology. In *Nature Reviews Cancer* (Vol. 11, Issue 12, pp. 865–878). https://doi.org/10.1038/nrc3143

Demarque, D. P., Dusi, R. G., de Sousa, F. D. M., Grossi, S. M., Silvério, M. R. S., Lopes, N. P., & Espindola, L. S. (2020). Mass spectrometry-based metabolomics approach in the isolation of bioactive natural products. *Scientific Reports*, *10*(1), 1051. https://doi.org/10.1038/s41598-020-58046-y

Dematteo, R. P., Heinrich, M. C., El-Rifai, W. M., & Demetri, G. (2002). Clinical management of gastrointestinal stromal tumors: Before and after STI-571. *Human Pathology*, *33*(5). https://doi.org/10.1053/hupa.2002.124122

DeMatteo, R. P., Lewis, J. J., Leung, D., Mudan, S. S., Woodruff, J. M., & Brennan, M. F. (2000). Two Hundred Gastrointestinal Stromal Tumors. *Annals of Surgery*, *231*(1), 51. https://doi.org/10.1097/00000658-200001000-00008

Demetri, G. D., Reichardt, P., Kang, Y.-K., Blay, J.-Y., Rutkowski, P., Gelderblom, H., Hohenberger, P., Leahy, M., von Mehren, M., Joensuu, H., Badalamenti, G., Blackstein, M., Le Cesne, A., Schöffski, P., Maki, R. G., Bauer, S., Nguyen, B. B., Xu, J., Nishida, T., … Casali, P. G. (2013). Efficacy and safety of regorafenib for advanced gastrointestinal stromal tumours after failure of imatinib and sunitinib (GRID): an international, multicentre, randomised, placebo-controlled, phase 3 trial. *The Lancet*, *381*(9863). https://doi.org/10.1016/S0140-6736(12)61857-1

Demetri, G. D., van Oosterom, A. T., Garrett, C. R., Blackstein, M. E., Shah, M. H., Verweij, J., McArthur, G., Judson, I. R., Heinrich, M. C., Morgan, J. A., Desai, J., Fletcher, C. D., George, S., Bello, C. L., Huang, X., Baum, C. M., & Casali, P. G. (2006). Efficacy and safety of sunitinib in patients with advanced gastrointestinal stromal tumour after failure of imatinib: a randomised controlled trial. *The Lancet*, *368*(9544), 1329–1338. https://doi.org/10.1016/S0140-6736(06)69446-4

Dhillon, S. (2020a). Avapritinib: First Approval. *Drugs*, *80*(4). https://doi.org/10.1007/s40265-020-01275-2

Dhillon, S. (2020b). Ripretinib: First Approval. *Drugs*, *80*(11), 1133–1138. https://doi.org/10.1007/s40265-020-01348-2

Di Vito, A., Ravegnini, G., Gorini, F., Aasen, T., Serrano, C., Benuzzi, E., Coschina, E., Monesmith, S., Morroni, F., Angelini, S., & Hrelia, P. (2023). The multifaceted landscape behind imatinib resistance in gastrointestinal stromal tumors (GISTs): A lesson from ripretinib. *Pharmacology & Therapeutics*, *248*, 108475. https://doi.org/10.1016/j.pharmthera.2023.108475

Dillekås, H., Rogers, M. S., & Straume, O. (2019). Are 90% of deaths from cancer caused by metastases? *Cancer Medicine*, *8*(12), 5574–5576. https://doi.org/10.1002/cam4.2474

Du, C., Duan, X., Yao, X., Wan, J., Cheng, Y., Wang, Y., Yan, Y., Zhang, L., Zhu, L., Ni, C., Wang, M., & Qin, Z. (2020). Tumour-derived exosomal miR-3473b promotes lung tumour cell intrapulmonary colonization by activating the nuclear factor-κB of local fibroblasts. *Journal of Cellular and Molecular Medicine*, *24*(14), 7802–7813. https://doi.org/10.1111/jcmm.15411

Duensing, A., Medeiros, F., McConarty, B., Joseph, N. E., Panigrahy, D., Singer, S., Fletcher, C. D., Demetri, G. D., & Fletcher, J. A. (2004). Mechanisms of oncogenic KIT signal transduction in primary gastrointestinal stromal tumors (GISTs). *Oncogene*, *23*(22), 3999–4006. https://doi.org/10.1038/sj.onc.1207525

Edmonson, J. H., Marks, R. S., Buckner, J. C., & Mahoney, M. R. (2002). Contrast of Response to Dacarbazine, Mitomycin, Doxorubicin, and Cisplatin (DMAP) Plus GM-CSF Between Patients with Advanced Malignant Gastrointestinal Stromal Tumors and Patients with Other Advanced Leiomyosarcomas. *Cancer Investigation*, *20*(5–6), 605–612. https://doi.org/10.1081/CNV-120002485

Erkekoglou, I., Nenadis, N., Samara, E., & Mantzouridou, F. Th. (2017). Functional Teas from the Leaves of Arbutus unedo: Phenolic Content, Antioxidant Activity, and Detection of Efficient Radical Scavengers. *Plant Foods for Human Nutrition*, *72*(2), 176–183. https://doi.org/10.1007/s11130-017-0607-4

Eslami-S, Z., Cortés-Hernández, L. E., Thomas, F., Pantel, K., & Alix-Panabières, C. (2022). Functional analysis of circulating tumour cells: the KEY to understand the biology of the metastatic cascade. *British Journal of Cancer*, *127*(5), 800–810. https://doi.org/10.1038/s41416-022-01819-1

Evans, E. K., Gardino, A. K., Kim, J. L., Hodous, B. L., Shutes, A., Davis, A., Zhu, X. J., Schmidt-Kittler, O., Wilson, D., Wilson, K., DiPietro, L., Zhang, Y., Brooijmans, N., LaBranche, T. P., Wozniak, A., Gebreyohannes, Y. K., Schöffski, P., Heinrich, M. C., DeAngelo, D. J., … Lengauer, C. (2017). A precision therapy against cancers driven by *KIT/PDGFRA* mutations. *Science Translational Medicine*, *9*(414). https://doi.org/10.1126/scitranslmed.aao1690

Fan, R., Zhong, J., Zheng, S., Wang, Z., Xu, Y., Li, S., Zhou, J., & Yuan, F. (2015). microRNA-218 increase the sensitivity of gastrointestinal stromal tumor to imatinib through PI3K/AKT pathway. *Clinical and Experimental Medicine*, *15*(2). https://doi.org/10.1007/s10238-014-0280-y

Fares, J., Fares, M. Y., Khachfe, H. H., Salhab, H. A., & Fares, Y. (2020). Molecular principles of metastasis: a hallmark of cancer revisited. *Signal Transduction and Targeted Therapy*, *5*(1), 28. https://doi.org/10.1038/s41392-020-0134-x

Foo, W. C., Liegl-Atzwanger, B., & Lazar, A. J. (2012). Pathology of Gastrointestinal Stromal Tumors. *Clinical Medicine Insights: Pathology*, *5*, CPath.S9689. https://doi.org/10.4137/CPath.S9689

Fretto, L. J., Snape, A. J., Tomlinson, J. E., Seroogy, J. J., Wolf, D. L., LaRochelle, W. J., & Giese, N. A. (1993). Mechanism of platelet-derived growth factor (PDGF) AA, AB, and BB binding to alpha and beta PDGF receptor. *The Journal of Biological Chemistry*, *268*(5), 3625–3631.

Gao, X., Shen, K., Wang, C., Ling, J., Wang, H., Fang, Y., Shi, Y., Hou, Y., Qin, J., Sun, Y., & Qin, X. (2014). MiR-320a downregulation is associated with imatinib resistance in gastrointestinal stromal tumors. *Acta Biochimica et Biophysica Sinica*, *46*(1). https://doi.org/10.1093/abbs/gmt118

García-Valverde, A., Rosell, J., Sayols, S., Gómez-Peregrina, D., Pilco-Janeta, D. F., Olivares-Rivas, I., de Álava, E., Maurel, J., Rubió-Casadevall, J., Esteve, A., Gut, M., Valverde, C., Barretina, J., Carles, J., Demetri, G. D., Fletcher, J. A., Arribas, J., & Serrano, C. (2021). E3 ubiquitin ligase Atrogin-1 mediates adaptive resistance to KIT-targeted inhibition in gastrointestinal stromal tumor. *Oncogene*, *40*(48), 6614–6626. https://doi.org/10.1038/s41388-021-02049-0

Gastrointestinal Stromal Tumor Meta-Analysis Group (MetaGIST). (2010). Comparison of Two Doses of Imatinib for the Treatment of Unresectable or Metastatic Gastrointestinal Stromal Tumors: A Meta-Analysis of 1,640 Patients. *Journal of Clinical Oncology*, *28*(7), 1247–1253. https://doi.org/10.1200/JCO.2009.24.2099

Gatto, L., Nannini, M., Saponara, M., Di Scioscio, V., Beltramo, G., Frezza, G. P., Ercolani, G., Pinna, A. D., Astolfi, A., Urbini, M., Brandi, G., Biasco, G., & Pantaleo, M. A. (2017). Radiotherapy in the management of gist: state of the art and new potential scenarios. *Clinical Sarcoma Research*, *7*(1). https://doi.org/10.1186/s13569-016-0065-z

George, S., Blay, J. Y., Casali, P. G., Le Cesne, A., Stephenson, P., DePrimo, S. E., Harmon, C. S., Law, C. N. J., Morgan, J. A., Ray-Coquard, I., Tassell, V., Cohen, D. P., & Demetri, G. D. (2009). Clinical evaluation of continuous daily dosing of sunitinib malate in patients with advanced gastrointestinal stromal tumour after imatinib failure. *European Journal of Cancer*, *45*(11), 1959–1968. https://doi.org/10.1016/j.ejca.2009.02.011

Gill, A. J. (2012). Succinate dehydrogenase (SDH) and mitochondrial driven neoplasia. *Pathology*, *44*(4), 285–292. https://doi.org/10.1097/PAT.0b013e3283539932

Graziani, V., Scognamiglio, M., Belli, V., Esposito, A., D'Abrosca, B., Chambery, A., Russo, R., Panella, M., Russo, A., Ciardiello, F., Troiani, T., Potenza, N., & Fiorentino, A. (2018). Metabolomic approach for a rapid identification of natural products with cytotoxic activity against human colorectal cancer cells. *Scientific Reports*, *8*(1), 5309. https://doi.org/10.1038/s41598-018-23704-9

Gupta, A., Roy, S., Lazar, A. J. F., Wang, W.-L., McAuliffe, J. C., Reynoso, D., McMahon, J., Taguchi, T., Floris, G., Debiec-Rychter, M., Schoffski, P., Trent, J. A., Debnath, J., & Rubin, B. P. (2010). Autophagy inhibition and antimalarials promote cell death in gastrointestinal stromal tumor (GIST). *Proceedings of the National Academy of Sciences*, *107*(32). https://doi.org/10.1073/pnas.1000248107

Hamid, A. B., & Petreaca, R. C. (2020). Secondary Resistant Mutations to Small Molecule Inhibitors in Cancer Cells. *Cancers*, *12*(4), 927. https://doi.org/10.3390/cancers12040927

Hanks, S. K., Quinn, A. M., & Hunter, T. (1988). The Protein Kinase Family: Conserved Features and Deduced Phylogeny of the Catalytic Domains. *Science*, *241*(4861), 42–52. https://doi.org/10.1126/science.3291115

Harrison, C. (2014). Patenting natural products just got harder. *Nature Biotechnology*, *32*(5), 403–404. https://doi.org/10.1038/nbt0514-403a

Hebert, J. D., Neal, J. W., & Winslow, M. M. (2023). Dissecting metastasis using preclinical models and methods. *Nature Reviews Cancer*, *23*(6), 391–407. https://doi.org/10.1038/s41568-023-00568-4

Heinrich, M. C., Griffith, D. J., Druker, B. J., Wait, C. L., Ott, K. A., & Zigler, A. J. (2000). Inhibition of c-kit receptor tyrosine kinase activity by STI 571, a selective tyrosine kinase inhibitor. *Blood*, *96*(3), 925–932. https://doi.org/10.1182/blood.V96.3.925

Heinrich, M. C., Jones, R. L., von Mehren, M., Schöffski, P., Serrano, C., Kang, Y.-K., Cassier, P. A., Mir, O., Eskens, F., Tap, W. D., Rutkowski, P., Chawla, S. P., Trent, J., Tugnait, M., Evans, E. K., Lauz, T., Zhou, T., Roche, M., Wolf, B. B., … George, S. (2020). Avapritinib in advanced PDGFRA D842V-mutant gastrointestinal stromal tumour (NAVIGATOR): a multicentre, open-label, phase 1 trial. *The Lancet Oncology*, *21*(7), 935–946. https://doi.org/10.1016/S1470-2045(20)30269-2

Henrich, C. J., & Beutler, J. A. (2013). Matching the power of high throughput screening to the chemical diversity of natural products. *Natural Product Reports*, *30*(10), 1284. https://doi.org/10.1039/c3np70052f

Hirota, S. (1998). Gain-of-Function Mutations of c-kit in Human Gastrointestinal Stromal Tumors. *Science*, *279*(5350). https://doi.org/10.1126/science.279.5350.577

Hirota, S., Nishida, T., Isozaki, K., Taniguchi, M., Nishikawa, K., Ohashi, A., Takabayashi, A., Obayashi, T., Okuno, T., Kinoshita, K., Chen, H., Shinomura, Y., & Kitamura, Y. (2002). Familial gastrointestinal stromal tumors associated with dysphagia and novel type germline mutation of KIT gene. *Gastroenterology*, *122*(5), 1493–1499. https://doi.org/10.1053/gast.2002.33024

Hirota, S., Ohashi, A., Nishida, T., Isozaki, K., Kinoshita, K., Shinomura, Y., & Kitamura, Y. (2003). Gain-of-function mutations of platelet-derived growth factor receptor α gene in gastrointestinal stromal tumors. *Gastroenterology*, *125*(3), 660–667. https://doi.org/10.1016/S0016-5085(03)01046-1

Hohenberger, P., Langer, C., Wendtner, C. M., Hohenberger, W., Pustowka, A., Wardelmann, E., Andre, E., & Licht, T. (2012). Neoadjuvant treatment of locally advanced GIST: Results of APOLLON, a prospective, open label phase II study in KIT- or PDGFRA-positive tumors. *Journal of Clinical Oncology*, *30*(15_suppl), 10031–10031. https://doi.org/10.1200/jco.2012.30.15_suppl.10031

Hu, X., Wang, Z., Su, P., Zhang, Q., & Kou, Y. (2022). Advances in the research of the mechanism of secondary resistance to imatinib in gastrointestinal stromal tumors. *Frontiers in Oncology*, *12*. https://doi.org/10.3389/fonc.2022.933248

Hubrecht, & Carter. (2019). The 3Rs and Humane Experimental Technique: Implementing Change. *Animals*, *9*(10), 754. https://doi.org/10.3390/ani9100754

Huh, H. D., Sub, Y., Oh, J., Kim, Y. E., Lee, J. Y., Kim, H.-R., Lee, S., Lee, H., Pak, S., Amos, S. E., Vahala, D., Park, J. H., Shin, J. E., Park, S. Y., Kim, H. S., Roh, Y. H., Lee, H.-W., Guan, K.-L., Choi, Y. S., … Park, H. W. (2023). Reprogramming anchorage dependency by adherent-to-suspension transition promotes metastatic dissemination. *Molecular Cancer*, *22*(1), 63. https://doi.org/10.1186/s12943-023-01753-7

Jiang, L., Tixeira, R., Caruso, S., Atkin-Smith, G. K., Baxter, A. A., Paone, S., Hulett, M. D., & Poon, I. K. H. (2016). Monitoring the progression of cell death and the disassembly of dying cells by flow cytometry. *Nature Protocols*, *11*(4), 655–663. https://doi.org/10.1038/nprot.2016.028

Jiang, L., Wang, D., Zhang, Y., Li, J., Wu, Z., Wang, Z., & Wang, D. (2017). Investigation of the pro-apoptotic effects of arbutin and its acetylated derivative on murine melanoma cells. *International Journal of Molecular Medicine*. https://doi.org/10.3892/ijmm.2017.3256

Jiang, Y., Pei, J., Zheng, Y., Miao, Y., Duan, B., & Huang, L. (2022). Gallic Acid: A Potential Anti-Cancer Agent. *Chinese Journal of Integrative Medicine*, *28*(7), 661–671. https://doi.org/10.1007/s11655-021-3345-2

Joensuu, H., Roberts, P. J., Sarlomo-Rikala, M., Andersson, L. C., Tervahartiala, P., Tuveson, D., Silberman, S. L., Capdeville, R., Dimitrijevic, S., Druker, B., & Demetri, G. D. (2001). Effect of the Tyrosine Kinase Inhibitor STI571 in a Patient with a Metastatic Gastrointestinal Stromal Tumor. *New England Journal of Medicine*, *344*(14), 1052–1056. https://doi.org/10.1056/NEJM200104053441404

Kang, S., Ryu, M.-H., Bang, Y. H., Kim, H.-D., Lee, H. E., & Kang, Y.-K. (2022). Adjuvant Imatinib Treatment for 5 Years versus 3 Years in Patients with Ruptured Localized Gastrointestinal Stromal Tumor: A Retrospective Analysis. *Cancer Research and Treatment*, *54*(4), 1167–1174. https://doi.org/10.4143/crt.2021.1040

Katt, M. E., Placone, A. L., Wong, A. D., Xu, Z. S., & Searson, P. C. (2016). In Vitro Tumor Models: Advantages, Disadvantages, Variables, and Selecting the Right Platform. *Frontiers in Bioengineering and Biotechnology*, *4*. https://doi.org/10.3389/fbioe.2016.00012

Kays, J. K., Sohn, J. D., Kim, B. J., Goze, K., & Koniaris, L. G. (2018). Approach to wild-type gastrointestinal stromal tumors. *Translational Gastroenterology and Hepatology*, *3*, 92–92. https://doi.org/10.21037/tgh.2018.10.13

Khan, H. (2014). Medicinal Plants in Light of History: Recognized Therapeutic Modality. *Journal of Evidence-Based Complementary & Alternative Medicine*, *19*(3), 216–219. https://doi.org/10.1177/2156587214533346

Kim, J. W., Choi, J., Park, M. N., & Kim, B. (2023). Apoptotic Effect of Gallic Acid via Regulation of p-p38 and ER Stress in PANC-1 and MIA PaCa-2 Cells Pancreatic Cancer Cells. *International Journal of Molecular Sciences*, *24*(20), 15236. https://doi.org/10.3390/ijms242015236

Kindblom, L. G., Remotti, H. E., Aldenborg, F., & Meis-Kindblom, J. M. (1998). Gastrointestinal pacemaker cell tumor (GIPACT): gastrointestinal stromal tumors show phenotypic characteristics of the interstitial cells of Cajal. *The American Journal of Pathology*, *152*(5), 1259–1269.

Kivçak, B., & Mert, T. (2001). Quantitative determination of α-tocopherol in Arbutus unedo by TLC-densitometry and colorimetry. *Fitoterapia*, *72*(6), 656–661. https://doi.org/10.1016/S0367-326X(01)00305-7

Klein, C. A. (2009). Parallel progression of primary tumours and metastases. *Nature Reviews Cancer*, *9*(4), 302–312. https://doi.org/10.1038/nrc2627

Langley, R. R., & Fidler, I. J. (2011). The seed and soil hypothesis revisited-The role of tumor-stroma interactions in metastasis to different organs. *International Journal of Cancer*, *128*(11), 2527–2535. https://doi.org/10.1002/ijc.26031

Lasota, J., Corless, C. L., Heinrich, M. C., Debiec-Rychter, M., Sciot, R., Wardelmann, E., Merkelbach-Bruse, S., Schildhaus, H.-U., Steigen, S. E., Stachura, J., Wozniak, A., Antonescu, C., Daum, O., Martin, J., del Muro, J. G., & Miettinen, M. (2008). Clinicopathologic profile of gastrointestinal stromal tumors (GISTs) with primary KIT exon 13 or exon 17 mutations: a multicenter study on 54 cases. *Modern Pathology*, *21*(4), 476–484. https://doi.org/10.1038/modpathol.2008.2

Lasota, J., & Miettinen, M. (2006). KIT and PDGFRA mutations in gastrointestinal stromal tumors (GISTs). *Seminars in Diagnostic Pathology*, *23*(2), 91–102. https://doi.org/10.1053/j.semdp.2006.08.006

Lev, S., Yarden, Y., & Givol, D. (1992). Dimerization and activation of the kit receptor by monovalent and bivalent binding of the stem cell factor. *The Journal of Biological Chemistry*, *267*(22), 15970–15977.

Liao, Y., Li, S., An, J., Yu, X., Tan, X., Gui, Y., Wang, Y., Huang, L., Zhou, S., & Wang, D. (2023). Ethyl acetate extract of Antenoron Filiforme inhibits the proliferation of triple negative breast cancer cells via suppressing Skp2/p21 signaling axis. *Phytomedicine*, *116*, 154856. https://doi.org/10.1016/j.phymed.2023.154856

Lin, H.-H., Chan, K.-C., Sheu, J.-Y., Hsuan, S.-W., Wang, C.-J., & Chen, J.-H. (2012). Hibiscus sabdariffa leaf induces apoptosis of human prostate cancer cells in vitro and in vivo. *Food Chemistry*, *132*(2), 880–891. https://doi.org/10.1016/j.foodchem.2011.11.057

Liu, S., Liao, G., Ding, J., Ye, K., Zhang, Y., Zeng, L., & Chen, S. (2014). Dysregulated expression of Snail and E-cadherin correlates with gastrointestinal stromal tumor metastasis. *European Journal of Cancer Prevention*, *23*(5), 329–335. https://doi.org/10.1097/CEJ.0000000000000072

Liu, Y., Perdreau, S. A., Chatterjee, P., Wang, L., Kuan, S.-F., & Duensing, A. (2008). Imatinib Mesylate Induces Quiescence in Gastrointestinal Stromal Tumor Cells through the CDH1-SKP2-p27 [Kip1] Signaling Axis. *Cancer Research*, *68*(21). https://doi.org/10.1158/0008-5472.CAN-08-1935

Lorusso, G., & Rüegg, C. (2012). New insights into the mechanisms of organ-specific breast cancer metastasis. *Seminars in Cancer Biology*, *22*(3), 226–233. https://doi.org/10.1016/j.semcancer.2012.03.007

Lostes-Bardaji, M. J., García-Illescas, D., Valverde, C., & Serrano, C. (2021). Ripretinib in gastrointestinal stromal tumor: the long-awaited step forward. *Therapeutic Advances in Medical Oncology*, *13*. https://doi.org/10.1177/1758835920986498

Luzzi, K. J., MacDonald, I. C., Schmidt, E. E., Kerkvliet, N., Morris, V. L., Chambers, A. F., & Groom, A. C. (1998). Multistep Nature of Metastatic Inefficiency. *The American Journal of Pathology*, *153*(3), 865–873. https://doi.org/10.1016/S0002-9440(10)65628-3

Majidpoor, J., & Mortezaee, K. (2021). Steps in metastasis: an updated review. *Medical Oncology*, *38*(1), 3. https://doi.org/10.1007/s12032-020-01447-w

Malandrino, A., Kamm, R. D., & Moeendarbary, E. (2018). In Vitro Modeling of Mechanics in Cancer Metastasis. *ACS Biomaterials Science & Engineering*, *4*(2), 294–301. https://doi.org/10.1021/acsbiomaterials.7b00041

Mani, J., Johnson, J., Hosking, H., Hoyos, B. E., Walsh, K. B., Neilsen, P., & Naiker, M. (2022). Bioassay Guided Fractionation Protocol for Determining Novel Active Compounds in Selected Australian Flora. *Plants*, *11*(21), 2886. https://doi.org/10.3390/plants11212886

Martins, J., Batista, T., Pinto, G., & Canhoto, J. (2021). Seasonal variation of phenolic compounds in Strawberry tree (Arbutus unedo L.) leaves and inhibitory potential on Phytophthora cinnamomi. *Trees*, *35*(5), 1571–1586. https://doi.org/10.1007/s00468-021-02137-4

Mazur, M. T., & Clark, H. B. (1983). Gastric stromal tumors Reappraisal of histogenesis. *The American Journal of Surgical Pathology*, *7*(6), 507–520. https://doi.org/10.1097/00000478-198309000-00001

Miettinen, M., Virolainen, M., & Maarit-Sarlomo-Rikala. (1995). Gastrointestinal Stromal Tumors—Value of CD34 Antigen in their Identification and Separation from True Leiomyomas and Schwannomas. *The American Journal of Surgical Pathology*, *19*(2), 207–216. https://doi.org/10.1097/00000478-199502000-00009

Miettinen, M., Wang, Z.-F., & Lasota, J. (2009). DOG1 Antibody in the Differential Diagnosis of Gastrointestinal Stromal Tumors. *American Journal of Surgical Pathology*, *33*(9), 1401–1408. https://doi.org/10.1097/PAS.0b013e3181a90e1a

Minn, A. J., Kang, Y., Serganova, I., Gupta, G. P., Giri, D. D., Doubrovin, M., Ponomarev, V., Gerald, W. L., Blasberg, R., & Massagué, J. (2005). Distinct organ-specific metastatic potential of individual breast cancer cells and primary tumors. *Journal of Clinical Investigation*, *115*(1), 44–55. https://doi.org/10.1172/JCI22320

Miranda, C., Nucifora, M., Molinari, F., Conca, E., Anania, M. C., Bordoni, A., Saletti, P., Mazzucchelli, L., Pilotti, S., Pierotti, M. A., Tamborini, E., Greco, A., & Frattini, M. (2012). KRAS and BRAF Mutations Predict Primary Resistance to Imatinib in Gastrointestinal Stromal Tumors. *Clinical Cancer Research*, *18*(6), 1769–1776. https://doi.org/10.1158/1078-0432.CCR-11-2230

Mol, C. D., Dougan, D. R., Schneider, T. R., Skene, R. J., Kraus, M. L., Scheibe, D. N., Snell, G. P., Zou, H., Sang, B.-C., & Wilson, K. P. (2004). Structural Basis for the Autoinhibition and STI-571 Inhibition of c-Kit Tyrosine Kinase. *Journal of Biological Chemistry*, *279*(30), 31655–31663. https://doi.org/10.1074/jbc.M403319200

Morgado, S., Morgado, M., Plácido, A. I., Roque, F., & Duarte, A. P. (2018). Arbutus unedo L.: From traditional medicine to potential uses in modern pharmacotherapy. *Journal of Ethnopharmacology*, *225*. https://doi.org/10.1016/j.jep.2018.07.004

Naeem, A., Hu, P., Yang, M., Zhang, J., Liu, Y., Zhu, W., & Zheng, Q. (2022). Natural Products as Anticancer Agents: Current Status and Future Perspectives. *Molecules*, *27*(23), 8367. https://doi.org/10.3390/molecules27238367

Nakabayashi, R., & Saito, K. (2013). Metabolomics for unknown plant metabolites. *Analytical and Bioanalytical Chemistry*, *405*(15), 5005–5011. https://doi.org/10.1007/s00216-013-6869-2

Newman, D. J., & Cragg, G. M. (2020). Natural Products as Sources of New Drugs over the Nearly Four Decades from 01/1981 to 09/2019. *Journal of Natural Products*, *83*(3), 770–803. https://doi.org/10.1021/acs.jnatprod.9b01285

Ni, B.-S., Tzao, C., & Huang, J.-H. (2019). Plug-and-Play In Vitro Metastasis System toward Recapitulating the Metastatic Cascade. *Scientific Reports*, *9*(1), 18110. https://doi.org/10.1038/s41598-019-54711-z

Niinuma, T., Suzuki, H., & Sugai, T. (2018). Molecular characterization and pathogenesis of gastrointestinal stromal tumor. *Translational Gastroenterology and Hepatology*, *3*. https://doi.org/10.21037/tgh.2018.01.02

Nishida, T., Blay, J.-Y., Hirota, S., Kitagawa, Y., & Kang, Y.-K. (2016). The standard diagnosis, treatment, and follow-up of gastrointestinal stromal tumors based on guidelines. *Gastric Cancer*, *19*(1), 3–14. https://doi.org/10.1007/s10120-015-0526-8

Nishida, T., Kanda, T., Nishitani, A., Takahashi, T., Nakajima, K., Ishikawa, T., & Hirota, S. (2008). Secondary mutations in the kinase domain of the KIT gene are predominant in imatinib-

resistant gastrointestinal stromal tumor. *Cancer Science*, *99*(4), 799–804. https://doi.org/10.1111/j.1349-7006.2008.00727.x

Noble, R. L. (1990). The discovery of the vinca alkaloids--chemotherapeutic agents against cancer. *Biochemistry and Cell Biology = Biochimie et Biologie Cellulaire*, *68*(12), 1344–1351.

Noma, K., Naomoto, Y., Gunduz, M., Matsuoka, J., Yamatsuji, T., Shirakawa, Y., Nobuhisa, T., Okawa, T., Takaoka, M., Tomono, Y., Hiroyuki, O., Gunduz, E., & Tanaka, N. (2005). Effects of imatinib vary with the types of KIT-mutation in gastrointestinal stromal tumor cell lines. *Oncology Reports*. https://doi.org/10.3892/or.14.3.645

Olivier, M., Langer√∏d, A., Carrieri, P., Bergh, J., Klaar, S., Eyfjord, J., Theillet, C., Rodriguez, C., Lidereau, R., Bi√®che, I., Varley, J., Bignon, Y., Uhrhammer, N., Winqvist, R., Jukkola-Vuorinen, A., Niederacher, D., Kato, S., Ishioka, C., Hainaut, P., & B√∏rresen-Dale, A.-L. (2006). The clinical value of somatic TP53 gene mutations in 1,794 patients with breast cancer. *Clinical Cancer Research*, *12*(4), 1157–1167. https://doi.org/10.1158/1078-0432.CCR-05-1029

Ozaki, T., & Nakagawara, A. (2011). Role of p53 in Cell Death and Human Cancers. *Cancers*, *3*(1), 994–1013. https://doi.org/10.3390/cancers3010994

Paget, S. (1989). The distribution of secondary growths in cancer of the breast. 1889. *Cancer Metastasis Reviews*, *8*(2), 98–101.

Panda, S., & Ravindran, B. (2013). Isolation of Human PBMCs. *BIO-PROTOCOL*, *3*(3). https://doi.org/10.21769/BioProtoc.323

Patel, M., Pandey, S., Kumar, M., Haque, M., Pal, S., & Yadav, N. (2021). Plants Metabolome Study: Emerging Tools and Techniques. *Plants*, *10*(11), 2409. https://doi.org/10.3390/plants10112409

Patel, N., & Benipal, B. (2019). Incidence of Gastrointestinal Stromal Tumors in the United States from 2001-2015: A United States Cancer Statistics Analysis of 50 States. *Cureus*. https://doi.org/10.7759/cureus.4120

Peng, X., Pan, W., Jiang, F., Chen, W., Qi, Z., Peng, W., & Chen, J. (2022). Selective PARP1 inhibitors, PARP1-based dual-target inhibitors, PROTAC PARP1 degraders, and prodrugs of PARP1 inhibitors for cancer therapy. *Pharmacological Research*, *186*, 106529. https://doi.org/10.1016/j.phrs.2022.106529

Pérez-González, A., Bévant, K., & Blanpain, C. (2023). Cancer cell plasticity during tumor progression, metastasis and response to therapy. *Nature Cancer*, *4*(8), 1063–1082. https://doi.org/10.1038/s43018-023-00595-y

Pessetto, Z. Y., Weir, S. J., Sethi, G., Broward, M. A., & Godwin, A. K. (2013). Drug Repurposing for Gastrointestinal Stromal Tumor. *Molecular Cancer Therapeutics*, *12*(7). https://doi.org/10.1158/1535-7163.MCT-12-0968

Plaat, B. E. C., Hollema, H., Molenaar, W. M., Broers, G. H. T., Pijpe, J., Mastik, M. F., Hoekstra, H. J., van den Berg, E., Scheper, R. J., & van der Graaf, W. T. A. (2000). Soft Tissue Leiomyosarcomas and Malignant Gastrointestinal Stromal Tumors: Differences in Clinical Outcome and Expression of Multidrug Resistance Proteins. *Journal of Clinical Oncology*, *18*(18), 3211–3220. https://doi.org/10.1200/JCO.2000.18.18.3211

Postow, M. A., & Robson, M. E. (2012). Inherited gastrointestinal stromal tumor syndromes: mutations, clinical features, and therapeutic implications. *Clinical Sarcoma Research*, *2*(1), 16. https://doi.org/10.1186/2045-3329-2-16

Poveda, A., García del Muro, X., López-Guerrero, J. A., Cubedo, R., Martínez, V., Romero, I., Serrano, C., Valverde, C., & Martín-Broto, J. (2017). GEIS guidelines for gastrointestinal sarcomas (GIST). *Cancer Treatment Reviews*, *55*, 107–119. https://doi.org/10.1016/j.ctrv.2016.11.011

Rajabi, S., Maresca, M., Yumashev, A. V., Choopani, R., & Hajimehdipoor, H. (2021). The Most Competent Plant-Derived Natural Products for Targeting Apoptosis in Cancer Therapy. *Biomolecules*, *11*(4), 534. https://doi.org/10.3390/biom11040534

Ran, F. A., Hsu, P. D., Wright, J., Agarwala, V., Scott, D. A., & Zhang, F. (2013). Genome engineering using the CRISPR-Cas9 system. *Nature Protocols*, *8*(11), 2281–2308. https://doi.org/10.1038/nprot.2013.143

Raut, C. P., Espat, N. J., Maki, R. G., Araujo, D. M., Trent, J., Williams, T. F., Purkayastha, D. Das, & DeMatteo, R. P. (2018). Efficacy and Tolerability of 5-Year Adjuvant Imatinib Treatment for Patients With Resected Intermediate- or High-Risk Primary Gastrointestinal Stromal Tumor. *JAMA Oncology*, *4*(12), e184060. https://doi.org/10.1001/jamaoncol.2018.4060

Ravegnini, G., Sammarini, G., Nannini, M., Pantaleo, M. A., Biasco, G., Hrelia, P., & Angelini, S. (2017). Gastrointestinal stromal tumors (GIST): Facing cell death between autophagy and apoptosis. *Autophagy*, *13*(3). https://doi.org/10.1080/15548627.2016.1256522

Reichardt, P., Blay, J.-Y., Boukovinas, I., Brodowicz, T., Broto, J. M., Casali, P. G., Decatris, M., Eriksson, M., Gelderblom, H., Kosmidis, P., Le Cesne, A., Pousa, A. L., Schlemmer, M., Verweij, J., & Joensuu, H. (2012). Adjuvant therapy in primary GIST: state-of-the-art. *Annals of Oncology*, *23*(11), 2776–2781. https://doi.org/10.1093/annonc/mds198

Rizzo, A., Pantaleo, M. A., Astolfi, A., Indio, V., & Nannini, M. (2021). The Identity of PDGFRA D842V-Mutant Gastrointestinal Stromal Tumors (GIST). *Cancers*, *13*(4), 705. https://doi.org/10.3390/cancers13040705

Rossari, F., Minutolo, F., & Orciuolo, E. (2018). Past, present, and future of Bcr-Abl inhibitors: from chemical development to clinical efficacy. *Journal of Hematology & Oncology*, *11*(1), 84. https://doi.org/10.1186/s13045-018-0624-2

Rubin, B. P., Singer, S., Tsao, C., Duensing, A., Lux, M. L., Ruiz, R., Hibbard, M. K., Chen, C. J., Xiao, S., Tuveson, D. A., Demetri, G. D., Fletcher, C. D., & Fletcher, J. A. (2001). KIT activation is a ubiquitous feature of gastrointestinal stromal tumors. *Cancer Research*, *61*(22), 8118–8121.

Sanders, K. M., Koh, S. D., & Ward, S. M. (2006). INTERSTITIAL CELLS OF CAJAL AS PACEMAKERS IN THE GASTROINTESTINAL TRACT. *Annual Review of Physiology*, *68*(1), 307–343. https://doi.org/10.1146/annurev.physiol.68.040504.094718

Sanna, C., Chiocchio, I., Mandrone, M., Bonvicini, F., Gentilomi, G. A., Trincia, S., & Poli, F. (2023). Metabolomic analysis and bioactivities of Arbutus unedo leaves harvested across the seasons in different natural habitats of Sardinia (Italy). *BMC Plant Biology*, *23*(1), 490. https://doi.org/10.1186/s12870-023-04497-0

Sawaki, A. (2017). Rare gastrointestinal stromal tumors (GIST): omentum and retroperitoneum. *Translational Gastroenterology and Hepatology*, *2*(12), 116–116. https://doi.org/10.21037/tgh.2017.12.07

Schaldenbrand, J. D., & Appelman, H. D. (1984). Solitary solid stromal gastrointestinal tumors in von recklinghausen's disease with minimal smooth muscle differentiation. *Human Pathology*, *15*(3), 229–232. https://doi.org/10.1016/S0046-8177(84)80184-7

Sepe, P. S., Moparty, B., Pitman, M. B., Saltzman, J. R., & Brugge, W. R. (2009). EUS-guided FNA for the diagnosis of GI stromal cell tumors: sensitivity and cytologic yield. *Gastrointestinal Endoscopy*, *70*(2), 254–261. https://doi.org/10.1016/j.gie.2008.11.038

Serrano, C., Mariño-Enríquez, A., Tao, D. L., Ketzer, J., Eilers, G., Zhu, M., Yu, C., Mannan, A. M., Rubin, B. P., Demetri, G. D., Raut, C. P., Presnell, A., McKinley, A., Heinrich, M. C., Czaplinski, J. T., Sicinska, E., Bauer, S., George, S., & Fletcher, J. A. (2019). Complementary activity of tyrosine kinase inhibitors against secondary kit mutations in imatinib-resistant gastrointestinal stromal tumours. *British Journal of Cancer*, *120*(6), 612–620. https://doi.org/10.1038/s41416-019-0389-6

Shen, C., Han, L., Liu, B., Zhang, G., Cai, Z., Yin, X., Yin, Y., Chen, Z., & Zhang, B. (2022). The KDM6A-SPARCL1 axis blocks metastasis and regulates the tumour microenvironment of gastrointestinal stromal tumours by inhibiting the nuclear translocation of p65. *British Journal of Cancer*, *126*(10), 1457–1469. https://doi.org/10.1038/s41416-022-01728-3

Shen, C., Yin, Y., Chen, H., Wang, R., Yin, X., Cai, Z., Zhang, B., Chen, Z., & Zhou, Z. (2018). Secreted protein acidic and rich in cysteine-like 1 suppresses metastasis in gastric stromal tumors. *BMC Gastroenterology*, *18*(1), 105. https://doi.org/10.1186/s12876-018-0833-8

Shlomovitz, I., Speir, M., & Gerlic, M. (2019). Flipping the dogma – phosphatidylserine in non-apoptotic cell death. *Cell Communication and Signaling*, *17*(1), 139. https://doi.org/10.1186/s12964-019-0437-0

Smith, B. D., Kaufman, M. D., Lu, W.-P., Gupta, A., Leary, C. B., Wise, S. C., Rutkoski, T. J., Ahn, Y. M., Al-Ani, G., Bulfer, S. L., Caldwell, T. M., Chun, L., Ensinger, C. L., Hood, M. M., McKinley, A., Patt, W. C., Ruiz-Soto, R., Su, Y., Telikepalli, H., … Flynn, D. L. (2019). Ripretinib (DCC-2618) Is a Switch Control Kinase Inhibitor of a Broad Spectrum of Oncogenic and Drug-Resistant KIT and PDGFRA Variants. *Cancer Cell*, *35*(5), 738-751.e9. https://doi.org/10.1016/j.ccell.2019.04.006

Søreide, K., Sandvik, O. M., Søreide, J. A., Giljaca, V., Jureckova, A., & Bulusu, V. R. (2016). Global epidemiology of gastrointestinal stromal tumours (GIST): A systematic review of population-based cohort studies. *Cancer Epidemiology*, *40*, 39–46. https://doi.org/10.1016/j.canep.2015.10.031

Strebhardt, K., & Ullrich, A. (2008). Paul Ehrlich's magic bullet concept: 100 years of progress. *Nature Reviews Cancer*, *8*(6). https://doi.org/10.1038/nrc2394

Strilic, B., & Offermanns, S. (2017). Intravascular Survival and Extravasation of Tumor Cells. *Cancer Cell*, *32*(3), 282–293. https://doi.org/10.1016/j.ccell.2017.07.001

Taguchi, T., Sonobe, H., Toyonaga, S., Yamasaki, I., Shuin, T., Takano, A., Araki, K., Akimaru, K., & Yuri, K. (2002). Conventional and Molecular Cytogenetic Characterization of a New Human Cell Line, GIST-T1, Established from Gastrointestinal Stromal Tumor. *Laboratory Investigation*, *82*(5), 663–665. https://doi.org/10.1038/labinvest.3780461

Tait, S. W. G., & Green, D. R. (2008). Caspase-independent cell death: leaving the set without the final cut. *Oncogene*, *27*(50), 6452–6461. https://doi.org/10.1038/onc.2008.311

Tarn, C., Skorobogatko, Y. V., Taguchi, T., Eisenberg, B., Von Mehren, M., & Godwin, A. K. (2006). Therapeutic effect of imatinib in gastrointestinal stromal tumors: AKT signaling dependent and independent mechanisms. *Cancer Research*, *66*(10), 5477–5486. https://doi.org/10.1158/0008-5472.CAN-05-3906

Tu, Y., Zuo, R., Ni, N., Eilers, G., Wu, D., Pei, Y., Nie, Z., Wu, Y., Wu, Y., & Ou, W.-B. (2018). Activated tyrosine kinases in gastrointestinal stromal tumor with loss of KIT oncoprotein expression. *Cell Cycle*, *17*(23). https://doi.org/10.1080/15384101.2018.1553335

Tuveson, D. A., Willis, N. A., Jacks, T., Griffin, J. D., Singer, S., Fletcher, C. D., Fletcher, J. A., & Demetri, G. D. (2001). STI571 inactivation of the gastrointestinal stromal tumor c-KIT oncoprotein: biological and clinical implications. *Oncogene*, *20*(36). https://doi.org/10.1038/sj.onc.1204704

van de Rijn, M., Hendrickson, M. R., & Rouse, R. V. (1994). CD34 expression by gastrointestinal tract stromal tumors. *Human Pathology*, *25*(8), 766–771. https://doi.org/10.1016/0046-8177(94)90245-3

van der Graaf, W. T. A., Tielen, R., Bonenkamp, J. J., Lemmens, V., Verhoeven, R. H. A., & de Wilt, J. H. W. (2018). Nationwide trends in the incidence and outcome of patients with gastrointestinal stromal tumour in the imatinib era. *British Journal of Surgery*, *105*(8), 1020–1027. https://doi.org/10.1002/bjs.10809

Vargas-Accarino, E., Herrera-Montávez, C., Ramón y Cajal, S., & Aasen, T. (2021). Spontaneous Cell Detachment and Reattachment in Cancer Cell Lines: An In Vitro Model of Metastasis and Malignancy. *International Journal of Molecular Sciences*, *22*(9), 4929. https://doi.org/10.3390/ijms22094929

Verweij, J., Casali, P. G., Zalcberg, J., LeCesne, A., Reichardt, P., Blay, J.-Y., Issels, R., van Oosterom, A., Hogendoorn, P. C., Van Glabbeke, M., Bertulli, R., & Judson, I. (2004). Progression-free survival in gastrointestinal stromal tumours with high-dose imatinib:

randomised trial. *The Lancet*, *364*(9440), 1127–1134. https://doi.org/10.1016/S0140-6736(04)17098-0

Wada, R., Arai, H., Kure, S., Peng, W.-X., & Naito, Z. (2016). "Wild type" GIST: Clinicopathological features and clinical practice. *Pathology International*, *66*(8), 431–437. https://doi.org/10.1111/pin.12431

Wani, M. C., Taylor, H. L., Wall, M. E., Coggon, P., & McPhail, A. T. (1971). Plant antitumor agents. VI. Isolation and structure of taxol, a novel antileukemic and antitumor agent from Taxus brevifolia. *Journal of the American Chemical Society*, *93*(9), 2325–2327. https://doi.org/10.1021/ja00738a045

Wardelmann, E., Merkelbach-Bruse, S., Pauls, K., Thomas, N., Schildhaus, H.-U., Heinicke, T., Speidel, N., Pietsch, T., Buettner, R., Pink, D., Reichardt, P., & Hohenberger, P. (2006). Polyclonal Evolution of Multiple Secondary *KIT* Mutations in Gastrointestinal Stromal Tumors under Treatment with Imatinib Mesylate. *Clinical Cancer Research*, *12*(6), 1743–1749. https://doi.org/10.1158/1078-0432.CCR-05-1211

West, R. B., Corless, C. L., Chen, X., Rubin, B. P., Subramanian, S., Montgomery, K., Zhu, S., Ball, C. A., Nielsen, T. O., Patel, R., Goldblum, J. R., Brown, P. O., Heinrich, M. C., & van de Rijn, M. (2004). The Novel Marker, DOG1, Is Expressed Ubiquitously in Gastrointestinal Stromal Tumors Irrespective of KIT or PDGFRA Mutation Status. *The American Journal of Pathology*, *165*(1), 107–113. https://doi.org/10.1016/S0002-9440(10)63279-8

Williams, S. D., Birch, R., Einhorn, L. H., Irwin, L., Greco, F. A., & Loehrer, P. J. (1987). Treatment of Disseminated Germ-Cell Tumors with Cisplatin, Bleomycin, and either Vinblastine or Etoposide. *New England Journal of Medicine*, *316*(23), 1435–1440. https://doi.org/10.1056/NEJM198706043162302

Wozniak, A., Rutkowski, P., Piskorz, A., Ciwoniuk, M., Osuch, C., Bylina, E., Sygut, J., Chosia, M., Rys, J., Urbanczyk, K., Kruszewski, W., Sowa, P., Siedlecki, J., Debiec-Rychter, M., & Limon, J. (2012). Prognostic value of KIT/PDGFRA mutations in gastrointestinal stromal tumours (GIST): Polish Clinical GIST Registry experience. *Annals of Oncology*, *23*(2), 353–360. https://doi.org/10.1093/annonc/mdr127

Wozniak, A., Rutkowski, P., Schöffski, P., Ray-Coquard, I., Hostein, I., Schildhaus, H.-U., Le Cesne, A., Bylina, E., Limon, J., Blay, J.-Y., Siedlecki, J. A., Wardelmann, E., Sciot, R., Coindre, J.-M., & Debiec-Rychter, M. (2014). Tumor Genotype Is an Independent Prognostic Factor in Primary Gastrointestinal Stromal Tumors of Gastric Origin: A European Multicenter Analysis Based on ConticaGIST. *Clinical Cancer Research*, *20*(23), 6105–6116. https://doi.org/10.1158/1078-0432.CCR-14-1677

Yang, D. Y., Wang, X., Yuan, W. J., & Chen, Z. H. (2019). Metastatic pattern and prognosis of gastrointestinal stromal tumor (GIST): a SEER-based analysis. *Clinical and Translational Oncology*, *21*(12), 1654–1662. https://doi.org/10.1007/s12094-019-02094-y

Yang, J., Ikezoe, T., Nishioka, C., Takezaki, Y., Hanazaki, K., Taguchi, T., & Yokoyama, A. (2012). Long-term exposure of gastrointestinal stromal tumor cells to sunitinib induces

epigenetic silencing of the PTEN gene. *International Journal of Cancer*, *130*(4). https://doi.org/10.1002/ijc.26095

Yeh, C.-N., Yen, C.-C., Chen, Y.-Y., Cheng, C.-T., Huang, S.-C., Chang, T.-W., Yao, F.-Y., Lin, Y.-C., Wen, Y.-S., Chiang, K.-C., Chen, J.-S., Yeh, T.-S., Tzeng, C.-H., Chao, T.-C., & Fletcher, J. A. (2014). Identification of aurora kinase A as an unfavorable prognostic factor and potential treatment target for metastatic gastrointestinal stromal tumors. *Oncotarget*, *5*(12). https://doi.org/10.18632/oncotarget.1705

Yuan, J., Kihara, T., Kimura, N., Yamasaki, T., Yoshida, M., Isozaki, K., Ito, A., & Hirota, S. (2022). *CADM1* promotes adhesion to vascular endothelial cells and transendothelial migration in cultured GIST cells. *Oncology Letters*, *23*(3), 86. https://doi.org/10.3892/ol.2022.13206

Zhang, J., Chen, K., Tang, Y., Luan, X., Zheng, X., Lu, X., Mao, J., Hu, L., Zhang, S., Zhang, X., & Chen, W. (2021). LncRNA-HOTAIR activates autophagy and promotes the imatinib resistance of gastrointestinal stromal tumor cells through a mechanism involving the miR-130a/ATG2B pathway. *Cell Death & Disease*, *12*(4). https://doi.org/10.1038/s41419-021-03650-7
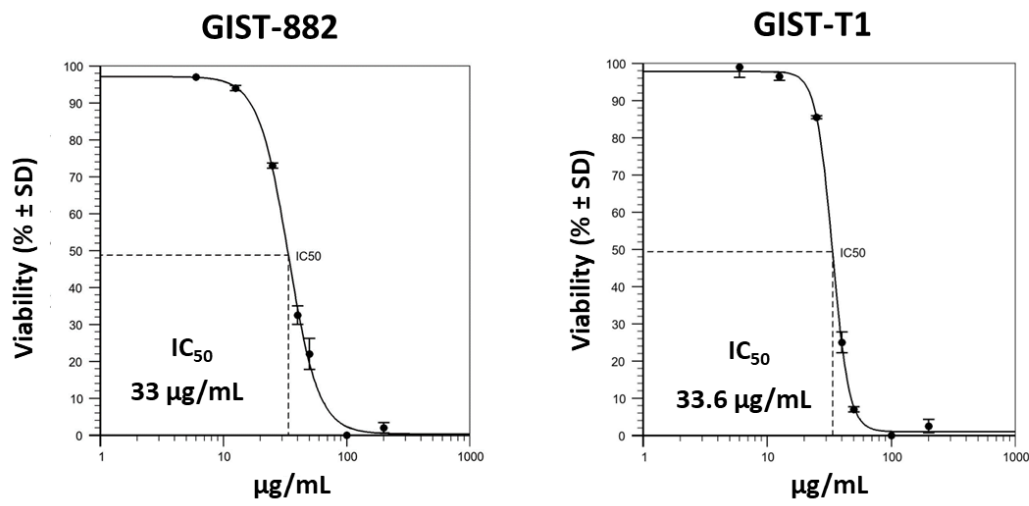
8. SUPPLEMENTARY DATA

Bio-guided fractionation of AUN to identify chemotherapeutics for GIST treatment
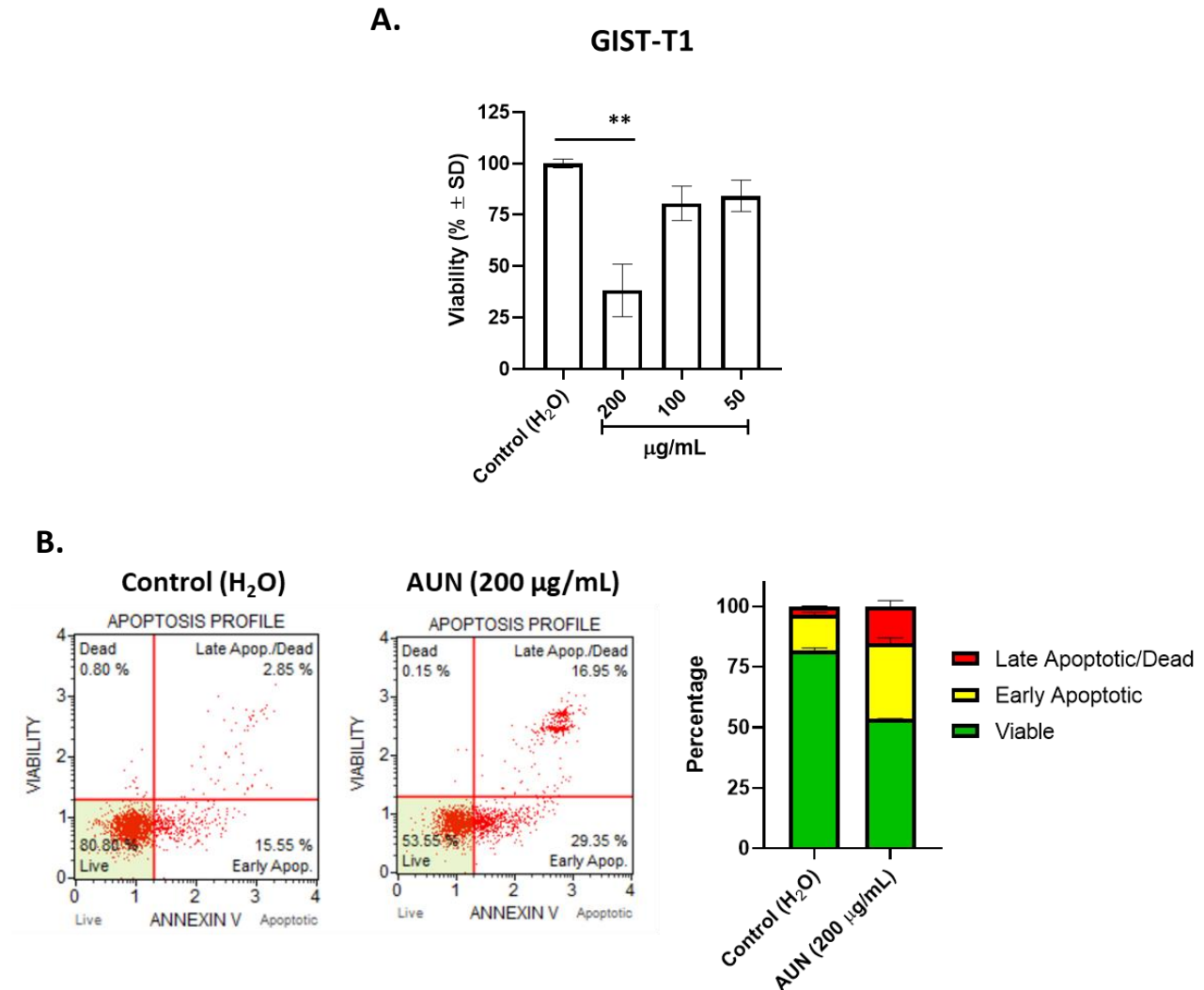
Supplementary Figure 1. AUN treatment in GIST-T1. A. Cells were treated at indicated final concentrations (μg/mL) for 72h. Viability is expressed in % ± SD with respect to Control. Viability was calculated based on the viable cells estimated with Guava® ViaCount™ staining. Adjusted p-value **<0.01 (One-way ANOVA-Dunnett's Multiple comparison test with respect to Control). **B.** Annexin-V/7-AAD staining of cells treated with 200 μg/mL AUN for 6h with respect to Control (left panel). Representative "apoptosis profiles" are shown. The percentage ± SD of viable (Annexin-V (-)/7-AAD (-)), early apoptotic (Annexin V (+)/7-AAD (-)), and late apoptotic/dead (Annexin V (+) and 7-AAD (+)) cell populations are displayed in the right graph. The average values are reported in the column. A representative experiment among two experimental replicates is shown.

A.

B.

C.
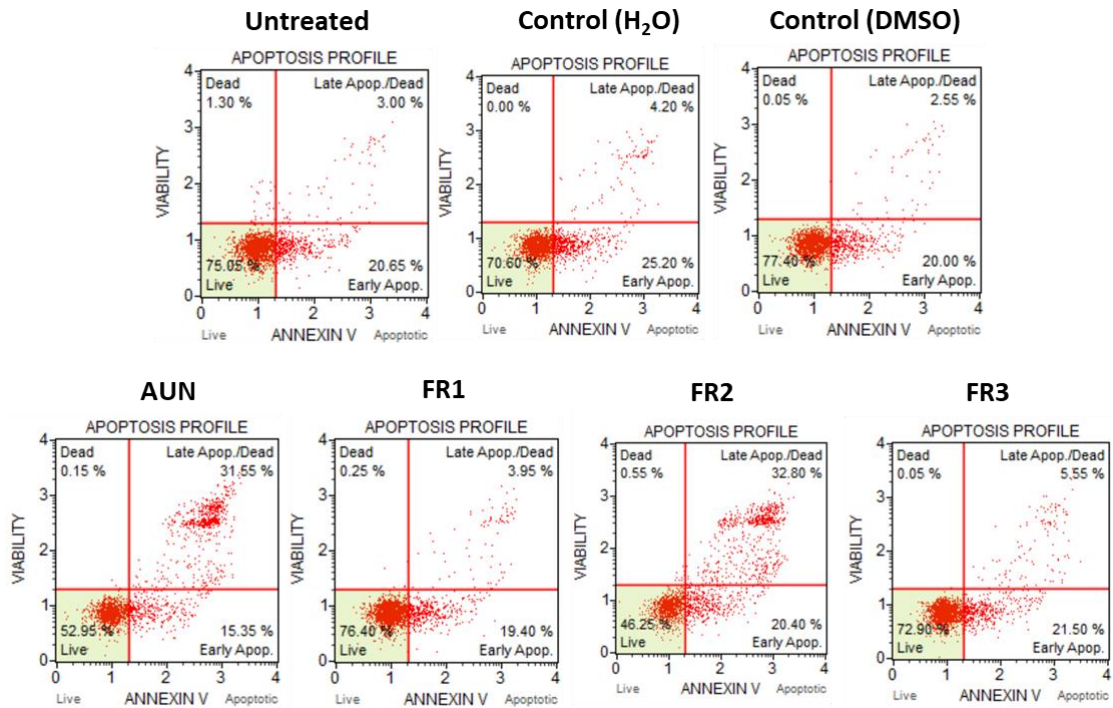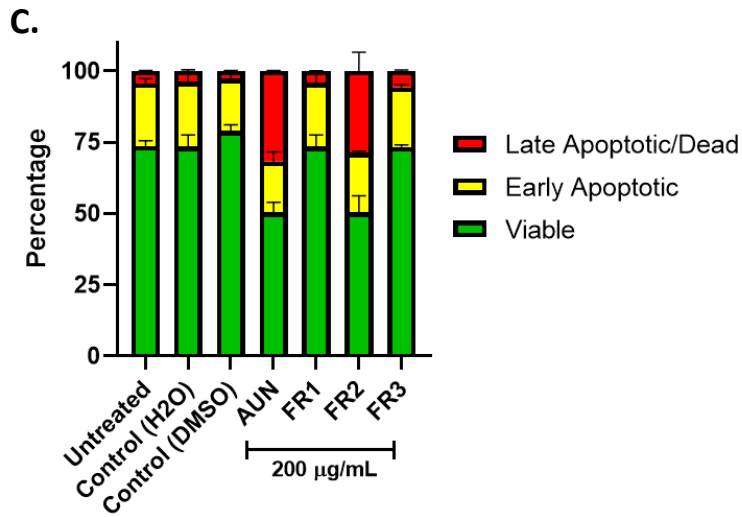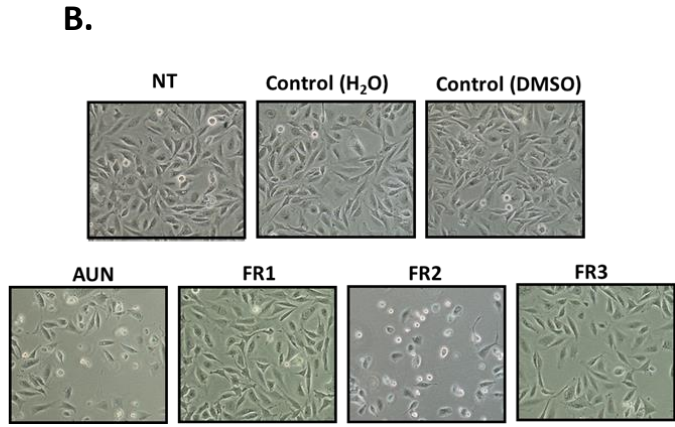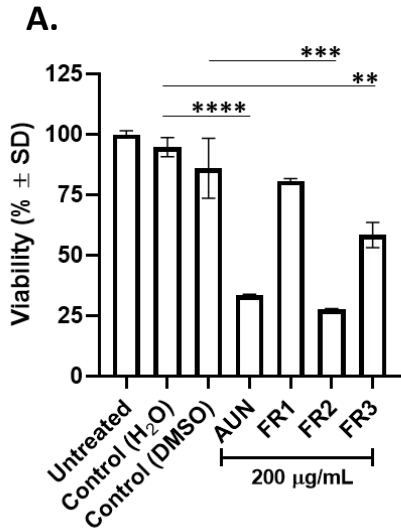
Supplementary Figure 2. Effect of AUN-derived FRs in GIST-T1. A. Cell viability after AUN or its derived FRs treatment (FR1-FR2-FR3). The length of the treatment was 24h. Viability is expressed in % ± SD with respect to the untreated sample. Adjusted p-value **** <0.0001, *** < 0.001, ** <0,01 - One-way ANOVA-Tuckey's Multiple comparison test with respect to the corresponding solvent-treated control sample (Control H_2O in the case of AUN and FR3, Control DMSO for FR2 and FR3). **B.** Brightfield microscopy pictures of each experimental sample before performing the staining and flow cytometry analysis are shown at a 10X magnification. **C.** Apoptosis profile obtained after Annexin-V/7-AAD staining of the experimental samples. The percentage ± SD of viable (Annexin-V (-)/ /7-AAD (-)), early apoptotic (Annexin V (+)/7-AAD (-)), and late apoptotic/dead (Annexin V (+) and 7-AAD (+)) cell populations are displayed. A representative experiment among three experimental replicates is shown.


Supplementary Figure 3. GIST-882 (on the left) and GIST-T1 (on the right) were treated with different concentrations of FR2-A, and the viability was measured through Guava® ViaCount™ staining and flow cytometry analysis. Cell viability is expressed in percentage with respect to Control ± SD. The calculated IC_{50} is reported at the bottom of the corresponding graph. A representative experiment among two experimental replicates is shown.

An *in vitro* model for the study of metastasis in GISTs
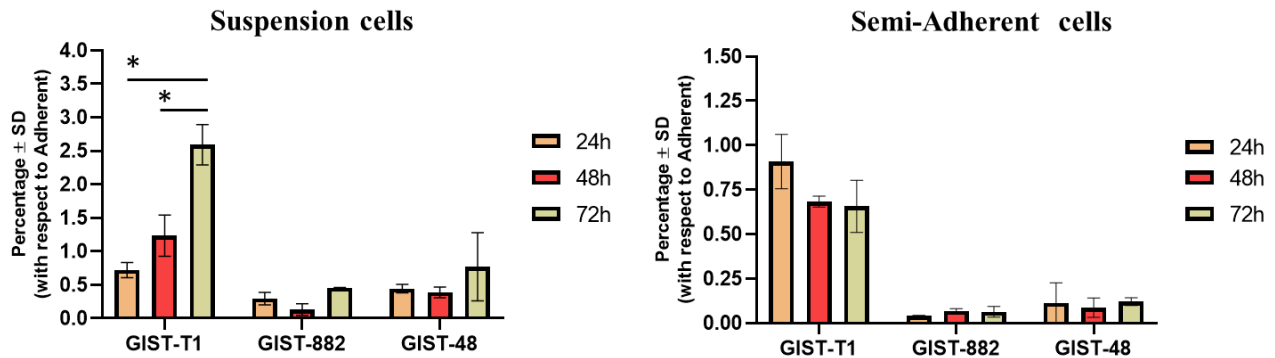
Supplementary Figure 4. Analysis of the percentage of Suspension and Semi-adherent subpopulations with respect to the corresponding Adherent observed at 24h. One-way ANOVA-Dunnett's Multiple comparison test with respect to the corresponding samples at 24h. * means an "adjusted p-value" <0.05. A representative experiment among three experimental replicates is shown.
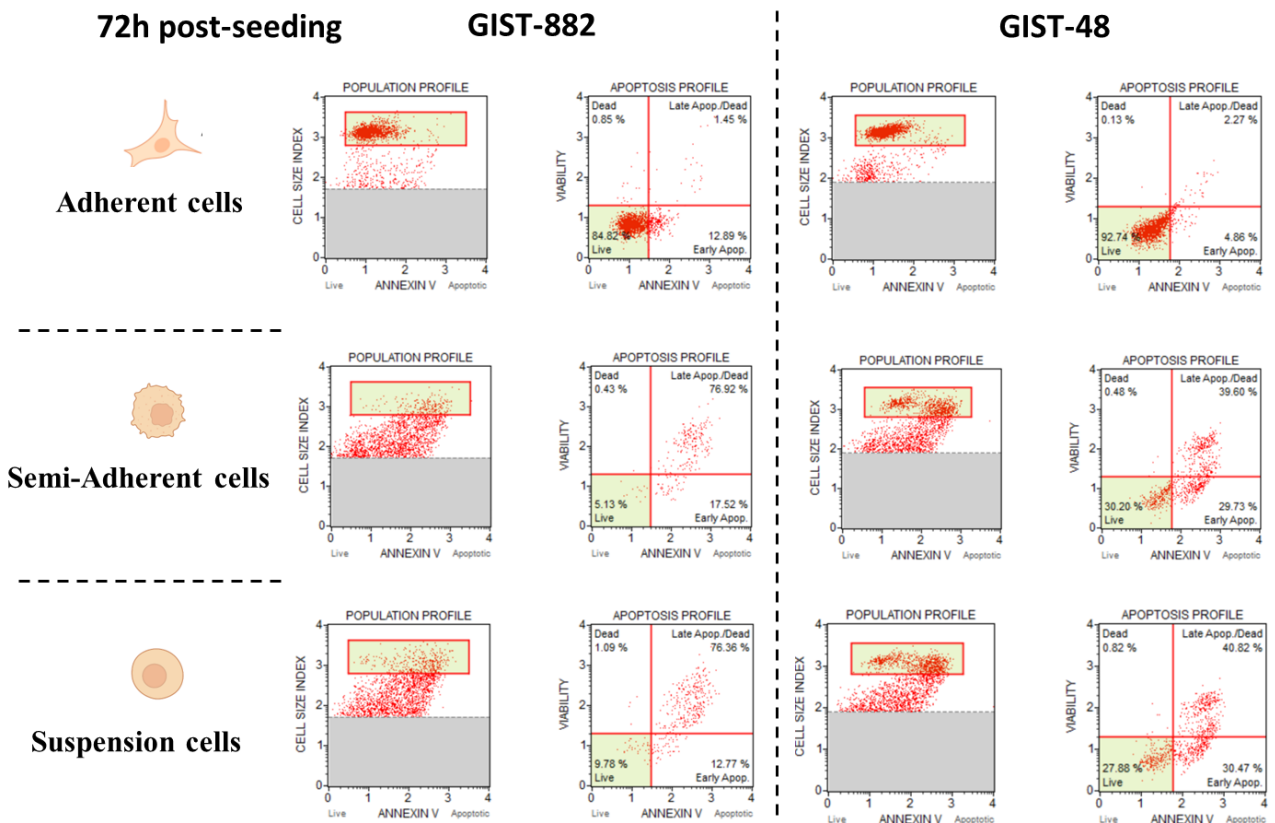
Supplementary Figure 5. The "Apoptosis profiles" in GIST-882 and GIST-48 sub-populations. Differentiation of live, early apoptotic, and late apoptotic/dead cells is shown. A representative experiment is shown among two experimental replicates.
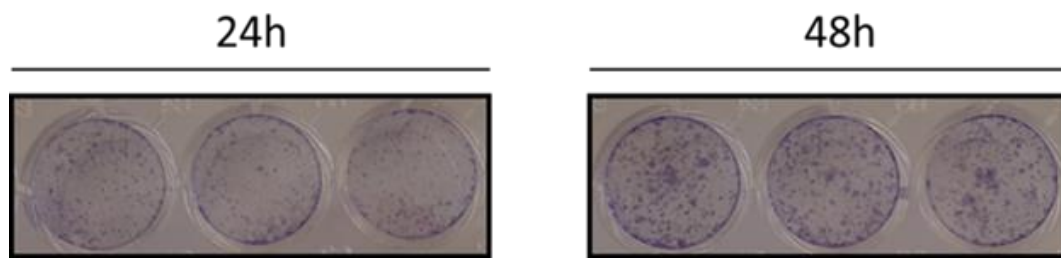
Supplementary Figure 6. Suspension cells can be collected 24h and 48h after Adh-F4-T1 seeding. Adh-F4-T1 were seeded, and suspension cells were collected 24h or 48h later. Crystal violet staining was performed 12 days after seeding. A technical triplicate is shown for each time point. A representative experiment is shown among two experimental replicates.
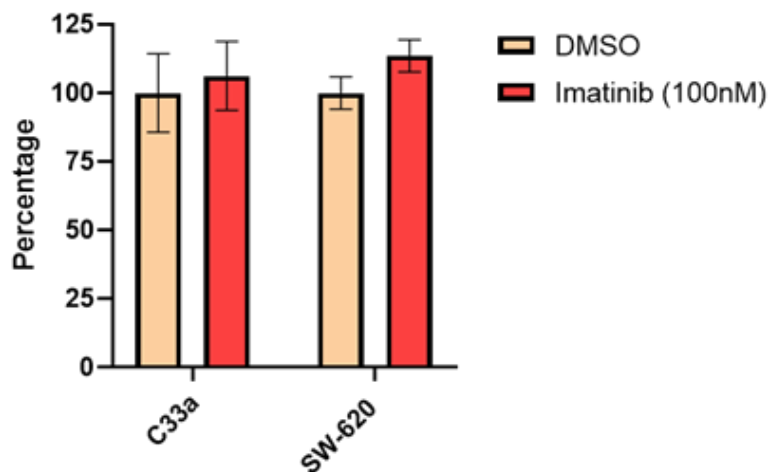
Supplementary Figure 7. Imatinib does not affect the *in vitro* metastatic model in C33a and SW-620. The percentage (± SD) of re-attached cells was calculated starting from crystal violet staining performed the day before the seeding of C33a and SW-620 suspension cells (595nm). The percentage is with respect to each DMSO-treated sample.

GIST-T1 Adherent
Stained TO-PRO-3
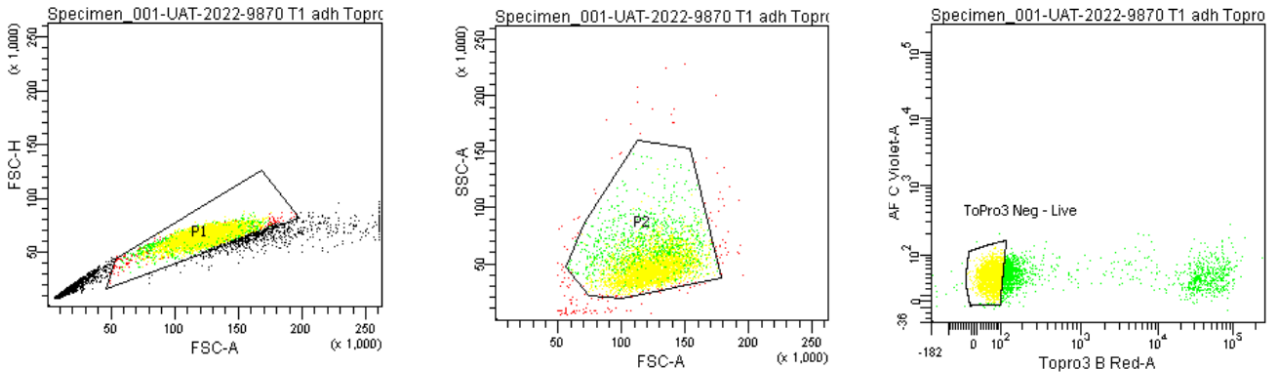
GIST-T1 Suspension
Stained with TO-PRO-3
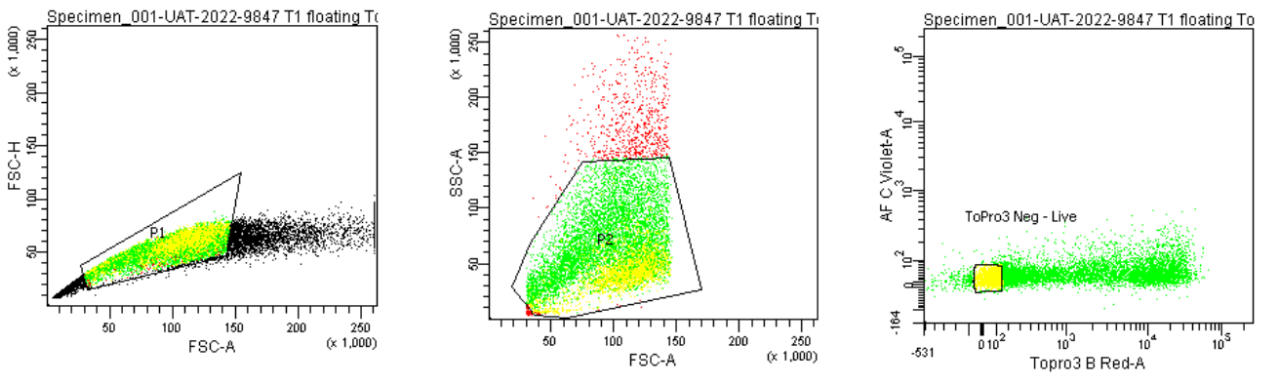

Supplementary Figure 8. Applied gates to sort viable cells in the Suspension subpopulation. GIST-T1 adherent subpopulation was used to define the FSC, SSC, and TO-PRO-3 parameters associated with viable cells. These parameters were then applied to sort the living population from the Floating subpopulation.

Population	#Events	%Parent	%Total
☐ All Events	16,979	####	100.0
■ P1	10,010	59.0	59.0
■ P2	9,219	92.1	54.3
☐ ToPro3 Neg - Live	2,018	21.9	11.9
☐ P3	0	0.0	0.0
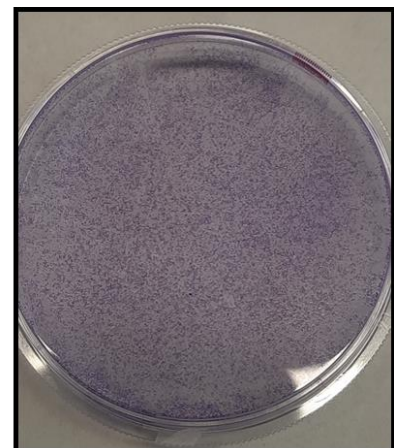
Supplementary Figure 9. TO PRO-3 negative cells represent about 12% of all events detected in GIST-T1 Suspension subpopulation with FACS-based sorting (red box in the right panel). The sorted TO-PRO-3 negative can settle down again. This suggests that the population that we have isolated reproduces the *in vitro* metastatic-like behavior of suspension cells present in the culture medium.
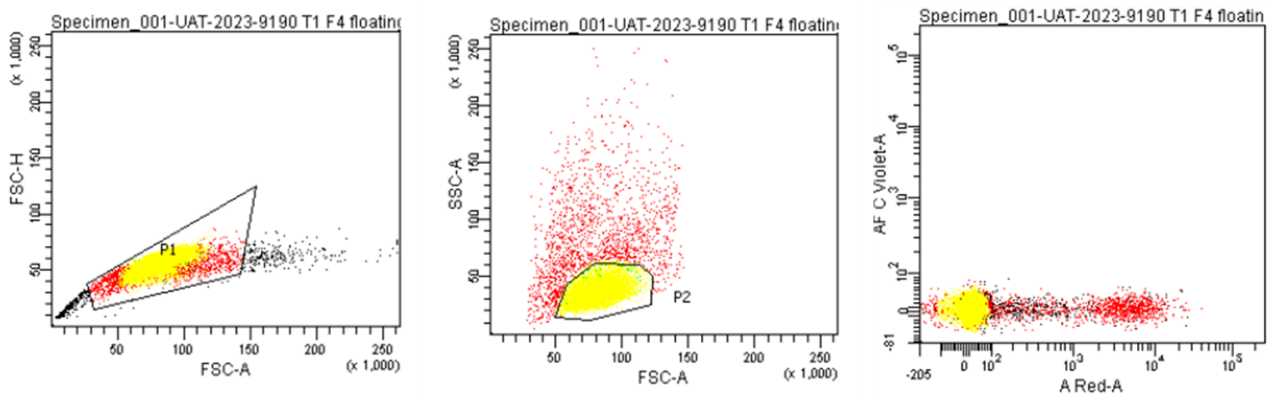
Tube: UAT-2023-9190 T1 F4 floating topro3			
Population	#Events	%Parent	%Total
☐ All Events	11,019	####	100.0
☐ P1	10,000	90.8	90.8
☐ P2	8,335	83.4	75.6
☐ P5	8,082	97.0	73.3

Supplementary Figure 10. TO PRO-3 negative cells represent about 73% of all events detected in Adh-F4-T1 Suspension subpopulation with FACS-based sorting. Red-A (x-axis) measures TO-PRO-3 related signal. The yellow population represents viable cells in the Suspension subpopulation.

Upregulated proteins in floating (C33a, SW-620 and GIST-T1) - n=180								
AAAS	BCS1L	DNPEP	GNAI2	MT-CO2	PAPOLA	PTCD3	RPS27	TBC1D13
ABCE1	BPIFB1	DYNC1H1	GOT1	NAMPT	PCYOX1	PTPN1	RPS8	TBRG4
ABR	BYSL	EFTUD2	GRIN2A	NARS1	PDP1	QRICH2	RPS9	TMED10
ACADVL	CAPN1	EHD4	GTF2H1	NCAPD2	PFKL	QSOX2	RRP9	TMED7-TICAM2
ACLY	CAPN2	EIF3K	HAT1	NCBP1	PFKM	RAB14	SACM1L	TMEM70
ACOX1	CARM1	EIF3L	HK1	NDUFA10	PGD	RAP1GDS1	SCFD1	TNPO3
ACTB	CDK5	EIF4A1	HSD17B11	NDUFS7	PICALM	RAP2C	SEC23B	TRAP1
ACTR1B	CISD1	EIF4A3	IDE	NMT1	PITPNB	RELB	SERPINB6	TRIP13
ADSL	CLTC	EMG1	IPO5	NOMO2	PLOD3	**RFC5**	SETD3	TUBAL3
AHCY	COPS3	ERLEC1	IPO7	NT5DC1	PMPCA	RHOT2	SFXN1	UFL1
AKT1	CPSF1	ERLIN2	**IPO9**	NUDC1	POLD1	RNMT	SLC25A3	USP14
ANAPC7	CS	ERO1A	KARS1	NUP155	PPP1CB	RPL13A	SNRNP200	USP7
ANXA5	**CTR9**	FAF1	MCM6	NUP160	PPP2CB	RPL15	SNRPD1	UTP15
AP2B1	CUL3	FASTKD2	MCU	NUP85	PPP2R5E	RPL18A	SPTBN1	UTP4
APEX1	CUL4A	GANAB	MEMO1	NUP93	PRKCI	RPL28	SRP72	VPS29
APMAP	DARS1	GDI2	MRPL38	OSBPL9	PSMB2	RPL3	STT3A	WDR12
ARPC2	DDB1	GEMIN5	MRPL48	OSTC	PSMB5	RPL4	STT3B	WDR18
ATG7	DDX39A	GFUS	MRPS27	OTUB1	PSMD13	RPL6	SUPT16H	WDR43
BCAT2	DHX15	GLB1	MRTFA	OTULIN	PSMD3	RPL7	SYNM	WDR75
BCHE	DHX9	GMPPB	MRTO4	PAFAH1B1	PSMD8	RPL7A	TARS1	XPOT

Supplementary Table 1. Alphabetic list of protein upregulated (N= 180) in C33a, SW-620, and GIST-T1 suspension cells with respect to adherents. According to Figure 33, proteins indicated in bold respect the highly stringent condition of analysis.

Downregulated proteins in floating (C33a, SW-620 and GIST-T1) - n=171									
AAMDC	CBX5	EEA1	ISCU	MRPL50	PPP1R14B	SH3BGRL	TIMM10B	USF2
AATF	CCDC12	ENY2	ITGA6	MRTFB	PRRC2A	SHARPIN	TIMM13	VASP
AIMP1	CDC26	EPS15	JPT2	MT1X	PRRC2C	SNRNP27	TIMM8A	WASH2P
AKAP2	CHCHD2	ERC1	KALRN	MTPN	PSAP	SORBS1	**TIMM8B**	WASH6P
APAF1	CHCHD4	FABP4	KIAA1191	NCOR1	PSMD4	SPTAN1	TJP1	WASHC2C
ARHGAP33	CLASRP	FBN2	KIF5C	NDUFS6	PTRHD1	SREK1	**TMF1**	YBX1
ATOX1	CNPY3	FIS1	**LASP1**	NEDD8-MDP1	PYGO2	SRRM2	TMOD3	ZC3H13
ATP5IF1	COL11A1	FKBP3	LIN7C	NFU1	RAD23A	SRSF1	TNIP1	ZFAND5
ATP5PF	COPS9	FNDC1	LRCH3	NUMB	RBM6	SRSF11	TNRC6B	ZNF207
BAD	COX5B	FOXO3	LUC7L2	NUP153	RCN2	SRSF7	TPD52L2	ZNF318
BANF1	COX6B1	GALNT18	LYRM7	PARK7	RHPN2	SRSF8	TRA2B	ZYX
BAP18	CREB1	GOLGA3	LZIC	PEX19	RMDN2	STAU1	TRIAP1	
BCL9	CRELD2	GON7	MAP4	PFDN2	RPL39	STMN1	TRIR	
BOD1	CRTC2	GSKIP	MBL2	PFDN4	RPLP2	**SUB1**	TRUB1	
BOD1L1	CSTB	GTF2F1	MCRIP1	PFDN6	RPS21	SUMF2	TSEN2	
C12orf43	CWC15	HEBP1	MEAF6	PFN1	**RPS29**	SUMO2	TTC1	
C1orf198	CYCS	HSBP1	MED9	PGLS	RRBP1	TAF4	TTC24	
CALM3	DBI	IK	MIX23	PHPT1	S100A4	TCF12	UBQLN1	
CAST	DBNL	IKBKG	MRPL12	PIN1	SCLY	THYN1	UCHL3	
CBX1	DHRS4	IRF2BP1	MRPL46	PIN4	SDE2	TIMM10	URI1	

Supplementary Table 2. Alphabetic list of downregulated protein (N= 171) in C33a, SW-620, and GIST-T1 suspension cells with respect to adherents. According to Figure 33, proteins indicated in bold respect the highly stringent condition of analysis.